

University of Nevada, Reno

**Reactivity of 1,3,5-triaza-7-phosphaadamantane-6-yl lithium (PTA-Li)
Towards Organotin, Silicon, and Boron Chlorides**

A thesis submitted in partial fulfillment of the
requirements for the degree of Master of Science in
Chemistry

by

June Pinky T. Acay

Dr. Brian J. Frost/Thesis Advisor

December, 2014

Copyright by June Pinky T. Acay 2014
All Rights Reserved



THE GRADUATE SCHOOL

We recommend that the thesis
prepared under our supervision by

JUNE PINKY T. ACAY

Entitled

**Reactivity Of 1,3,5-Triaza-7-Phosphaadamantane-6-Yllithium (PTA-Li)
Towards Organotin, Silicon, And Boron Chlorides**

be accepted in partial fulfillment of the
requirements for the degree of

MASTER OF SCIENCE

Brian J. Frost, Ph.D., Advisor

Vincent J. Catalano, Ph.D., Committee Member

Michael P. Branch, Ph.D., Graduate School Representative

David W. Zeh, Ph.D., Dean, Graduate School

December, 2014

Abstract

In this thesis, the synthesis and preliminary characterization of a library of 1,3,5-triaza-7-phosphaadamantane derivatives with Sn, Si, and B moieties are presented. Various electrophiles were reacted with lithiated PTA (PTA-Li) including SnR_3Cl , SnR_2Cl_2 , SiR_2Cl_2 ($\text{R}=\text{CH}_3$, Ph), and BR_2Cl ($\text{R}=\text{Cy}$, Ph). The α -stannylated PTA, PTA-SnMe₃, was successfully isolated along with the oxide, O=PTA-SnMe₃, characterized through solution NMR ($^{31}\text{P}\{^1\text{H}\}$, $^{13}\text{C}\{^1\text{H}\}$, $^{119}\text{Sn}\{^1\text{H}\}$, and ^1H) and ESI-MS. These water soluble compounds are also soluble in other organic solvents like chloroform, methylene chloride, hexanes, pentane, etc. PTA-SnMe₃ has been found to oxidize in solution but is more stable in the solid state. Preliminary observations on the reactions of PTA-Li with other tin, silicon, and boron electrophiles show various side products that become more abundant upon increasing the reaction scale. This may be a consequence of the air and moisture sensitivity of the starting materials and the products. Attempts to isolate the products were limited by a small yield. Most of the compounds were observed to decompose into O=PTA. Future attempts should consider measures to test effective moisture removal from solvents and starting materials.

Acknowledgements

First and foremost, I would like to thank my advisor Professor Brian J. Frost for providing me an opportunity to conduct research under his supervision. I was able to learn a lot about organometallic chemistry and green chemistry from his classes. I would also like to thank my committee members: Professor Brian J. Frost, Professor Vincent J. Catalano and Professor Michael P. Branch. I would like to express my appreciation for the support and friendship of former and current Frost research group members – Nathan Gelman, Dr. Jocelyn Pineda-Lanorio, Whalmany Ounkham, Ralph Enow, Dr. Jason Weeden, Jeremiah Sears, Travis Cournoyer, and Jonathan Rhea. It has been a very fortunate circumstance to be able to work with you all.

I would like to thank the Chemistry department faculty members, staff, and the graduate student association who encourage, help, and guide us through our academic and research goals. Thank you to Dr. Stephen M. Spain for his guidance in operating the various instruments in the department.

To my friends, thank you for all your encouragement.

To my parents and my siblings Joan, Jules, Joni, and Jenn -- thank you so much for the love and support.

To Nate, thank you for always being there for me. You never fail to put a smile on my face.

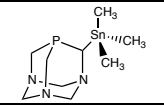
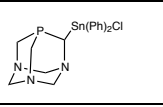
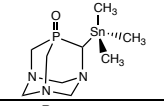
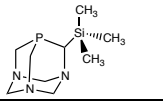
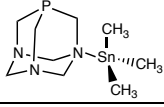
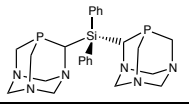
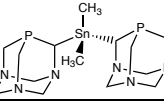
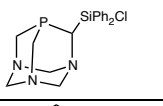
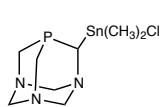
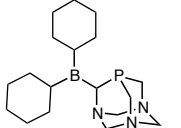
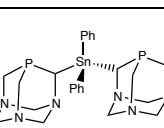
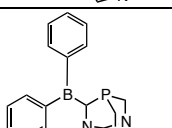
Table of Contents

Abstract	i
Acknowledgements	ii
Table of Contents	iii
Compounds Numbers	vi
List of Figures	vii
List of Schemes	xii
List of Tables	xiv
Chapter 1. General Introduction	1
1.1. Phosphines	1
1.2. PTA Synthesis and Properties	2
1.3. PTA-Li Synthesis and Upper-rim Derivatives	4
1.4. Thesis Organization	7
1.5. References	7
Chapter 2. Stannylated and Silylated PTA derivatives	8
2.1 Introduction	8
2.1.1 Upper-rim PTA derivatives via PTA-Li	8
2.1.2 Stannylated and Silylated phosphines	10

2.2 Results and Discussion	11
2.2.1 PTA-Sn derivatives via PTA-Li	11
2.2.1.1 Reaction of PTA with SnMe ₃ Cl	22
2.2.2 Attempts at PTA-Si derivatives	35
2.2.2.1 Reaction of PTA with SiMe ₃ Cl	37
2.3 Concluding Remarks	39
2.4 Experimental	40
2.4.1 General	40
2.4.2 Water Solubility	41
2.4.3 Synthesis	41
2.5 References	45
Chapter 3. PTA Phosphinoboranes	47
3.1 Introduction	47
3.1.1 Frustrated Lewis Pairs (FLPs)	47
3.1.2 P/B FLP compounds	49
3.1.3 Synthesis of Phosphinoborates and related compounds	50
3.2 Results and Discussion	52
3.2.1 Reaction of PTA-Li with BCy ₂ Cl	52
3.2.2 Reaction of PTA with BCy ₂ Cl	59
3.2.3 Attempted Synthesis of PTA-BPh ₂	60
3.3 Concluding Remarks	64

3.4 Experimental	65
3.4.1 General	65
3.4.2 Synthesis	65
3.5 References	70
Chapter 4. General Conclusions	73
APPENDIX	75
CURRICULUM VITAE	91

Compound Numbers

Compound	Number	Compound	Number
	1		7
	2		8
	3		9
	4		10
	5		11
	6		12

List of Figures

<u>Figure</u>		<u>Page</u>
1.1	Examples of water soluble phosphines.	2
1.2	Upper and lower rim of PTA.	4
1.3	PTA lower-rim derivatives	4
1.4	$^{31}\text{P}\{^1\text{H}\}$ NMR spectra of PTA-D in D_2O (top) and CDCl_3 (bottom).	5
1.5	$^{13}\text{C}\{^1\text{H}\}$ NMR spectra of PTA-D in D_2O (top) and CDCl_3 (bottom).	5
1.6	^1H NMR spectra of PTA-D in D_2O (top) and CDCl_3 (bottom).	6
2.1	PTA diphosphine derivatives from chlorophosphines.	9
2.2	First bis-PTA derivatives.	10
2.3	$^{31}\text{P}\{^1\text{H}\}$ NMR spectrum of the crude reaction mixture of PTA-Li and SnMe_3Cl in THF.	12
2.4	$^{31}\text{P}\{^1\text{H}\}$ NMR spectrum of PTA- SnMe_3 in CDCl_3 (* traces of the oxidized product).	13
2.5	$^{119}\text{Sn}\{^1\text{H}\}$ NMR spectrum of PTA- SnMe_3 (1) in CDCl_3 .	14
2.6	$^{31}\text{P}\{^1\text{H}\}$ NMR spectrum of PTA- SnMe_3 and traces of $\text{O}=\text{PTA}-\text{SnMe}_3$ in CDCl_3 .	14
2.7	Expanded ^1H NMR spectrum of PTA- SnMe_3 in CDCl_3 (without TMS). Full spectrum is presented in the appendix. *Traces of unreacted SnMe_3Cl	15
2.8	Expanded ^1H NMR spectrum of PTA- SnMe_3 in CDCl_3 showing ^{119}Sn and ^{117}Sn satellites.	15
2.9	Expanded $^{13}\text{C}\{^1\text{H}\}$ NMR spectrum of PTA- SnMe_3 in CDCl_3 . Full spectrum is presented in the appendix.	17
2.10	Expanded $^{13}\text{C}\{^1\text{H}\}$ NMR spectrum of PTA- SnMe_3 in CDCl_3 showing SnCH_3 protons.	17

2.11	Expanded $^{13}\text{C}\{^1\text{H}\}$ NMR spectrum of PTA-SnMe ₃ in CDCl ₃ showing PCH ₂ N and PCHSn protons.	18
2.12	Expanded $^{13}\text{C}\{^1\text{H}\}$ NMR spectrum of PTA-SnMe ₃ in CDCl ₃ showing NCH ₂ N protons.	18
2.13	$^{31}\text{P}\{^1\text{H}\}$ NMR spectrum of O=PTA-SnMe ₃ in CDCl ₃ .	20
2.14	Expanded ^1H NMR spectrum of O=PTA-SnMe ₃ in CDCl ₃ . *unreacted SnMe ₃ Cl	20
2.15	$^{119}\text{Sn}\{^1\text{H}\}$ NMR spectrum of O=PTA-SnMe ₃ in CDCl ₃ .	20
2.16	$^{119}\text{Sn}\{^1\text{H}\}$ NMR spectrum of a mixture of PTA-SnMe ₃ and OPTA-SnMe ₃ in CDCl ₃ .	21
2.17	$^{13}\text{C}\{^1\text{H}\}$ NMR spectrum of O=PTA-SnMe ₃ in CDCl ₃ . *oxide	22
2.18	Electrospray mass spectrum (positive mode) of PTA-SnMe ₃ and O=PTA-SnMe ₃ . Inset shows the simulated isotopic distribution pattern for $[\text{MH}]^+$.	22
2.19	^1H NMR spectrum of PTA with 1.1 equiv. SnMe ₃ Cl in CDCl ₃ . Inset shows the expanded resonance for SnCH ₃ protons. *trace amount of HMTA (hexamethylenetetramine) from PTA synthesis	24
2.20	$^{31}\text{P}\{^1\text{H}\}$ NMR spectrum of PTA with 1.1 equiv. SnMe ₃ Cl in CDCl ₃ . *Unidentified	24
2.21	$^{119}\text{Sn}\{^1\text{H}\}$ NMR spectrum of PTA with 1.1 equiv. SnMe ₃ Cl in CDCl ₃ .	24
2.22	$^{31}\text{P}\{^1\text{H}\}$ NMR spectrum of PTA with 1.1 equiv. SnMe ₃ Cl in D ₂ O.	26
2.23	Expanded ^1H NMR spectrum of PTA with 1.1 equiv. SnMe ₃ Cl in D ₂ O.	26
2.24	$^{31}\text{P}\{^1\text{H}\}$ NMR spectrum of previous sample of PTA with SnMe ₃ Cl in D ₂ O after addition of PTA.	26
2.25	Expanded ^1H NMR spectrum of previous sample of PTA with SnMe ₃ Cl in D ₂ O after addition of PTA.	27
2.26	$^{119}\text{Sn}\{^1\text{H}\}$ NMR spectrum of PTA with SnMe ₃ Cl in D ₂ O.	27

2.27	Expanded $^{119}\text{Sn}\{^1\text{H}\}$ NMR spectrum of a crude mixture of PTA-Li and SnMe_3Cl in D_2O . *Unidentified	27
2.28	Stereochemistry of $(\text{PTA})_2\text{SnMe}_2$ products.	28
2.29	$^{31}\text{P}\{^1\text{H}\}$ NMR spectrum of the crude sample of PTA-Li and SnMe_2Cl_2 in THF. *Unidentified	30
2.30	$^{31}\text{P}\{^1\text{H}\}$ NMR spectrum of the pentane-soluble product from the reaction of SnMe_2Cl_2 with PTA-Li in CDCl_3 . *Possibly an open-cage PTA derivative	30
2.31	Expanded $^{31}\text{P}\{^1\text{H}\}$ NMR spectrum of the pentane-soluble product from the reaction of SnMe_2Cl_2 with PTA-Li in CDCl_3 . *Possibly an open-cage PTA derivative	30
2.32	$^{119}\text{Sn}\{^1\text{H}\}$ NMR spectrum of the pentane-soluble product from the reaction of SnMe_2Cl_2 with PTA-Li in CDCl_3 . *Possibly an open-cage PTA derivative	31
2.33	Expanded $^{31}\text{P}\{^1\text{H}\}$ NMR spectrum of the decomposition of the crude sample of SnMe_2Cl_2 with PTA-Li in CDCl_3 . (top: starting sample. bottom: after 1 day)	33
2.34	Expanded electrospray mass spectrum (positive mode) of a sample of SnMe_2Cl_2 with PTA-Li. Inset shows the simulated isotopic distribution pattern (MH^+) for $(\text{PTA})_2\text{SnMe}_2$.	33
2.35	$^{31}\text{P}\{^1\text{H}\}$ NMR spectrum of the PTA-Li and SnPh_2Cl_2 reaction mixture in THF. *Unidentified. The full $^{31}\text{P}\{^1\text{H}\}$ NMR spectrum is presented in the appendix.	34
2.36	$^{31}\text{P}\{^1\text{H}\}$ NMR spectrum after washing the crude mixture of the PTA-Li and SnPh_2Cl_2 with hexanes. *Unidentified.	34
2.37	Possible side-products for the reaction of PTA-Li with SiMe_3Cl .	35
2.38	$^{31}\text{P}\{^1\text{H}\}$ NMR spectra of the reaction mixture of PTA-Li and SiMe_3Cl in THF (top) and the formation of oxides (bottom).	36
2.39	$^{31}\text{P}\{^1\text{H}\}$ NMR spectra of a PTA-Li and SiMe_3Cl in CDCl_3 .	36
2.40	$^{31}\text{P}\{^1\text{H}\}$ NMR spectrum of PTA with SiMe_3Cl in CD_2Cl_2 . *Unidentified,	37

	possible digital noise	
2.41	^1H NMR spectrum of PTA with SiMe_3Cl in CD_2Cl_2 .	38
2.42	$^{31}\text{P}\{^1\text{H}\}$ NMR spectrum of the crude reaction mixture of PTA-Li and SiPh_2Cl_2 reaction in THF.	39
2.43	$^{31}\text{P}\{^1\text{H}\}$ NMR spectrum of the crude reaction mixture of PTA-Li and SiPh_2Cl_2 pulled dry and dissolved in C_6D_6 .	39
3.1	Examples of FLPs	48
3.2	Examples of P/B FLP combinations	49
3.3	Depiction of PTA- BCy_2 (12)	52
3.4	Kinetic $^{31}\text{P}\{^1\text{H}\}$ NMR spectra of the reaction of PTA-Li and BCy_2Cl in THF at 35°C . Time elapsed can be calculated from the multiplication of the spectrum number by 5 minutes. Full study is shown in the appendix.	53
3.5	$^{31}\text{P}\{^1\text{H}\}$ NMR spectra of the reaction of PTA-Li and BCy_2Cl in THF at 25°C after 23 hours.	54
3.6	$^{31}\text{P}\{^1\text{H}\}$ NMR spectrum of the crude reaction mixture of PTA-Li and BCy_2Cl after filtering over celite.	55
3.7	Depiction of possible side products of the reaction of PTA-Li with BCy_2Cl	55
3.8	$^{31}\text{P}\{^1\text{H}\}$ NMR spectrum of the THF-soluble product from the reaction of PTA-Li and BCy_2Cl in C_6D_6 .	56
3.9	$^{31}\text{P}\{^1\text{H}\}$ NMR spectrum of the THF-soluble product from the crude reaction mixture of PTA-Li and BCy_2Cl in CD_3OD .	56
3.10	^1H NMR spectrum of the THF-soluble product from the crude reaction mixture of PTA-Li and BCy_2Cl in CD_3OD .	57
3.11	$^{31}\text{P}\{^1\text{H}\}$ NMR spectrum of the crude yellow precipitate from the reaction of PTA-Li and BCy_2Cl in CD_3OD .	57
3.12	ESI+ mass spectrum of a crude reaction mixture of PTA-Li and BCy_2Cl in methanol. Inset shows the simulated isotopic distribution pattern for M^+ .	58

3.13	$^{31}\text{P}\{^1\text{H}\}$ NMR spectrum of PTA-Li and BCy_2Cl in THF	58
3.14	$^{31}\text{P}\{^1\text{H}\}$ NMR spectrum of PTA and BCy_2Cl in toluene. The PTA peak (top) disappears and a new peak downfield appears (bottom).	60
3.15	$^{31}\text{P}\{^1\text{H}\}$ NMR spectrum for air-sensitivity of PTA and BCy_2Cl in toluene. The solution in toluene (top) oxidizes and decomposes within 3 hours (bottom). *Unidentified.	60
3.16	Depiction of PTA-BPh ₂ (12)	62
3.17	$^{31}\text{P}\{^1\text{H}\}$ NMR spectrum of PTA-Li with BPh_2Cl in THF	62
3.18	$^{31}\text{P}\{^1\text{H}\}$ NMR spectrum of PTA-Li with BPh_2Cl in CDCl_3	62
3.19	$^{31}\text{P}\{^1\text{H}\}$ NMR spectrum of PTA-Li with BPh_2Cl in CDCl_3 after washing with hexanes	63
3.20	ESI+ mass spectrum of PTA-Li with BPh_2Cl in methanol. Inset shows the simulated isotopic distribution curve for PTA-BPh ₂ (M^+).	63

List of Schemes

<u>Scheme</u>	<u>Page</u>
1.1	PTA synthesis (a) and oxidation(b) 3
1.2	PTA-Li synthesis. 4
2.1	Upper-rim PTA derivatives via PTA-Li 8
2.2	Synthesis of $\text{PhP(R)CH}_2\text{EMe}_3$ (R =H/Ph, E=Si/Sn). 11
2.3	Synthesis of PTA-SnMe ₃ (1). 11
2.4	Synthesis of O=PTA-SnMe ₃ (2). 18
2.5	Reaction of PTA with SnMe ₃ Cl. 22
2.6	General synthesis of stannylated and silylated bis-PTA via PTA-Li. 28
2.7	Depicted reaction products of SnMe ₂ Cl ₂ and PTA-Li. 28
2.8	Reaction of PTA-Li with SnPh ₂ Cl ₂ depicting the expected products 33
2.9	Reaction of PTA-Li with SiMe ₃ Cl depicting the expected product and side-product 35
2.10	Reaction of PTA with SiMe ₃ Cl depicting the expected product PTA(N-SiMe ₃) 37
2.11	Reaction of PTA-Li with SiPh ₂ Cl ₂ depicting the expected product and side-product 38
3.1	Reaction of trimethylborane with different Lewis bases. 47
3.2	Example of an intramolecular FLP system 48
3.3	Example of an intermolecular FLP system 49
3.4	Synthesis of bis(phosphine) borates. (R = p-MePh, m,m-(CH ₃) ₂ Ph, p-tBuPh, p-MeOPh, p-CF ₃ Ph, o-MeOPh, o,o- (MeO) ₂ Ph, o-CF ₃ Ph and R' = tBu, iPr, Ph, p-tBuPh, p-CF ₃ Ph) 50

3.5	Reaction of PTA-Li with R_2BCl .	52
3.6	Synthesis of BR_2PTA via BR_2Cl .	61

List of Tables

<u>Table</u>		<u>Page</u>
2.1	NMR properties of Sn isotopes with nuclear spin $\frac{1}{2}$	14
2.2	Comparison of NMR data for PTA-SnMe ₃ and related compounds. Coupling constants with tin refer to ¹¹⁹ Sn.	17
3.1	³¹ P{ ¹ H} NMR shifts of PTA-BH ₃ adducts in THF	54

Chapter 1

General Introduction

1.1 Phosphines

Phosphines are common ligands in organometallic chemistry that can be easily tuned depending on the desired steric (size) and electronic (σ -donor/ π -acceptor) properties with metal complexes. Tolman proposed a method of quantifying electronic and steric effects of phosphines by measuring the CO stretching frequencies and cone angles of PR_3 phosphines in Ni complexes, $\text{Ni}(\text{PR}_3)_2(\text{CO})_2$.^{1,2} Different metal carbonyl complexes can be utilized to measure the electronic effects of phosphines but trans- $\text{Rh}(\text{L})_2(\text{CO})\text{Cl}$ complexes are often recommended because it is a more straightforward approach.³ Other methods of predicting properties of phosphines have been reported such as the Lever parameter that provides electrochemical data for coordination compounds and the bite angle which is a measurement of the P-M-P angle for chelating ligands.⁴ Due to the wide range of steric and electronic properties that have some level of predictability, phosphines are regarded as versatile ligands. The availability of reactivity data and trends for various phosphines provides a convenient way to alter steric properties without altering electronic properties and *vice versa* by modifying the substituent on the phosphine.

A growing number of catalysts involve phosphines due to their ability to stabilize low metal oxidation states. This may be attributed to their intermediate hardness and π -acceptor ability.⁴ Phosphine ligands have also been utilized to improve water solubility of transition metal complexes by simple modification of the substituents on the phosphine

such as adding a polar or ionic hydrophilic group.⁵⁻⁷ These water-soluble phosphines (WSPs) are commonly used in aqueous and biphasic catalysis because it provides an alternative to volatile organic solvents. Some examples of water-soluble phosphines (WSPs) are shown in Figure 1.1. This list includes 1,3,5-triaza-7-phosphaadamantane (PTA), which is the phosphine of interest in this thesis.

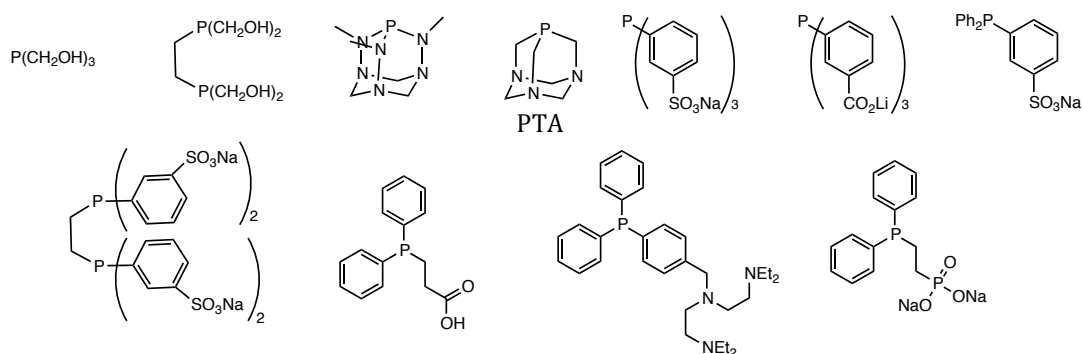
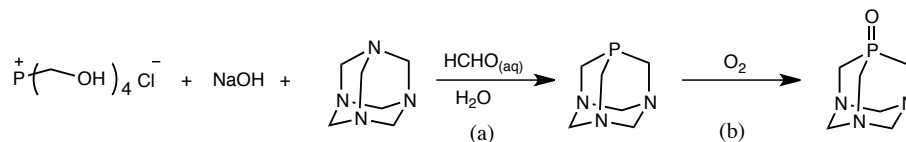


Figure 1.1. Examples of water soluble phosphines.

1.2 PTA Synthesis and Properties

In 1974, Daigle *et al.* synthesized and isolated 1,3,5-triaza-7-phosphaadamantane (PTA).⁸ This discovery was a by product of their initial goal to develop flame retardant polymers. PTA is thermally stable up to 260°C. In 1998, synthetic improvements to increase percent yield was reported in literature.⁹ In this procedure (Scheme 1.1a), tetrakis(hydroxymethyl)phosphonium chloride was treated with sodium hydroxide, formaldehyde, and hexamethylenetetramine in ice water under air. In a synthetic scale of ~80-90 grams, the yield can vary from 65-80%. PTA can be recrystallized from hot ethanol (20 mL for 1 g of product) and allowing the solution to cool to room temperature. The nitrogen atoms in PTA form hydrogen bonds with water, resulting in good water solubility ($S_{25^\circ} = 235 \text{ g/L}$, $\sim 1.5 \text{ M}$).⁹ It is also soluble in methanol, dichloromethane,

chloroform, acetonitrile, and DMSO. In the solid state, PTA is stable but it undergoes slow oxidation in solution (Scheme 1.1b).



Scheme 1.1. PTA synthesis (a) and oxidation (b)

The potential of PTA as a water-soluble ligand led to further investigation of its properties relative to other phosphines.^{10–13} Darensbourg and Daigle observed similar ^{31}P chemical shifts and force constants of $\nu(\text{CO})$ in the PMe_3 and PTA complexes of $(\text{CO})_5\text{MoL}$.¹⁴ This has led to the idea of PTA as an alternative to PMe_3 in transition metal complexes since it is much more stable and easier to handle. In recent review articles, PTA and its derivatives were highlighted for their application in transition metal chemistry, their medicinal and photoluminescent properties as well as their applications in catalytic reactions. PTA's water solubility give it tremendous potential for aqueous biphasic catalysis, allowing for green chemical processes.^{11–13}

PTA has a diverse array of derivatives due to the availability of various sites of modification on the upper rim and lower rim, giving it flexibility as a ligand (Figure 1.2). Our group is interested in upper- and lower-rim derivatives. PTA can be alkylated on the nitrogen and ring-opened by treatment with alkyl halides and acid, respectively. This modification allows formation of lower-rim derivatives such as those shown in Figure 1.3. Upper-rim modifications are accessible through the lithiation of the α -methylene carbon to generate a chiral nucleophile which can be easily reacted with various electrophiles, more of which will be discussed in the following chapter.

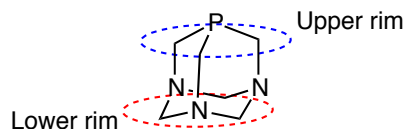


Figure 1.2. Upper and lower rim of PTA.

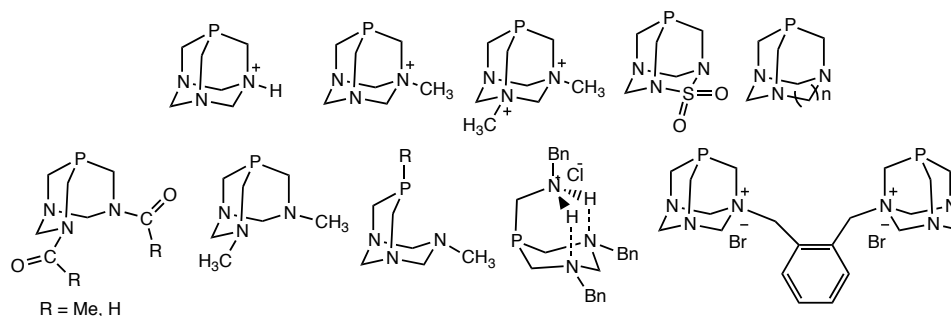
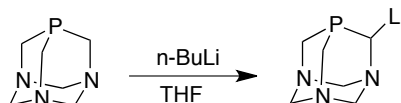


Figure 1.3. PTA lower-rim derivatives.¹¹⁻¹³

1.3 PTA-Li Synthesis and Upper-rim Derivatives



Scheme 1.2. PTA-Li synthesis.¹⁵

1,3,5-triaza-7-phosphaadamantane-6-yllithium (PTA-Li) can be prepared in high yield by treatment of a THF solution of PTA with *n*-butyllithium at room temperature (Scheme 1.2).¹⁵ Lithiation occurs at the methylene carbon adjacent to the phosphorus atom. PTA-Li is isolated as a white, highly pyrophoric powder that is readily oxidized upon exposure to air. The weak C-Li bond makes it a strong nucleophile and a strong base. This leads to deprotonation of electrophiles with acidic protons.

PTA-Li can be characterized by quenching with D₂O. Two ³¹P resonance peaks, -98.2 and -98.6, appear in the ³¹P {¹H} NMR spectrum corresponding to PTA and PTA-D, respectively. Integration of the peaks corresponds to the %yield, which is usually above 90% (Figure 1.4). Characterization by ¹³C {¹H} NMR shows the two inequivalent

PCH₂N carbons as doublets at 47.7 and 47.6 ppm (¹J_{PC}=19.6 Hz) (Figure 1.5). A quartet centered at 47.3 ppm (~1:2:2:1) arises from the coupling of the phosphorus and deuterium to the PCHD carbon (¹J_{PC} ~ ¹J_{DC} ~21 Hz). A variable triplet at 70.57 ppm arises from the three inequivalent NCH₂N carbons. The ¹H NMR of PTA-D consists of an AB quartet due to the NCH₂N protons (4.48 – 4.43 ppm, J = 12.4 Hz) and a doublet due to the PCH₂N and PCHD protons (3.91 ppm, ²J_{PH} = 8.8 Hz) (Figure 1.6). PTA-D was also characterized in CDCl₃ and details are presented in the experimental section.

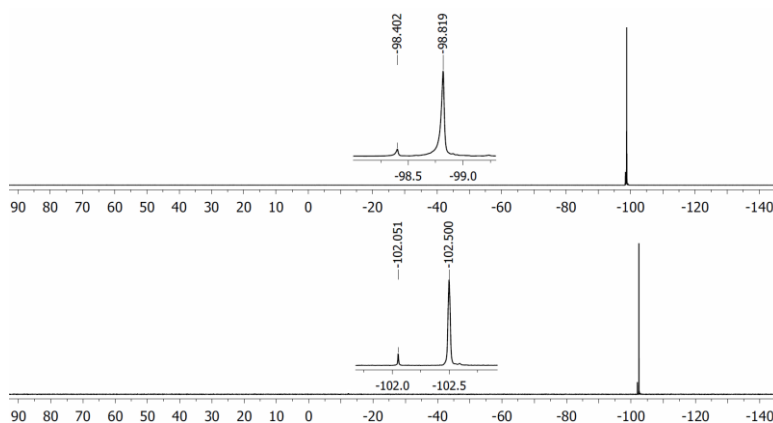


Figure 1.4. ³¹P {¹H} NMR spectra of PTA-D in D₂O (top) and CDCl₃ (bottom).

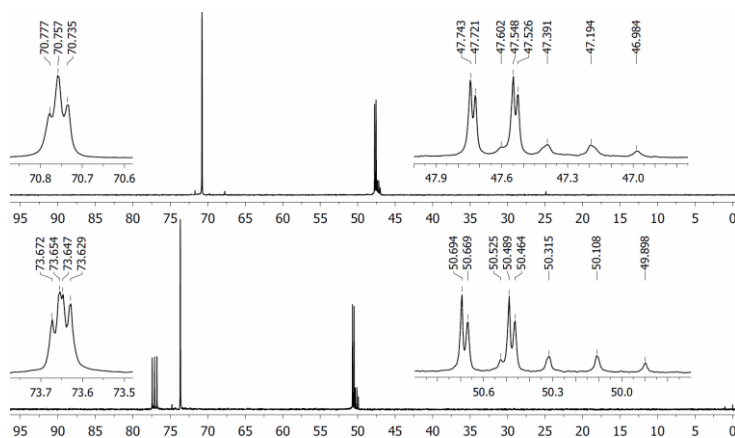


Figure 1.5. ¹³C {¹H} NMR spectra of PTA-D in D₂O (top) and CDCl₃ (bottom).

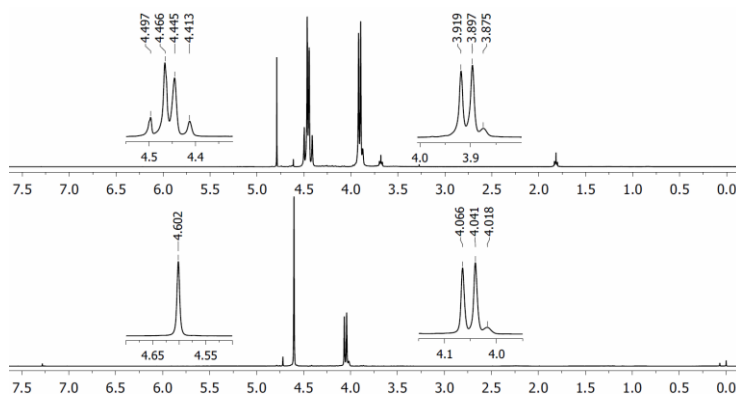


Figure 1.6. ^1H NMR spectra of PTA-D in D_2O (top) and CDCl_3 (bottom).

Insertion of electrophilic substrates into the C-Li bond of PTA-Li is considered a general, straightforward method for generating upper-rim PTA derivatives. The electronic and steric effects surrounding the phosphorus atom is tunable depending on the substituent at the α -methylene carbon. A number of upper-rim PTA modifications have been synthesized with the addition of aldehydes, ketones, imines, carbon dioxide, and chlorophosphines to PTA-Li.^{13,15,16} This method of modification allows access to a wide array of chiral phosphines with the stereogenic carbon in close proximity to the phosphorus as opposed to lower-rim derivatives that are further away from the phosphorus atom. The next chapter provides a more detailed discussion on these compounds. These potential multidentate ligands can be utilized for transition metal complexes. Of interest in this thesis is the expansion of the library of PTA derivatives to include boron, tin and silicon moieties.

1.4 Thesis Organization

This thesis contains 4 chapters starting with Chapter 1, a general introduction. Chapter 2 reports various PTA derivatives with tin and silicon moieties and attempted isolation of the compounds. Various boron-containing derivatives are presented in chapter three which then leads to chapter four, a general conclusion. An appendix containing experimental data (NMR, mass spectroscopy, etc.) is presented thereafter.

1.5 References

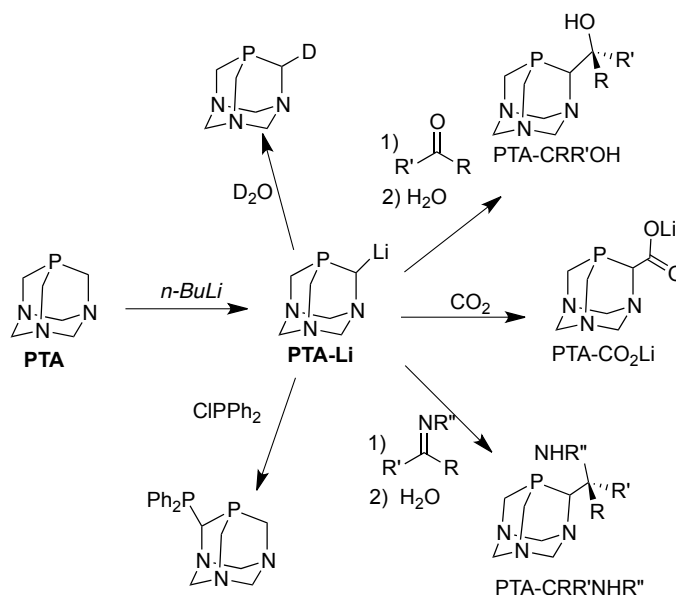
- (1) Tolman, C. A. *J. Am. Chem. Soc.* **1970**, *92*, 2953–2956.
- (2) Tolman, C. A. *Chem. Rev.* **1977**, *77*, 313–348.
- (3) Clarke, M. L.; Frew, J. J. R. In *Organometallic Chemistry: Volume 35*; 2009.
- (4) Crabtree, R. H. *The organometallic chemistry of the transition metals*; Wiley, 1994.
- (5) Pinault, N.; Bruce, D. W. *Coord. Chem. Rev.* **2003**, *241*, 1–25.
- (6) Shaughnessy, K. H. *Chem Rev* **2009**, *109*, 643–710.
- (7) Zablocka, M.; Hameau, A.; Caminade, A.-M.; Majoral, J.-P. *Adv. Synth. Catal.* **2010**, *352*, 2341–2358.
- (8) Daigle, D. J.; Pepperman, A. B., Jr.; Vail, S. L. *J. Heterocycl. Chem.* **1974**, *11*, 407–408.
- (9) Daigle, D. *J. Inorg. Synth.* **1998**, *32*, 40–45.
- (10) Darensbourg, D. J.; Decuir, T. J.; Reibenspies, J. H. *NATO ASI Ser. Ser. 3 High Technol.* **1995**, *5*, 61–80.
- (11) Phillips, A. D.; Gonsalvi, L.; Romerosa, A.; Vizza, F.; Peruzzini, M. *Coord. Chem. Rev.* **2004**, *248*, 955–993.
- (12) Bravo, J.; Bolano, S.; Gonsalvi, L.; Peruzzini, M. *Coord. Chem. Rev.* **2010**, *254*, 555–607.
- (13) Gonsalvi, L.; Guerriero, A.; Hapiot, F.; Krogstad, D. A.; Monflier, E.; Reginato, G.; Peruzzini, M. *Pure Appl. Chem.* **2013**, *85*, 385–396.
- (14) Darensbourg, M. Y.; Daigle, D. *Inorg. Chem.* **1975**, *14*, 1217–1218.
- (15) Wong, G. W.; Harkreader, J. L.; Mebi, C. A.; Frost, B. J. *Inorg. Chem.* **2006**, *45*, 6748–6755.
- (16) Wong, G. W.; Lee, W.-C.; Frost, B. J. *Inorg. Chem.* **2008**, *47*, 612–620.

Chapter 2

Stannylated and Silylated PTA derivatives

2.1 Introduction

2.1.1 Upper-rim PTA derivatives via PTA-Li



Scheme 2.1. Upper-rim PTA derivatives via PTA-Li. ¹⁻⁴

Various upper-rim PTA derivatives via 1,3,5-triaza-7-phosphaadamantane-6-ylolithium (PTA-Li) have been successfully synthesized (Scheme 2.1). PTA-Li is a convenient precursor for electrophilic addition to the α -phosphorus methylene in order to generate chiral phosphines while preserving the cage structure. The C-Li bond is weak enough to easily react with different electrophiles like ClPPh₂,⁴ CO₂,³ aryl ketones and aldehydes.^{3,5-7} In 2006, our group reported the first upper-rim PTA derivative, PTA-PPh₂, from the reaction of PTA-Li with PPh₂Cl in 1,2-dimethoxyethane. Our group was interested in water-soluble bidentate phosphines with application in aqueous catalysis; however, this new upper-rim PTA derivative was isolated in low yield, and it is not

water-soluble. In 2008, the reaction of PTA-Li with various aryl ketones and aldehydes were independently reported at about the same time by our group and Peruzzini and coworkers.^{3,5} This upper-rim modification generated a small library of β -phosphine alcohol derivatives of PTA, PTA-CRR'OH, that exhibited some evidence of bidentate coordination.^{3,5-7} In an attempt to expand the library of PTA-PR₂ derivatives, a previous research group member, Jeremiah Sears, was able to successfully isolate water-soluble diphosphines via PTA-Li and chlorophosphines (Figure 2.1).⁸

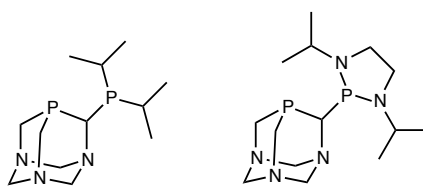


Figure 2.1. PTA diphosphine derivatives from chlorophosphines.⁸

Our group recently reported the successful synthesis of β -aminophosphines from the reaction of PTA-Li with imines -- PhN=CPh₂, PhN=CHC₆H₅, PhN=CHC₆H₄OCH₃.² These PTA derivatives of the general form PTA-CR¹R²NHPh, were coordinated to 0.5 equiv. [(η^6 -C₆H₅CH₃)-RuCl(μ -Cl)]₂. Analysis of the resulting ruthenium arene complexes displayed evidence of coordination to Ru in either a monodentate (κ^1 -P) or bidentate (κ^2 -P,N) manner with hemilability. These functionalized PTA derivatives proved to be active catalysts in the aqueous hydration of benzonitrile in the presence of air. So far, these upper-rim PTA derivatives are only slightly water-soluble in comparison to PTA. Therefore, it is of continued interest in our group to synthesize PTA derivatives with improved water solubility that can coordinate to metals in a bidentate manner.

We initially envisioned the synthesis of bis-PTA compounds by reacting PTA-Li with either R₂SnCl₂ or R₂SiCl₂ to form R₂Sn(PTA)₂ and R₂Si(PTA)₂. These

functionalized PTAs with two chiral centers have the potential to bind to a metal via a five-atom, P-C-Sn/Si-C-P, linker. Furthermore, the presence of two PTA entities may improve water-solubility. The first bis-phosphines with two PTAs were reported by Krogstad and coworkers in 2009 by reacting bis(bromomethyl)benzene synthons with PTA⁹ (Scheme 2.3). These derivatives exhibited interesting water solubility with one particular compound, 1,10-[1,2-phenylenebis(methylene)]bis-3,5-diaza-1-azonia-7-phosphatricyclo-[3.3.1.1]decane dibromide, about eight times more soluble than PTA (Figure 2.2 – a).

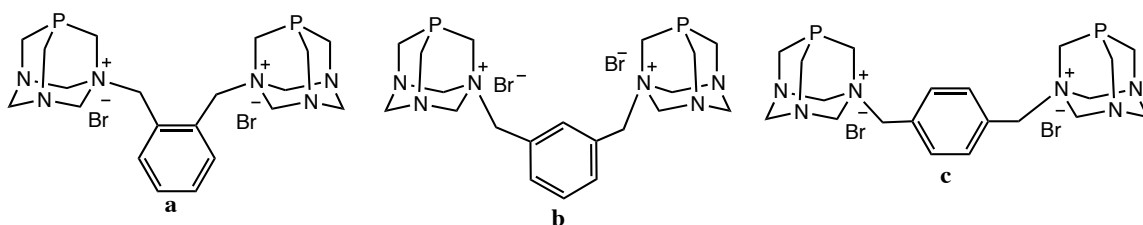
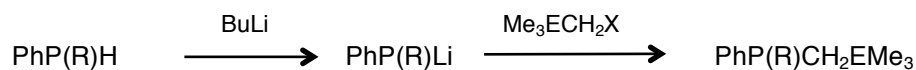


Figure 2.2. First bis-PTA derivatives.¹⁰

2.1.2 Stannylated and Silylated Phosphines

Organostannanes have been extensively studied with ω -phosphino or P(O)R₂ groups due to the dual reactivity at both the tin and phosphorus centers, in addition to their interesting structural properties.^{11–17} There has been a limited number of studies in α -stannylated phosphines compared to β - or γ -P-substituted organostannanes, which have been points of interest in the study of intermolecular interactions and the synthesis of heterocycles.^{18,19} Kowall and Heinicke were able to synthesize α -stannyl and α -silyl phosphines in two ways. One of the synthetic methods involved the generation of the lithiated primary or secondary phenyl phosphine with BuLi followed by the reaction with

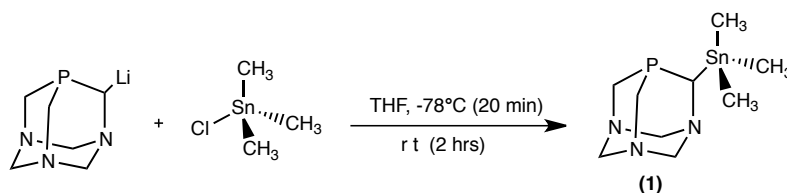
halotrimethylstannane or halotrimethylsilane (Scheme 2.2). For the synthesis of $\text{Ph}_2\text{PCH}_2\text{SiMe}_3$, a similar method by Wolfsberger utilized Ph_2PNa as the starting material but contamination with Ph_2PCH_3 was observed at 7%.²⁰ The second method presented was the lithiation of $\text{Ph}_2\text{PCH}_2\text{SiMe}_3$ with BuLi/TMEDA and subsequent reaction with either trimethyltin chloride or dimethyltin dibromide to get both silyl and stannyl groups on the phosphine. These stannylated and silylated phosphines were characterized spectroscopically and used as comparison for the PTA derivatives presented herein.



Scheme 2.2. Synthesis of $\text{PhP(R)CH}_2\text{EMe}_3$ (R =H/Ph, E=Si/Sn, X=Cl, Br).

2.2 Results and Discussion

2.2.1 PTA-Sn derivatives via PTA-Li



Scheme 2.3. Synthesis of PTA-SnMe₃ (**1**)

The reaction of PTA-Li and trimethyltin chloride resulted in a mixture of the α -stannylated phosphine (-86.5 ppm) and PTA (-101.1 ppm) that show up as two singlets in the $^{31}\text{P}\{^1\text{H}\}$ NMR spectrum of the crude THF solution (Figure 2.3). Satellites on the singlet at -86.5 ppm appear due to Sn coupling ($^2J_{\text{PSn}} = 107$ Hz). A small amount of PTA was added to the crude NMR sample, and a noticeable increase in the peak at -101.1 ppm was observed, confirming that the resonance is due to PTA. The crude reaction mixture was pulled dry, and a minimum amount of dry pentane was added. The undissolved

residual PTA and LiCl were separated via filtration. The filtrate was then pulled dry under vacuum to give PTA-SnMe₃ (**1**) as a white solid in 46% yield. The compound is readily soluble in organic solvents, (e.g. tetrahydrofuran, chloroform, dichloromethane) and water. Solubility of compound **1** in water at 25°C is 22 g/L (0.069 M) which is comparable to and even higher than previous PTA derivatives such as the PTA-CR₂OH (R=Ph, *p*-C₆H₄OMe, *H/p*-C₆H₄OMe) compounds (0.02-0.04 M).³ Compound **1** appears as a singlet at -86.8 ppm in the ³¹P{¹H} NMR spectrum, flanked with ¹¹⁹Sn/¹¹⁷Sn satellites (Figure 2.4). The ratio of the coupling constants for the Sn isotopes is comparable to the ratio of the gyromagnetic ratios (1.05), a characteristic feature in NMR spectroscopy.²¹ Therefore, the coupling due to ¹¹⁹Sn (²J_{31P¹¹⁹Sn} = 107 Hz) is expected to be larger in comparison to ¹¹⁷Sn (²J_{31P¹¹⁷Sn} = 104 Hz). The coupling constants are in the upper range in comparison to reported α-stannylated phosphines Ph₂PCH₂SnMe₃ (²J_{SnP} = 93.9 Hz, δ ³¹P -17.5 ppm in C₆D₆), H₂PCH₂SnMe₃ (²J_{SnP} = 55.9 Hz, δ ³¹P -57.6 ppm in C₆D₆), and Me₂PCH₂SnMe₃ (²J_{SnP} = 88.0 Hz, δ ³¹P -51.0 ppm in C₆D₆).^{18,22}

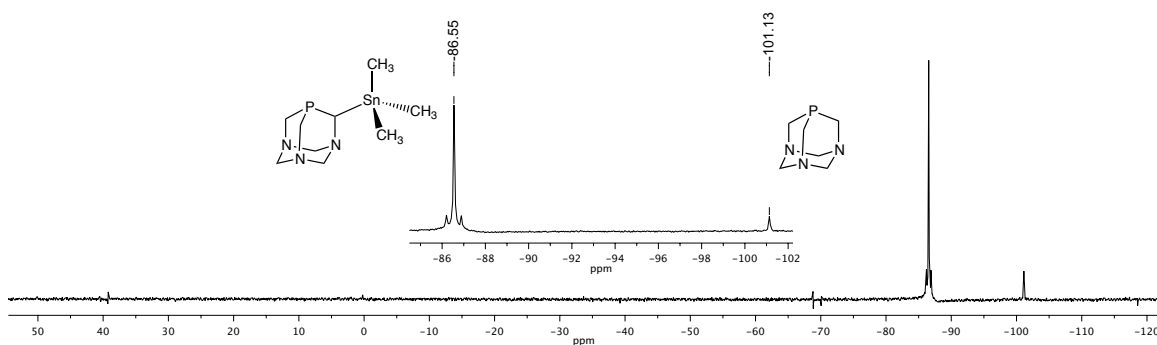


Figure 2.3. ³¹P{¹H} NMR spectrum of the crude reaction mixture of PTA-Li and SnMe₃Cl in THF.

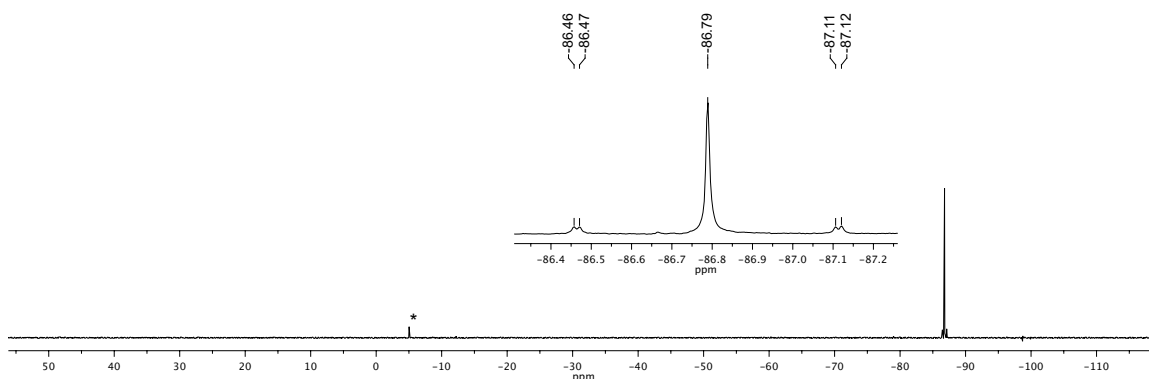
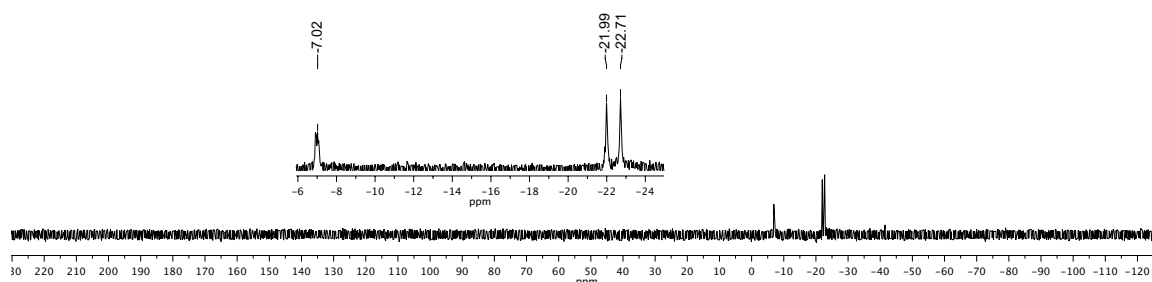
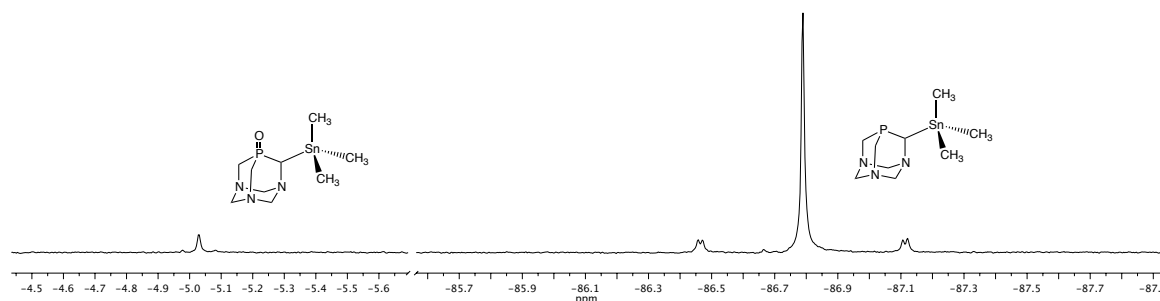


Figure 2.4. $^{31}\text{P}\{^1\text{H}\}$ NMR spectrum of PTA-SnMe₃ in CDCl₃ (* traces of oxidized product).

There are ten Sn isotopes but only three of which have spin $\frac{1}{2}$ -- ^{119}Sn , ^{117}Sn , ^{115}Sn . ^{119}Sn has the largest natural abundance and relative receptivity to ^1H and ^{13}C , and is commonly chosen for NMR characterization of tin compounds (Table 2.1). Coupling constants and the wide chemical shift range of tin spectroscopy offers structural information regarding coordination compounds. The $^{119}\text{Sn}\{^1\text{H}\}$ NMR of **1** (Figure 2.5) exhibits a prominent doublet centered at -22.35 ppm, with $^2J_{\text{SnP}} = 106$ Hz, close to $^2J_{^{31}\text{P}^{119}\text{Sn}} = 107$ Hz obtained from the ^{31}P NMR spectrum. The peak at -7.02 ppm corresponds to the oxidized product, O=PTA-SnMe₃, which correlates to the observed peak in the $^{119}\text{Sn}\{^1\text{H}\}$ NMR upon addition of H₂O₂ to **1**. Details on the experimental data for O=PTA-SnMe₃ shall be presented towards the end of this chapter. Integration of the $^{31}\text{P}\{^1\text{H}\}$ NMR acquired after 24 hrs (Figure 2.6) showed a 5% increase in the intensity of the oxide peak (Refer to Appendix, Figure A-14). The immediate formation of the oxide confirms the susceptibility of the compound to oxidation in solution.

Table 2.1. NMR properties of Sn isotopes with nuclear spin $\frac{1}{2}$.

Isotope	Natural Abundance	Gyromagnetic ratio ($\gamma/10^7 \text{ rad T}^{-1} \text{ s}^{-1}$)	Relative Receptivity	
			^1H	^{13}C
^{119}Sn	8.58	-10.021	4.51×10^{-3}	25.6
^{117}Sn	7.61	-9.578	3.49×10^{-3}	19.8
^{115}Sn	0.35	-8.792	1.24×10^{-4}	0.705

**Figure 2.5.** $^{119}\text{Sn}\{^1\text{H}\}$ NMR spectrum of PTA-SnMe₃ (**1**) in CDCl₃.**Figure 2.6.** $^{31}\text{P}\{^1\text{H}\}$ NMR spectrum of PTA-SnMe₃ and traces of O=PTA-SnMe₃ in CDCl₃.

The ^1H NMR spectrum (Figure 2.7) of **1** exhibits multiplets from 4.50 to 4.80 ppm that arise from inequivalent NCH₂N protons. The multiplets upfield from 4.00 to 4.20 ppm is assigned as PCH₂N protons, overlapping with the PCHSn proton. The methyl protons on the tin moiety appear as a singlet at 0.24 ppm, upfield with respect to unbound SnMe₃Cl (0.63 ppm). This is expected since the Cl atom is replaced by a less electronegative group. The coupling constant, $^2J_{^{119}\text{Sn-H}} = 56 \text{ Hz}$, is comparable to that of

the coupling constants for $\text{Ph}_2\text{PCH}_2\text{SnMe}_3$ ($^2J_{\text{SnH}} = 54.6$ Hz), $\text{PhHPCH}_2\text{SnMe}_3$ ($^2J_{\text{SnH}} = 54.5$ Hz), and $\text{Me}_2\text{PCH}_2\text{SnMe}_3$ ($^2J_{\text{SnH}} = 56.3$ Hz). It is slightly lower than that of free SnMe_3Cl ($^2J_{\text{SnH}} = 58$ Hz) due to a decrease in s character of the Sn-CH₃ bond. A summary of NMR data for comparison between these stannylated phosphines are shown in Table 2.2, more of which will be discussed as additional NMR parameters are presented.

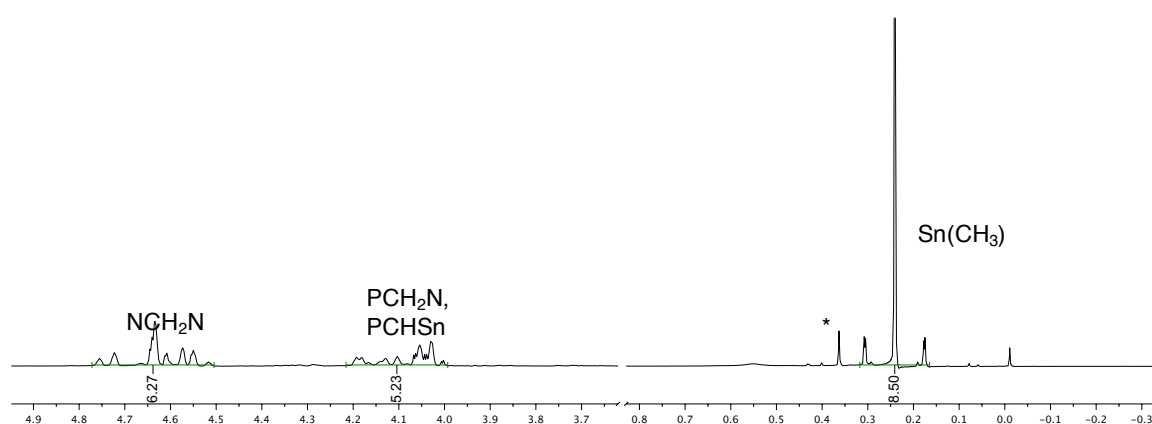


Figure 2.7. Expanded ^1H NMR spectrum of PTA- SnMe_3 in CDCl_3 (without TMS). Full spectrum is presented in the appendix. * Traces of unreacted SnMe_3Cl

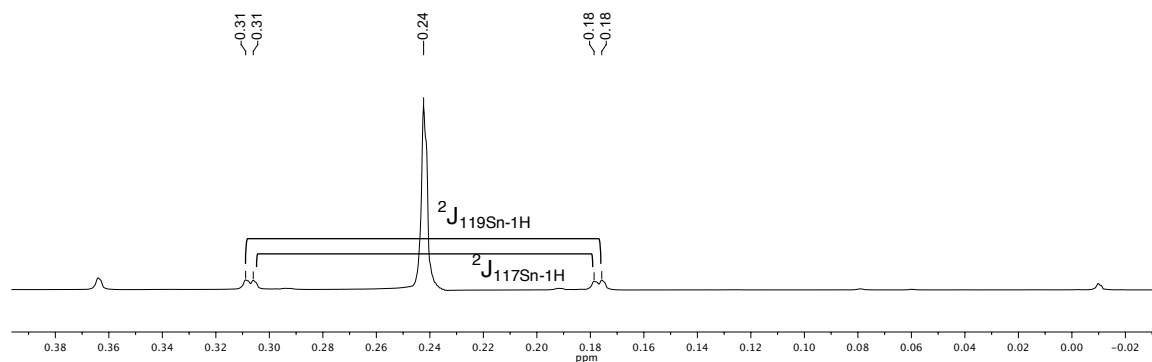


Figure 2.8. Expanded ^1H NMR spectrum of PTA- SnMe_3 in CDCl_3 showing ^{119}Sn and ^{117}Sn satellites.

The $^{13}\text{C}\{^1\text{H}\}$ NMR spectrum in Figure 2.9 shows the range at which doublets from the NCH_2N and PCH_2N carbons appear. The tin methylene carbons of **1** appear upfield (9.10 ppm) with tin satellites (Figure 2.10). The Sn-C coupling (319 Hz) is lower than that of $\text{Ph}_2\text{PCH}_2\text{SnMe}_3$ and $\text{PhHPCH}_2\text{SnMe}_3$ (both $^1J_{\text{SnC}} = 339$ Hz), $\text{Me}_2\text{PCH}_2\text{SnMe}_3$ ($^1J_{\text{SnC}} = 346$ Hz) and the free SnMe_3Cl ($^1J_{\text{SnC}} = 380$ Hz). The three-bond coupling constant, $^3J_{\text{PC}} = 3.8$ Hz, is similar to the observed $^3J_{\text{PC}} = 3.9$ Hz for $\text{Me}_2\text{PCH}_2\text{SnMe}_3$.

The PCH_2N carbons and the α -stannylated carbon, PCHSn , appear as doublets from 50 to 54 ppm (Figure 2.11). One PCH_2N carbon ($^1J_{\text{PC}} = 24$ Hz) centered at 53.3 ppm has tin satellites that are not resolved to show coupling with two isotopes. The coupling constant shall be referred to simply as $^3J_{\text{SnC}} = 33$ Hz. The other PCH_2N carbon ($^1J_{\text{PC}} = 20$ Hz) appears upfield at 50.0 ppm. The PCHSn signal centered at 52.7 ppm ($^1J_{\text{PC}} = 36$ Hz) has a larger coupling constant than the PCH_2N carbons, as expected. It is somehow larger than the coupling constants of $\text{Ph}_2\text{PCH}_2\text{SnMe}_3$ ($^1J_{\text{PC}} = 33.1$ Hz), $\text{PhHPCH}_2\text{SnMe}_3$ ($^1J_{\text{PC}} = 28.0$ Hz), and $\text{Me}_2\text{PCH}_2\text{SnMe}_3$ ($^1J_{\text{PC}} = 30.3$ Hz). Furthermore, the observed increase in $^1J_{\text{PC}}$ from the free phosphines to the α -stannylated phosphines of PMe_3 and PTA is similar (~ 16 Hz).

The three inequivalent NCH_2N carbons appear as doublets from 77 ppm to 73 ppm (Figure 2.12). One NCH_2N resonance at 76.8 ppm ($^3J_{\text{PC}} = 3.8$ Hz) lies the furthest downfield. This doublet exhibits tin satellites ($^3J_{\text{SnC}} = 40$ Hz) that somehow overlap with the solvent signal. The two other NCH_2N carbons appear as doublets at 74.5 ppm ($^3J_{\text{PC}} = 2.5$ Hz) and 73.0 ppm ($^3J_{\text{PC}} = 2.5$ Hz). All three coupling constants are relatively larger than PTA ($^3J_{\text{PC}} = 2.2$ Hz).

Table 2.2. Comparison of NMR data for PTA-SnMe₃ and related compounds. Coupling constants with tin refer to ¹¹⁹Sn.

	Compound	PTA-SnMe ₃ ^a	Ph ₂ PCH ₂ -SnMe ₃ ^b	PhHPCH ₂ -SnMe ₃ ^b	Me ₂ PCH ₂ -SnMe ₃ ^b	SnMe ₃ Cl ^a
¹ H	δ SnCH ₃ (² J _{SnH})	0.24 (54 Hz)	-0.03 ppm (54.6 Hz)	0.05 ppm (54.5 Hz)	0.12 ppm (56.3 Hz)	0.64 ppm (58 Hz ^c)
¹³ C	δ SnCH ₃ (¹ J _{SnC}) (³ J _{PC})	-9.11 ppm (319 Hz) (3.8 Hz)	-8.3 ppm (339 Hz) (4.3 Hz)	-8.6 ppm (339 Hz) (3.4 Hz)	-8.9 ppm (346 Hz) (3.9 Hz)	0.77 ppm (377 Hz ^d) (--)
	δ PCH ₂ /PCH (¹ J _{PC}) (¹ J _{SnC})	52.70 ppm ^f (36 Hz) (352 Hz)	8.4 ppm (33.1 Hz) (--) ^e	1.2 ppm (28.0 Hz) (231.4 Hz)	12.7 ppm (30.3 Hz) (292 Hz)	--
³¹ P	δ (² J _{SnP})	-86.8 ppm (107 Hz)	-17.5 ppm (93.9 Hz)	-57.6 ppm (55.9 Hz)	-51.0 ppm (--) ^e	--
¹¹⁹ Sn	δ (² J _{SnP})	-22.35 ppm (106 Hz)	3.6 ppm	5.8 ppm	-2.19 ppm (88.0 Hz)	164 ppm

^a in CDCl₃ ^b in C₆D₆ ^c Literature value = 58.1 Hz ^d Literature value = 380 Hz ^e not reported
^f PTA ³¹P δ -102.3 ppm, ¹³C δ 50.6 ppm, ¹J_{PC} = 20.2 Hz

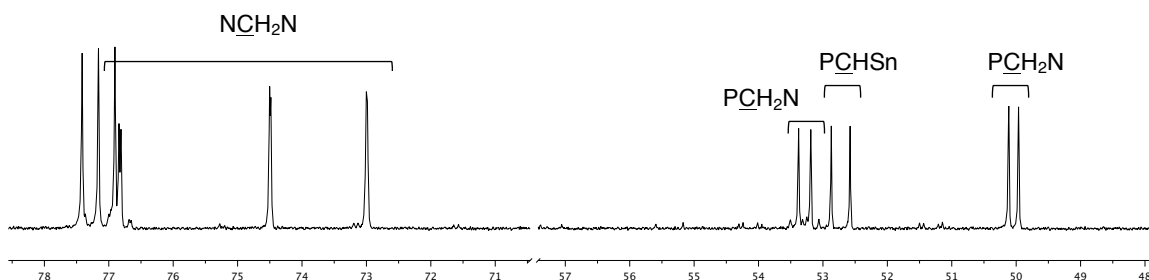


Figure 2.9. Expanded ¹³C{¹H} NMR spectrum of PTA-SnMe₃ in CDCl₃. Full spectrum is presented in the appendix.

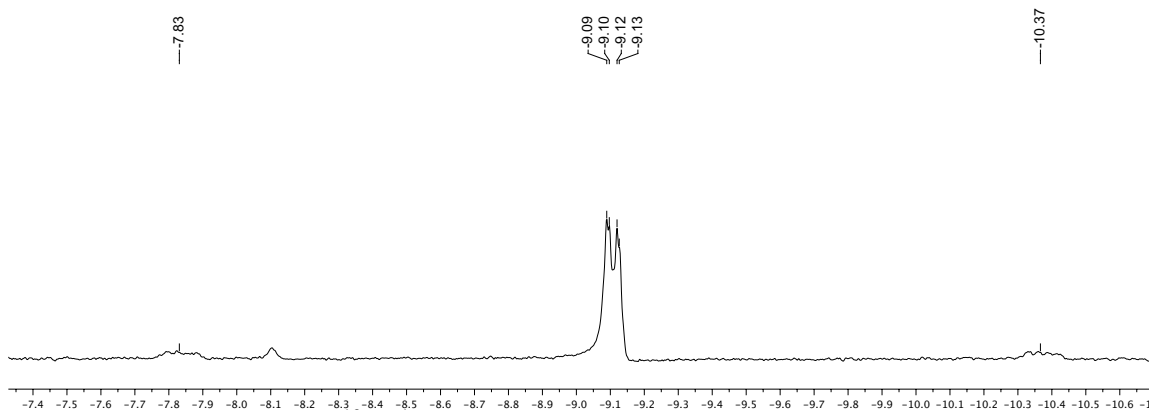


Figure 2.10. Expanded ¹³C{¹H} NMR spectrum of PTA-SnMe₃ in CDCl₃ showing SnCH₃ protons.

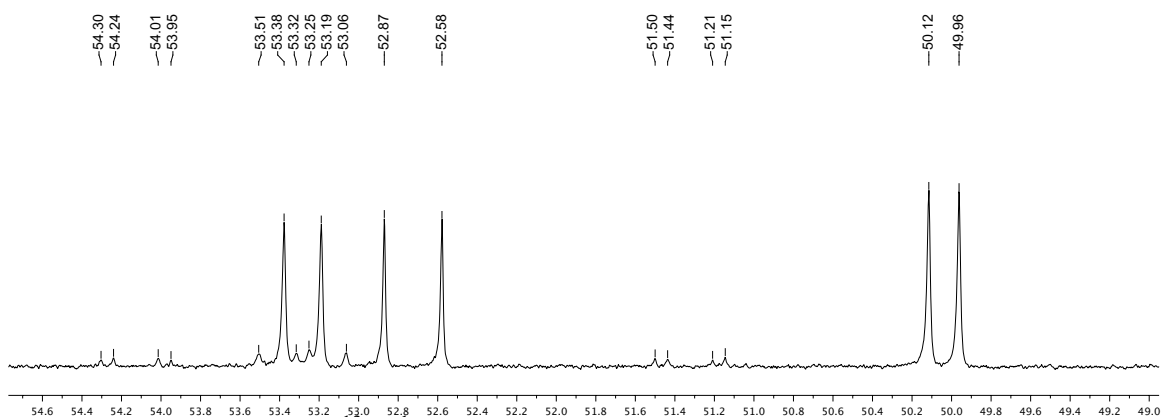


Figure 2.11. Expanded $^{13}\text{C}\{^1\text{H}\}$ NMR spectrum of PTA-SnMe₃ in CDCl₃ showing PCH₂N and PCHSn protons.

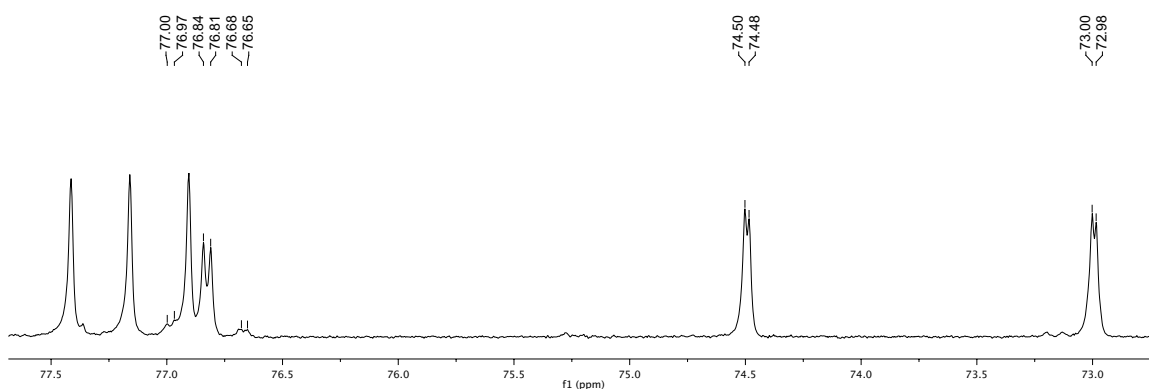
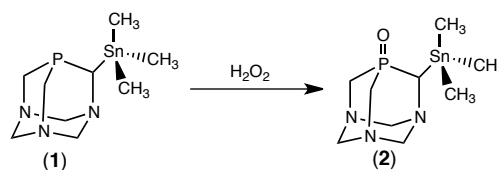


Figure 2.12. Expanded $^{13}\text{C}\{^1\text{H}\}$ NMR spectrum of PTA-SnMe₃ in CDCl₃ showing NCH₂N protons.

Oxidation with H₂O₂



Scheme 2.4. Synthesis of O=PTA-SnMe₃ (2).

The oxidation of **1** with H₂O₂ (Scheme 2.4) was proven successful with the disappearance of the $^{31}\text{P}\{^1\text{H}\}$ NMR peak at -86.8 ppm and the formation of a new singlet at -4.54 ppm (Figure 2.13). This is within the range of the reported chemical shift of

O=PTA (-2.49 ppm)²³ and other PTA oxide derivatives, O=PTA-CRR'OH (4.14 ppm to -3.20 ppm).³ The coupling value shall simply be referred to as ${}^2J_{\text{PSn}}$ since the individual ${}^{119}\text{Sn}$ and ${}^{117}\text{Sn}$ satellites are not resolved in the spectrum. The calculated coupling constant of compound **2** (${}^2J_{\text{PSn}} = 18$ Hz) is significantly smaller than compound **1** (${}^2J_{\text{PSn}} = 105$ Hz). This is expected due to a decrease in s character along the bond. Compound **2** showed a set of ${}^1\text{H}$ NMR multiplets from 3.6 to 4.4 ppm for the NCH₂N, PCH₂N, and PCHN protons (Figure 2.14). The SnCH₃ protons appeared as a singlet at 0.35 ppm with ${}^2J_{\text{SnH}} = 56.0$ Hz, upfield from traces of unreacted SnMe₃Cl at -0.54 ppm.

The ${}^{119}\text{Sn}\{{}^1\text{H}\}$ NMR of compound **2** in CDCl₃ exhibits a broad singlet at -6.64 ppm, without any traces of the starting compound **1** (Figure 2.15). The signal is at the same range as the minor peak (δ -7.02 ppm) observed in the ${}^{119}\text{Sn}\{{}^1\text{H}\}$ NMR spectrum of PTA-SnMe₃ sample in Figure 2.5. Compound **2** is expected to exhibit a doublet from phosphorus-tin coupling but appears as a broad singlet probably due to the low concentration of the sample. Nevertheless, a ${}^{119}\text{Sn}\{{}^1\text{H}\}$ NMR spectrum of a concentrated sample of PTA-SnMe₃ in CDCl₃ showed two sets of doublets that appear to be a mixture of (**1**) and (**2**) (Figure 2.16). The intense doublet centered at -8.45 ppm is assigned as PTA-SnMe₃ (**1**) (${}^2J_{\text{PSn}} = 100$ Hz), comparable to the purified product (${}^2J_{\text{PSn}} = 105$ Hz). The less intense doublet centered at -5.68 ppm is attributed to O=PTASnMe₃ (**2**) with a coupling constant of ${}^2J_{\text{PSn}} = 16$ Hz. This correlates to ${}^2J_{\text{PSn}} = 18$ Hz from the ${}^{31}\text{P}\{{}^1\text{H}\}$ NMR spectrum of the oxidized PTA-SnMe₃ with H₂O₂ discussed earlier. The differences in the chemical shifts of these three ${}^{119}\text{Sn}\{{}^1\text{H}\}$ NMR spectra may be attributed to some error in NMR referencing or the differences in the concentration of the samples. Nevertheless, the coupling constants seem to correlate.

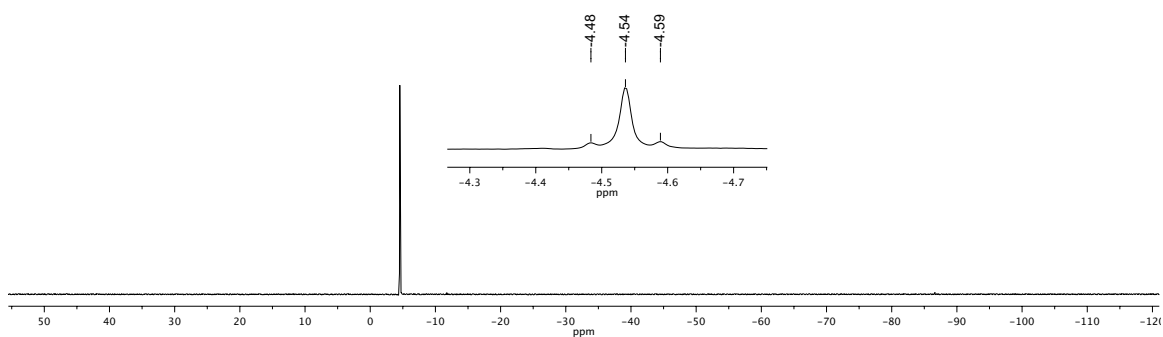


Figure 2.13. $^{31}\text{P}\{^1\text{H}\}$ NMR spectrum of $\text{O}=\text{PTA}-\text{SnMe}_3$ in CDCl_3 .

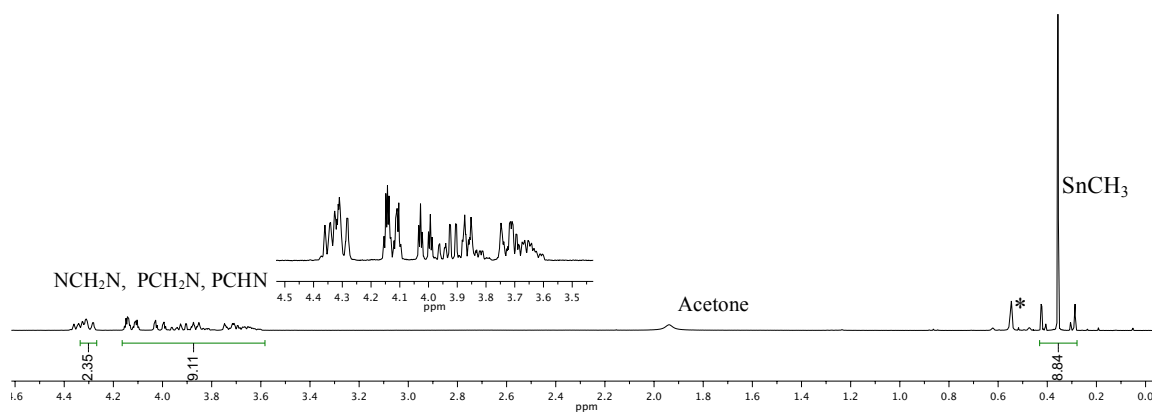


Figure 2.14. Expanded ^1H NMR spectrum of $\text{O}=\text{PTA}-\text{SnMe}_3$ in CDCl_3 . *unreacted SnMe_3Cl .

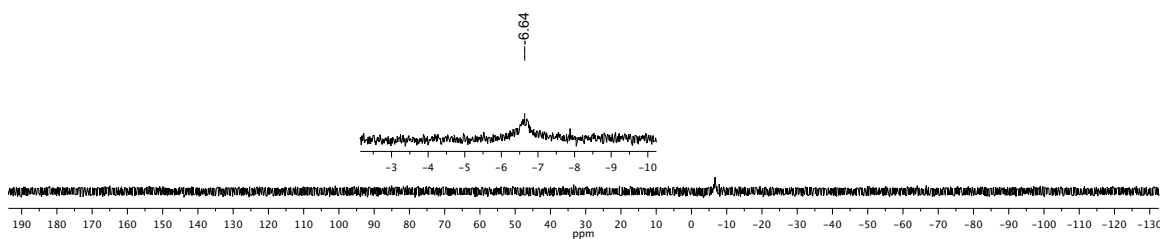


Figure 2.15. $^{119}\text{Sn}\{^1\text{H}\}$ NMR spectrum of $\text{O}=\text{PTA}-\text{SnMe}_3$ in CDCl_3 .

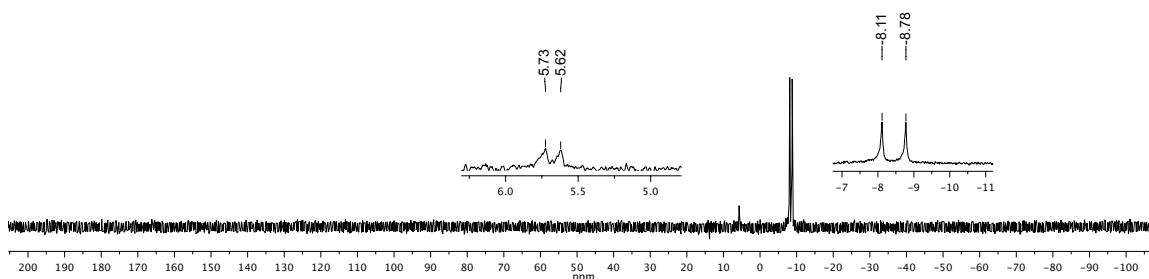


Figure 2.16. $^{119}\text{Sn}\{^1\text{H}\}$ NMR spectrum of a mixture of PTA-SnMe₃ and OPTA-SnMe₃ in CDCl₃.

The analysis of the $^{13}\text{C}\{^1\text{H}\}$ NMR spectrum of compound **2** reveals pairs of doublets assigned to NCH₂N, PCH₂N, and PCHSn carbons (Figure 2.17). The three NCH₂N carbons appear downfield as doublets centered at 75.2 ppm, 73.1 ppm, and 71.6 ppm ($J_{\text{PC}} = 9$ Hz). The two PCH₂N carbons are doublets centered at 58.4 ppm ($J_{\text{PC}} = 48$ Hz) and 55.3 ppm ($J_{\text{PC}} = 54$ Hz). The doublet centered at 57.1 ppm ($J_{\text{PC}} = 40$ Hz) is assigned to the PCHSn carbon. Visible ^{119}Sn and ^{117}Sn satellites overlap with the PCH₂N resonance. Nevertheless, the coupling J_{SnC} can be estimated at 260 Hz. This is significantly lower than PTA-SnMe₃ (**1**) ($J_{\text{SnC}} = 360$ Hz). Meanwhile, the SnCH₃ carbons appear as a singlet at -8.11 ppm ($J_{\text{SnCH}_3} = 330$ Hz) next to a minor peak at -0.78 ppm which correspond to SnMe₃Cl (Appendix, Figure A-12). The presence of peaks of lower intensities at 72 ppm and 56 ppm may be due to O=PTA. The ESI mass spectrum of compound **1** in water has m/z peaks at 322.47 and 338.5 that are comparable to the theoretical isotopic distribution pattern for MH⁺ species of compounds **1** and **2** (Figure 2.18).

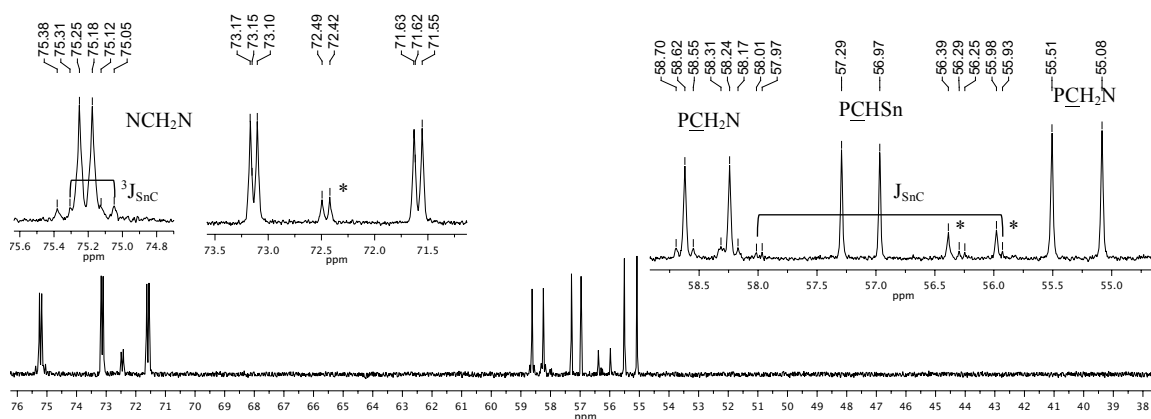


Figure 2.17. $^{13}\text{C}\{^1\text{H}\}$ NMR spectrum of $\text{O}=\text{PTA}-\text{SnMe}_3$ in CDCl_3 . *oxide

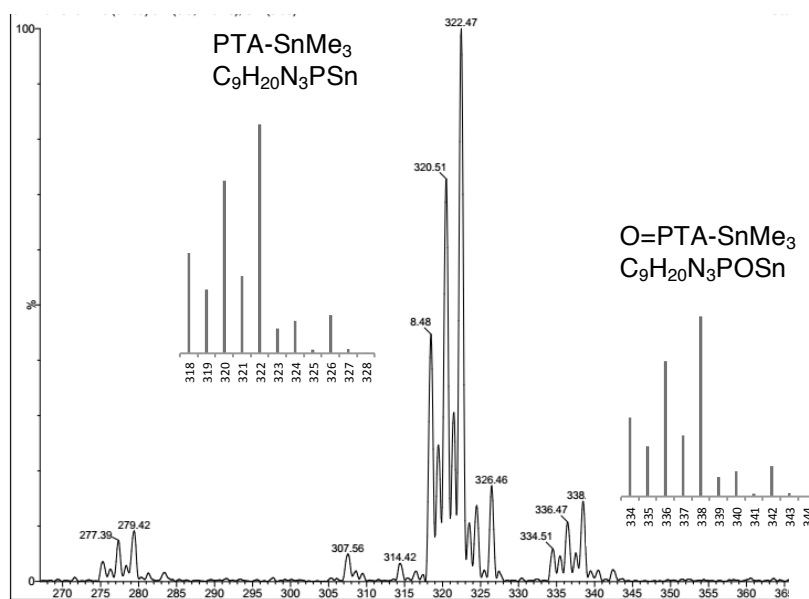
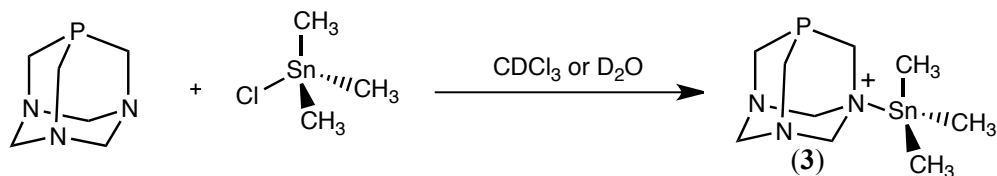


Figure 2.18. Electrospray mass spectrum (positive mode) of $\text{PTA}-\text{SnMe}_3$ and $\text{O}=\text{PTA}-\text{SnMe}_3$. Inset shows the simulated isotopic distribution pattern for $[\text{MH}]^+$.

2.2.1.1 Reaction of PTA with SnMe_3Cl



Scheme 2.5. Reaction of PTA with SnMe_3Cl .

The reactivity of PTA towards some of the tin electrophiles discussed earlier was also studied in order to aid in characterizing the potential side-products of the reactions in PTALi. It is not surprising that the N-Sn coordination complexes of PTA may form (Scheme 2.5). The Frost group reported the first known coordination complex of PTA with only nitrogen involved in bonding -- PTA-BH₃.²⁴

In CDCl₃, treatment of 1.1 equiv. of SnMe₃Cl to PTA did not appear to react as evidenced by the identical ¹H NMR spectrum as compared to the starting materials. However, the ³¹P{¹H} NMR spectrum has shifted from -102.3 ppm to -97.1 ppm (Figure 2.19). With regards to the ¹H NMR, the N-bound Sn-PTA derivative would be expected to generate a set of multiplets since the loss of symmetry in PTA would result in inequivalent protons. Instead, the NCH₂N and the PCH₂N protons remain as a singlet (4.55 ppm) and a doublet (centered at 4.00 ppm, ²J_{PH} = 12 Hz), respectively (Figure 2.20). The possibility of generating an acidic solution from the reaction of SnMe₃Cl and trace amounts of water can cause protonation of PTA. In the ³¹P{¹H} NMR spectrum, it would appear at around -90 ppm. The SnCH₃ protons remain as a singlet at 0.53 ppm, with the same coupling constant as unbound SnMe₃Cl. The singlet at -10 ppm is not suggestive of O=PTA, usually near -2 ppm. It is closer to the reported ³¹P{¹H} NMR resonance for O=PTA(N-BH₃) at -9.8 ppm.²⁴ If so, the absence of a PTA(N-SnMe₃) peak may be due to its susceptible oxidation to O=PTA(N-SnMe₃). The ¹¹⁹Sn{¹H} NMR resonance at 170.2 ppm is comparable to the starting material SnMe₃Cl at 164 ppm (Figure 2.21). The addition of up to 4 equiv. SnMe₃Cl gave similar NMR results. Since this reaction was carried out at 25°C, for future attempts, increasing the reaction

temperature and monitoring the progression of the reaction through $^{31}\text{P}\{^1\text{H}\}$ NMR would be a useful approach in understanding the chemistry behind this particular reaction.

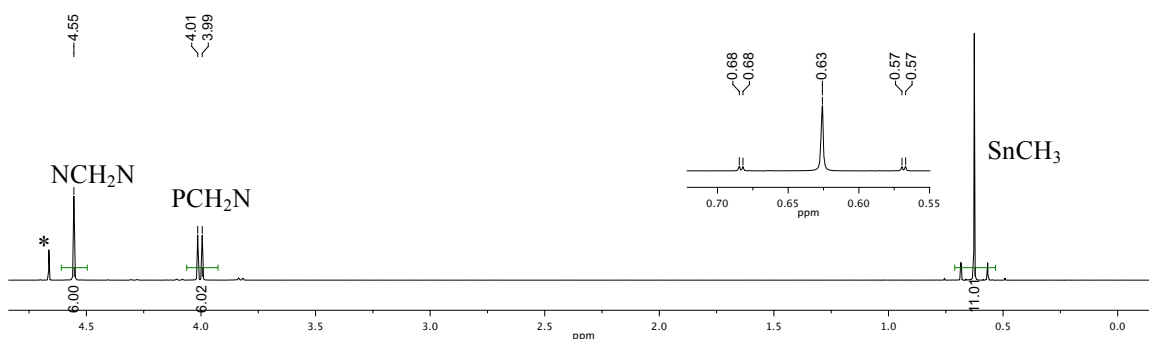


Figure 2.19. ^1H NMR spectrum of PTA with 1.1 equiv. SnMe_3Cl in CDCl_3 . Inset shows the expanded resonance for SnCH_3 protons. *trace amount of HMTA (hexamethylenetetramine) from PTA synthesis

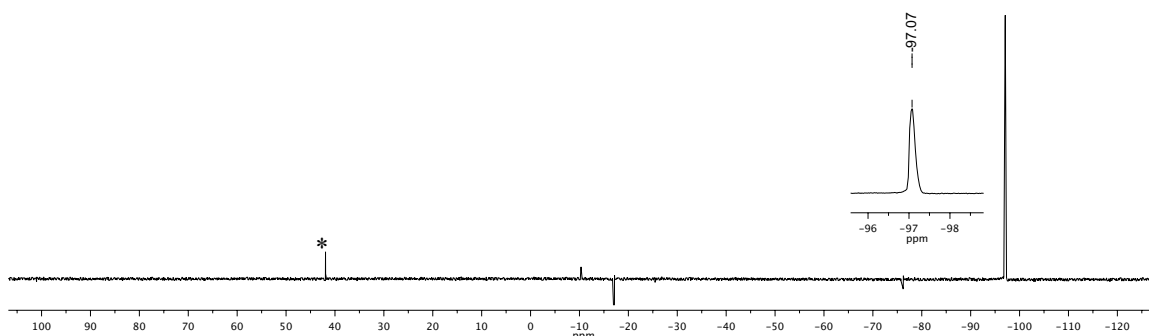


Figure 2.20. $^{31}\text{P}\{^1\text{H}\}$ NMR spectrum of PTA with 1.1 equiv. SnMe_3Cl in CDCl_3 . *Unidentified

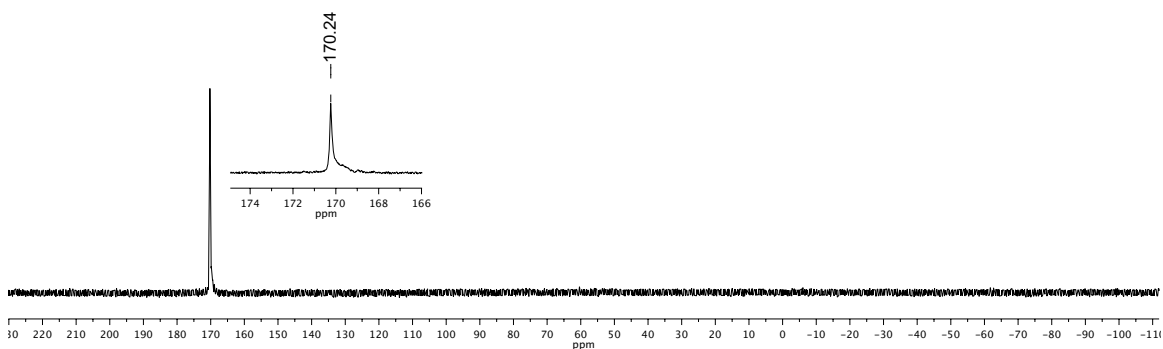


Figure 2.21. $^{119}\text{Sn}\{^1\text{H}\}$ NMR spectrum of PTA with 1.1 equiv. SnMe_3Cl in CDCl_3 .

In D₂O, addition of 1.1 equiv. SnMe₃Cl to PTA exhibited a singlet in the ³¹P{¹H} NMR spectrum at -90.35 ppm (Figure 2.22). This is also a downfield shift from free PTA (-98.30 ppm), similar to the observed chemical shift from CDCl₃. This peak at -90.35 ppm could be the protonated form of PTA since SnMe₃Cl can readily decompose in water to form an acidic solution. The minor peak at -2.09 ppm is comparable to O=PTA (-2.49 ppm). In the ¹H NMR (Figure 2.23), similar peaks to PTA appear and the coupling constants are comparable to unreacted PTA, ²J_{PH} = 8 Hz and ²J_{H_AH_B} = 12.4 Hz. Furthermore, the methyl groups on tin have ²J_{SnH} = 68 Hz, similar to unreacted SnMe₃Cl (²J_{SnH} = 67.5 Hz). To test whether the peak at -90.35 ppm is a newly formed compound, the NMR sample was spiked with PTA. No new peaks appeared and traces of O=PTA remained at around -2 ppm but the dominant singlet shifted slightly upfield to -91.93 ppm (Figure 2.24). The ¹H NMR (Figure 2.25) has the same characteristic peaks as that of PTA. This may suggest some weak Sn-P interaction present or the protonated PTA.

The ¹¹⁹Sn{¹H} NMR spectrum of the same sample exhibits a singlet at 56.33 ppm (Figure 2.26), downfield with respect to unreacted SnMe₃Cl (164 ppm) and SnMe₃OH (122.24 ppm). This peak may be attributed to the same unidentified species (-59 ppm) in a crude sample of PTALi and SnMe₃Cl in D₂O show in Figure 2.27. It is relatively broad in comparison with that of compound **1** and **2**. ¹H NMR of SnMe₃Cl taken after a month in D₂O did not show signs of decomposition based on the absence of SnMe₃OH peaks (Appendix) and the SnCH₃ peaks exhibited the same ²J_{Sn-H} as SnMe₃Cl. Particular Sn compounds with Sn-N bond like Me₃Sn-NMe₃ and Me₃Sn-NEt₂ have δ¹¹⁹Sn at 75.5 ppm and 60 ppm, respectively. The ¹¹⁹Sn{¹H} NMR peak at 56.33 ppm may imply that there is some form of interaction between tin and the nitrogen on PTA. There is some

confusion as to why the δ ^1H NMR of the sample resembles PTA and the starting material. Repeated experiments in different solvent systems at a longer period of time, higher temperature, and at a larger scale may provide insight on this inconsistency.

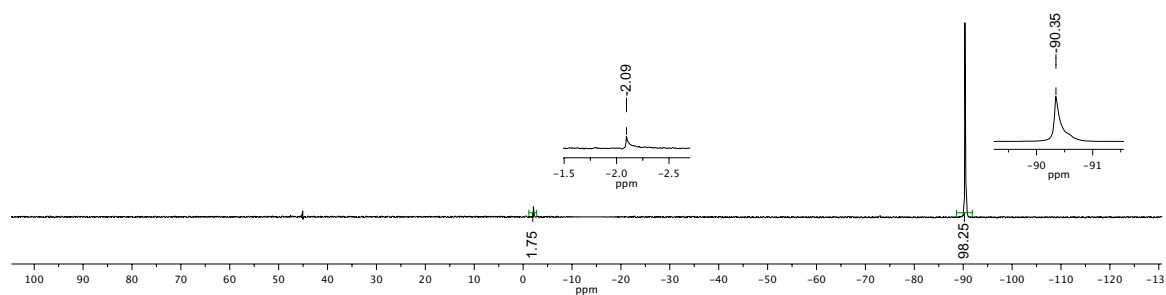


Figure 2.22. $^{31}\text{P}\{^1\text{H}\}$ NMR spectrum of PTA with 1.1 equiv. SnMe_3Cl in D_2O .

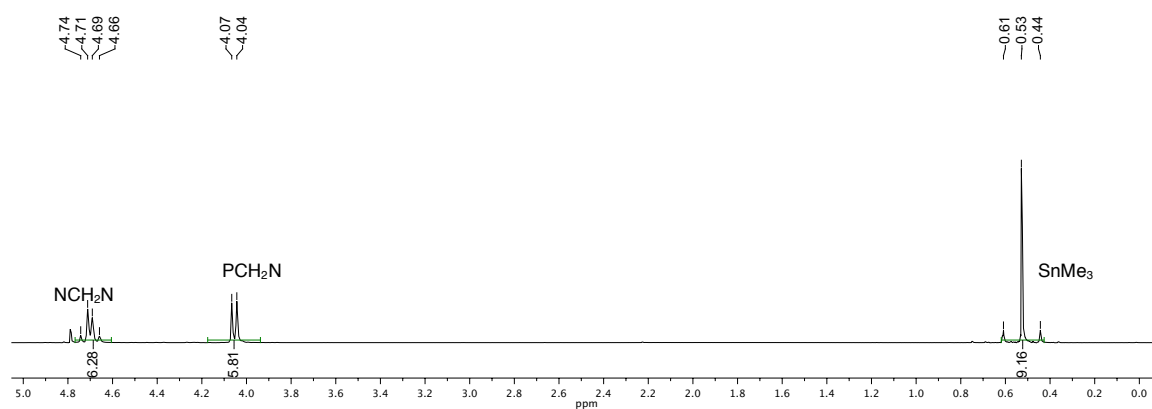


Figure 2.23. Expanded ^1H NMR spectrum of PTA with 1.1 equiv. SnMe_3Cl in D_2O .

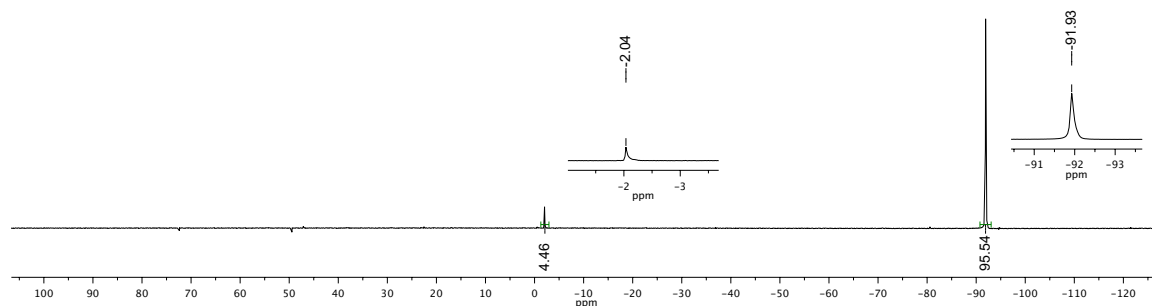


Figure 2.24. $^{31}\text{P}\{^1\text{H}\}$ NMR spectrum of previous sample of PTA with SnMe_3Cl in D_2O after addition of PTA.

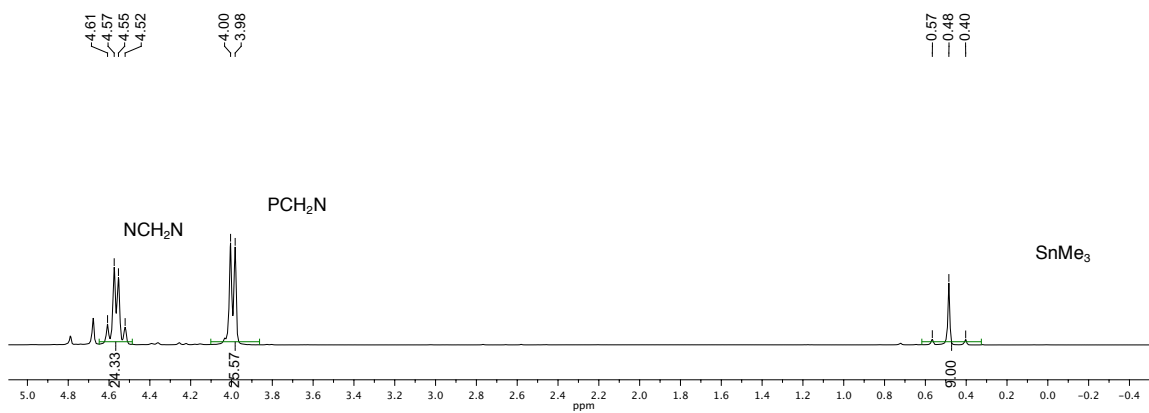


Figure 2.25. Expanded ^1H NMR spectrum of previous sample of PTA with SnMe_3Cl in D_2O after addition of PTA.

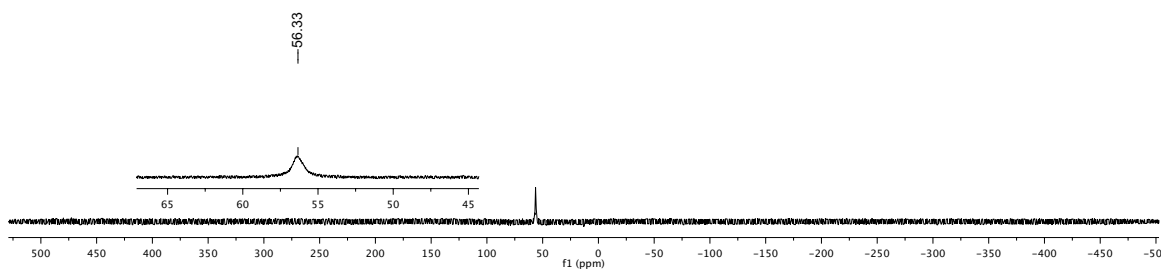


Figure 2.26. $^{119}\text{Sn}\{^1\text{H}\}$ NMR spectrum of PTA with SnMe_3Cl in D_2O .

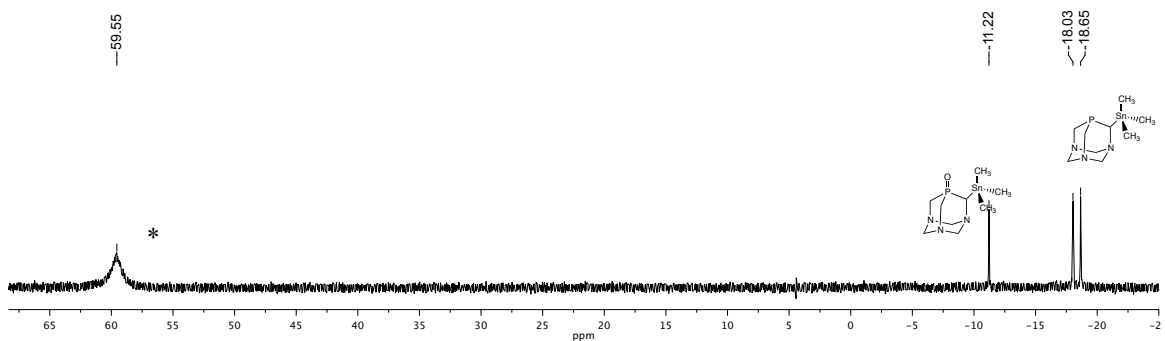
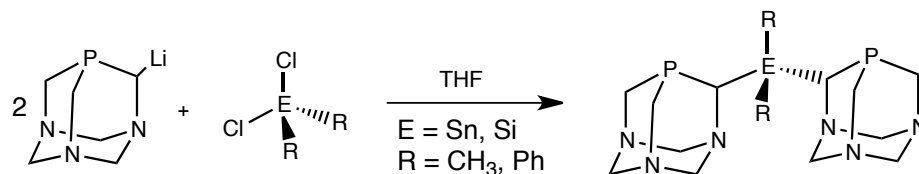


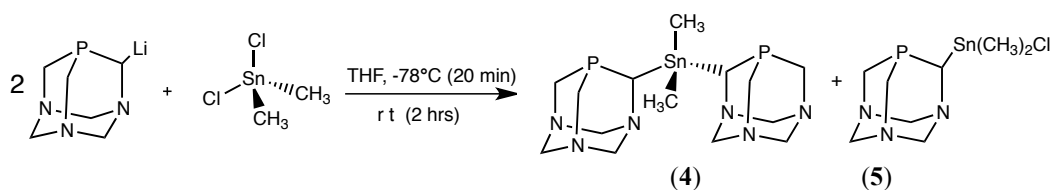
Figure 2.27. Expanded $^{119}\text{Sn}\{^1\text{H}\}$ NMR spectrum of a crude mixture of PTALi and SnMe_3Cl in D_2O . *Unidentified

Attempts on the synthesis of tin and silicon bis-PTA derivatives



Scheme 2.6. General synthesis of stannylated and silylated bis-PTA via PTA-Li.

Reaction of PTA-Li with SnMe_2Cl_2



Scheme 2.7. Depicted reaction products of SnMe_2Cl_2 and PTA-Li.

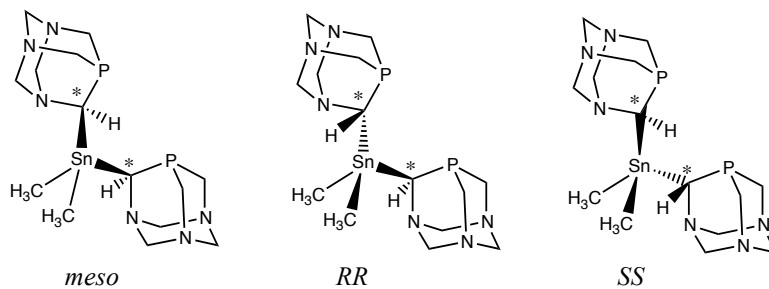


Figure 2.28 . Stereochemistry of $(\text{PTA})_2\text{SnMe}_2$ products.

Pursuit in synthesizing $(\text{PTA})_2\text{-SnMe}_2$ involved the addition of 0.5 equiv. SnMe_2Cl_2 to a THF solution of PTA-Li. What was initially a turbid, white suspension of PTA-Li turns into a clear solution after about 10 minutes of adding SnMe_2Cl_2 . After about 30 minutes of stirring, the clear solution started to appear cloudy white, attributed to the formation of LiCl . The $^{31}\text{P}\{^1\text{H}\}$ NMR spectrum of the crude milky white mixture resulted in closely set singlets from -84 to -87 ppm and starting material PTA at -101.5 ppm (Figure 2.29). Integration of peaks reveal 12% PTA and 87% products. A minor

unidentified peak at -45 ppm was present but only at 0.1%. The more abundant peaks with tin satellites may signify the formation of the mono- and di-substituted SnMe_2Cl_2 .

In an attempt to separate the Sn-bound products from residual PTA and LiCl, the crude mixture was pulled dry and dissolved in a minimum amount of dry pentane. The solution was filtered over celite and the collected filtrate was pulled dry. Dissolution in CDCl_3 resulted in a $^{31}\text{P}\{^1\text{H}\}$ NMR with peaks at 7.3 ppm, -4.9 ppm, -5.1 ppm, -5.3 ppm, -12.0 ppm, -63.5 ppm, -86.6 ppm, -86.8 ppm, -102 ppm (Figure 2.30, 2.31). The signals of low intensity at -5 ppm could be the oxidized material from an open-ring side-product and the disubstituted products, which is around the range at which $\text{O}=\text{PTASnMe}_3$ and most PTA oxides form. The minor peaks at 7.3 ppm and -12.0 ppm have not been identified. The close set of singlets with tin satellites (-86.6 ppm, -86.8 ppm) may represent the meso and RR/SS products. The individual ^{119}Sn and ^{117}Sn satellites are not evident so the coupling constants shall be referred to simply as $J_{\text{PSn}}/J_{\text{SnP}}$. Both singlets have $^2J_{\text{PSn}} = 108$ Hz, slightly larger than PTA- SnMe_3 ($^2J_{\text{PSn}} = 105$ Hz). Integration of the main peaks show a 1:2 ratio. These compounds appear as two sets of triplets in the $^{119}\text{Sn}\{^1\text{H}\}$ NMR spectrum from -40 ppm to -42 ppm (Figure 2.32). Both triplets have $^2J_{\text{SnP}} = 112$ Hz, comparable to the coupling value from the $^{31}\text{P}\{^1\text{H}\}$ NMR spectrum. The peak at -63.5 ppm ($^2J_{\text{PSn}} = 50.2$ Hz) is likely an open-ring side product that could form from an acidic solution as HCl can be generated upon decomposition of the starting material, SnMe_2Cl_2 , in the presence of water. This corresponds to a doublet observed in the $^{119}\text{Sn}\{^1\text{H}\}$ NMR, centered at -25.6 ppm, with $^2J_{\text{SnP}} = 50.7$ Hz (Figure 2.19). A monosubstituted product can be ruled out since the mass spectrum did not exhibit a peak for this possible side product. Furthermore, the $^{31}\text{P}\{^1\text{H}\}$ NMR shift would be expected to

be closer to -86 ppm where the meso and RR/SS peaks appear, with a greater tin-phosphorus coupling.

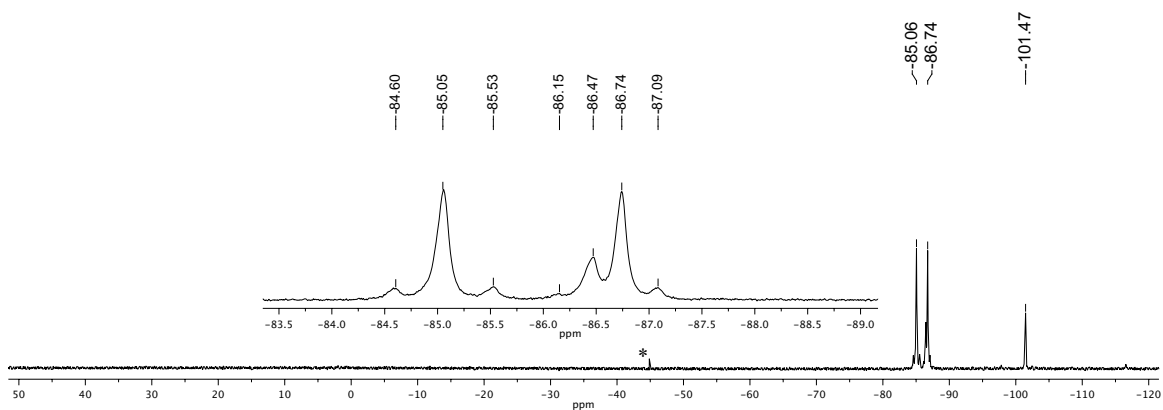


Figure 2.29. $^{31}\text{P}\{^1\text{H}\}$ NMR spectrum of the crude sample of PTA-Li and SnMe_2Cl_2 in THF. *Unidentified

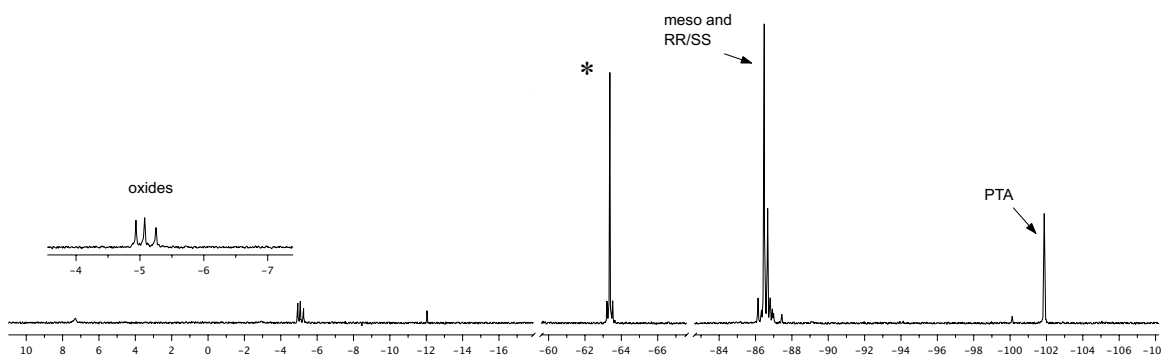


Figure 2.30. $^{31}\text{P}\{^1\text{H}\}$ NMR spectrum of the pentane-soluble product from the reaction of SnMe_2Cl_2 with PTA-Li in CDCl_3 . * Possibly an open-cage PTA derivative

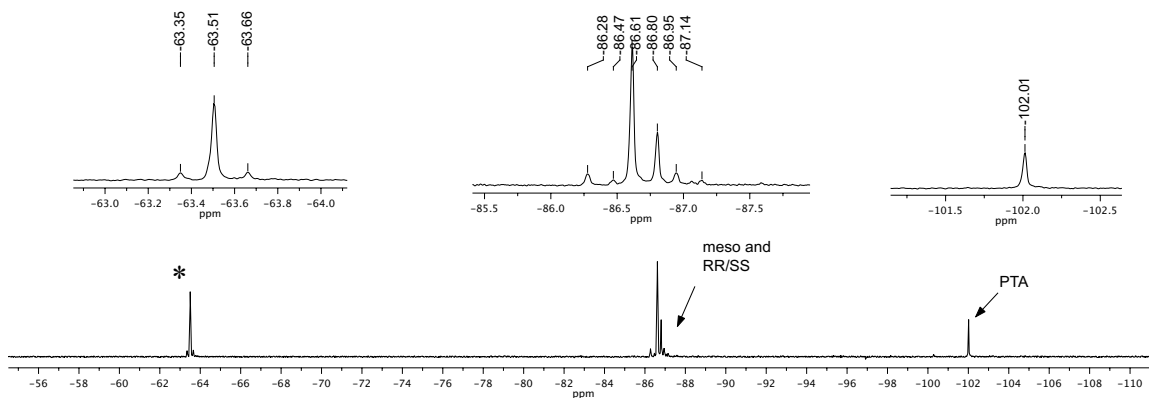


Figure 2.31. Expanded $^{31}\text{P}\{^1\text{H}\}$ NMR spectrum of the pentane-soluble product from the reaction of SnMe_2Cl_2 with PTA-Li in CDCl_3 . * Possibly an open-cage PTA derivative

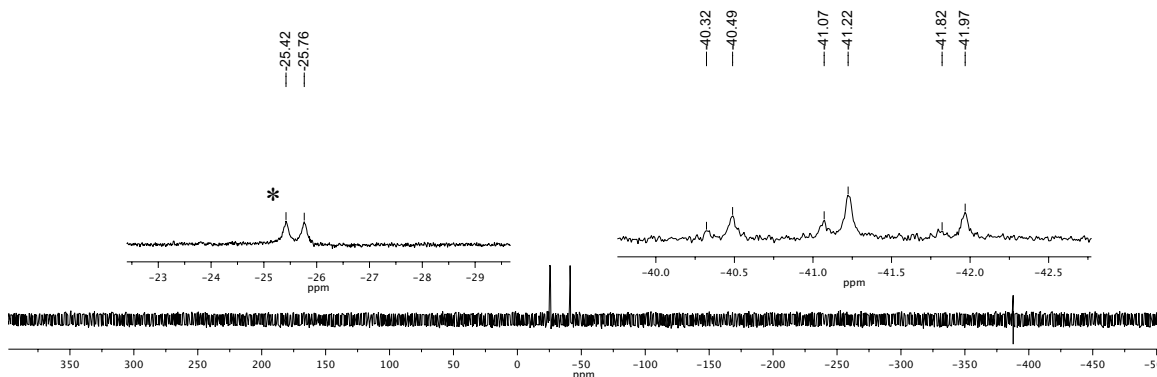


Figure 2.32. $^{119}\text{Sn}\{^1\text{H}\}$ NMR spectrum of the pentane-soluble product from the reaction of SnMe_2Cl_2 with PTA-Li in CDCl_3 . * Possibly an open-cage PTA derivative

Careful integration of the relative peaks on the $^{31}\text{P}\{^1\text{H}\}$ NMR spectra of a crude sample of PTA-Li and SnMe_2Cl_2 in CDCl_3 showed a slight increase in oxidized product over 1 day (Figure 2.33). The significant decrease in %PTA could mean that it is more prone to oxidation than the rest of the compounds because of the lack of bulky groups around the phosphorus atom. The ESI+ data shows a peak at 466 m/z, similar to the simulated distribution pattern (Figure 2.34). Further experimental data (e.g. Sn NMR, IR, MS) are needed to further examine the chemistry and nature of the crude product and to eventually isolate each compound. The relatively large PTA peak may be a result of the presence of moisture in the starting materials (SnMe_2Cl_2) and solvents in addition to the PTA present in the starting PTA-Li. The use of dry chemicals and the addition of more PTA-Li may improve the percent yield. To improve the separation of residual PTA, other organic solvents like benzene may be used.

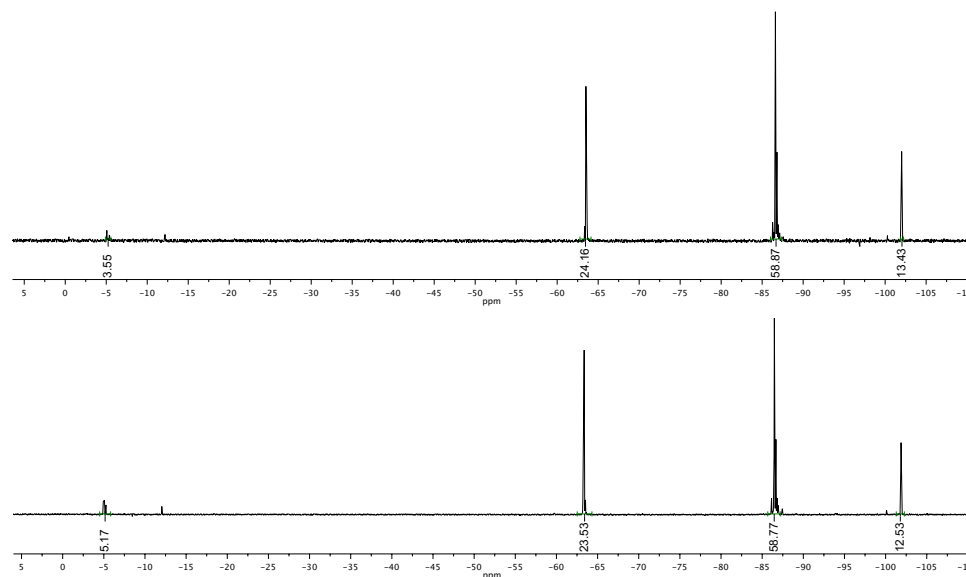


Figure 2.33. Expanded $^{31}\text{P}\{^1\text{H}\}$ NMR spectrum of the decomposition of the pentane-soluble product from the reaction of SnMe_2Cl_2 with PTA-Li in CDCl_3 . (top: starting sample. bottom: after 1 day)

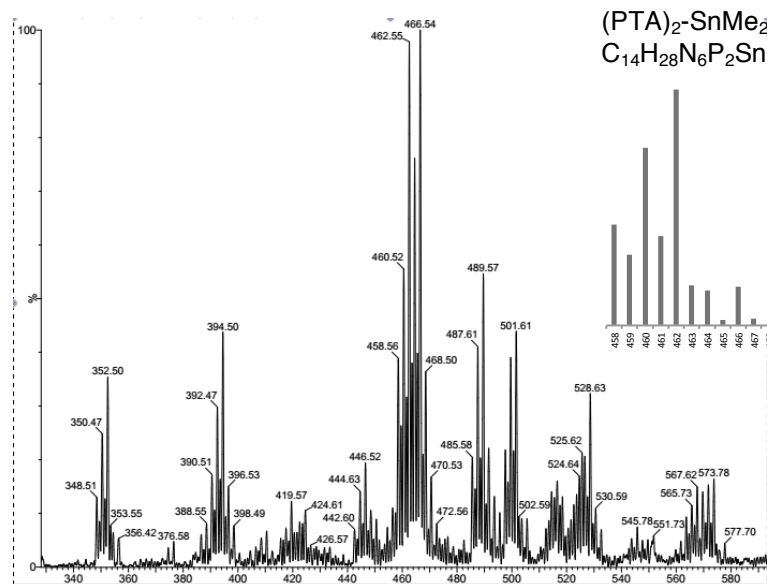
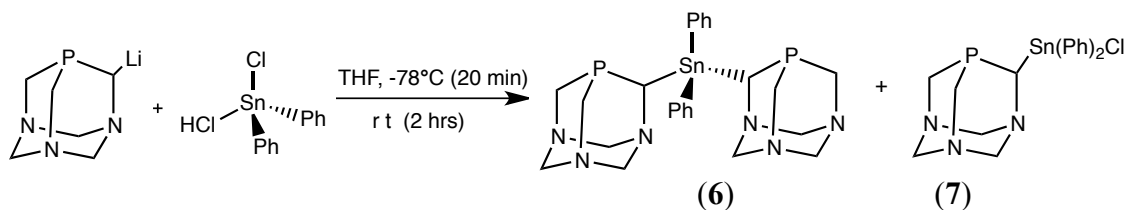


Figure 2.34. Expanded electrospray mass spectrum (positive mode) of a sample of SnMe_2Cl_2 with PTA-Li. Inset shows the simulated isotopic distribution pattern (M^+) for $(\text{PTA})_2\text{SnMe}_2$.

Reaction of PTA-Li with SnPh_2Cl_2



Scheme 2.8. Reaction of PTA-Li with SnPh_2Cl_2 depicting the expected products.

As further proof of concept for the reactivity of PTA-Li with other tin moieties, we have also attempted to react it with a more bulky group, SnPh_2Cl_2 . The crude product mixture in THF showed a set of singlets with tin satellites between -82 to -87 ppm on the $^{31}\text{P}\{^1\text{H}\}$ NMR spectrum (Figure 2.35). The resonance at -101.5 ppm is assigned to PTA. A singlet of low intensity at -85 ppm could be the monosubstituted product, PTA- SnPh_2Cl . The intense singlets at -83 ppm ($^2J_{\text{PSn}} = 153.6$ Hz) and -86 ppm ($^2J_{\text{PSn}} = 97.2$ Hz) could be the diastereomers of $\text{PTA}_2\text{-SnPh}_2$. These peaks are slightly downfield of the observed $^{31}\text{P}\{^1\text{H}\}$ NMR peaks from the reaction of SnMe_2Cl_2 with PTA-Li. The relatively large coupling constant can be attributed to the same steric dependence reported by Gudat and co-workers.²⁵ In their study of sterically crowded stannylphosphines and stannylamines, they observed an increase in coupling constant as the sterics on the tin moiety is increased.

An attempt to isolate the product by washing with hexanes showed remaining PTA residue (Figure 2.36). Repeated washings led to decomposition, probably due to moisture sensitivity. In addition to the initial PTA (usually 10% at the most) in the starting PTA-Li, the large amount of PTA in the product mixture may be due to PTA-Li reacting with traces of water in the solvent and the starting materials. Additional experimental data (e.g. Sn NMR, IR, MS, solubility) are needed to further examine the

chemistry and nature of the crude product and to eventually isolate the pure compound. Future attempts can be improved by assuring the use of dry solvent and adding more PTA-Li.

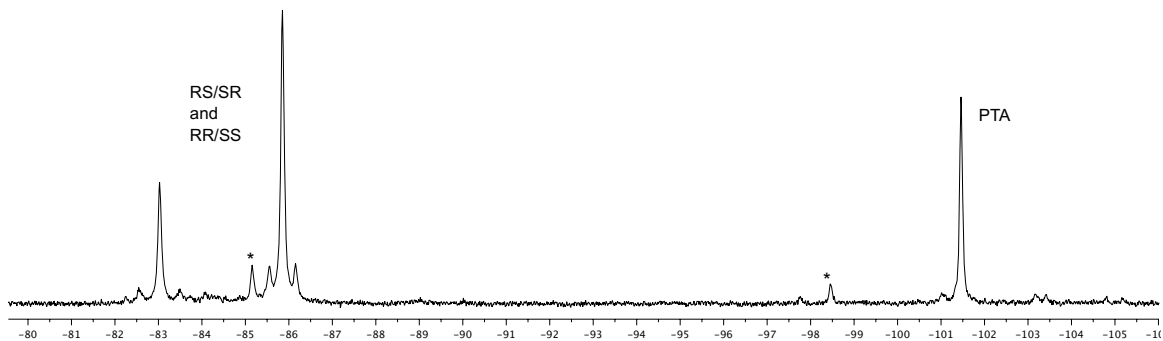


Figure 2.35. $^{31}\text{P}\{^1\text{H}\}$ NMR spectrum of the PTA-Li and SnPh_2Cl_2 reaction mixture in THF. *Unidentified. The full $^{31}\text{P}\{^1\text{H}\}$ NMR spectrum is presented in the appendix.

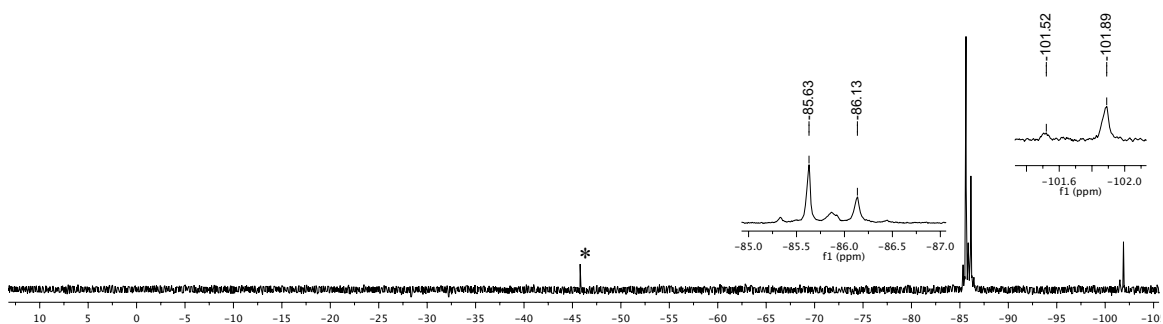
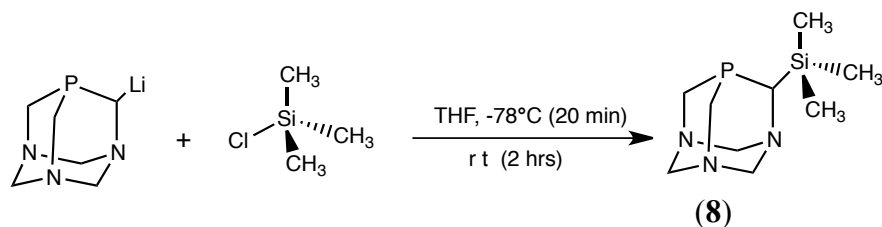


Figure 2.36. $^{31}\text{P}\{^1\text{H}\}$ NMR spectrum after washing the crude mixture of the PTA-Li and SnPh_2Cl_2 with hexanes. *Unidentified.

2.2.2 Attempts at PTA-Si derivatives

2.2.2.1 Reaction of PTA-Li with SiMe₃Cl



Scheme 2.9. Reaction of PTA-Li with SiMe₃Cl depicting the expected product, PTA-SiMe₃.

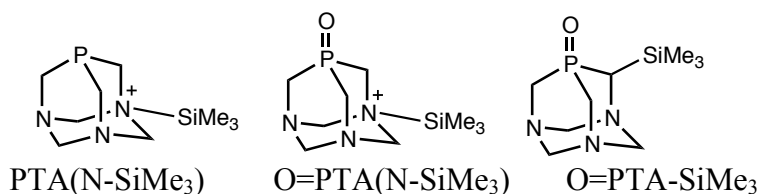


Figure 2.37. Possible side-products for the reaction of PTA-Li with SiMe₃Cl.

The reaction of PTA-Li with SiMe₃Cl in a 1:1 mole ratio resulted in three ³¹P{¹H} NMR peaks at -88.6 ppm, -93.2 ppm, and -95.6 ppm which are presumably the α -silylated phosphine PTA-SiMe₃, the N-silylated phosphine PTA(N-SiMe₃), and PTA respectively (Figure 2.38). Integration of the three peaks from downfield to upfield gives 3.32%, 83.9%, 12.8%. After a few weeks, the peak at -88.6 ppm disappeared with the appearance of a peak at -2 ppm, suggestive of oxidized product. The solution turned cloudy and turbid which could be the oxide deposits that are sparingly soluble. Furthermore, the two upfield peaks that started as a ratio of 6.6:1 changed to 2.1:1. This may suggest that the rate of oxidation for the peak at -93.2 ppm is faster compared to the peak at -95.6 ppm. If so, this may support the presumption that the resonance at -93.2 ppm corresponds to the N-Si PTA derivative since the similar compound, N-BH₃ PTA, was found to be more susceptible to oxidation than PTA.²⁴ The crude mixture was pulled

dry and minimum dry pentane was added. Filtration afforded a clear filtrate that was pulled dry under vacuum. The resulting white powder was dissolved in CDCl_3 and three $^{31}\text{P}\{^1\text{H}\}$ NMR peaks were observed (-93.4 ppm, -97.9 ppm, and -101.8 ppm, Figure 2.39). A small singlet at -5 ppm is representative of oxidized product. Due to the moisture sensitivity of the starting materials, future attempts should focus on using dry solvent and distillation of SiMe_3Cl over calcium hydride. The reaction should also be considered in a solvent other than THF and for a longer period of time to allow completion of the reaction.

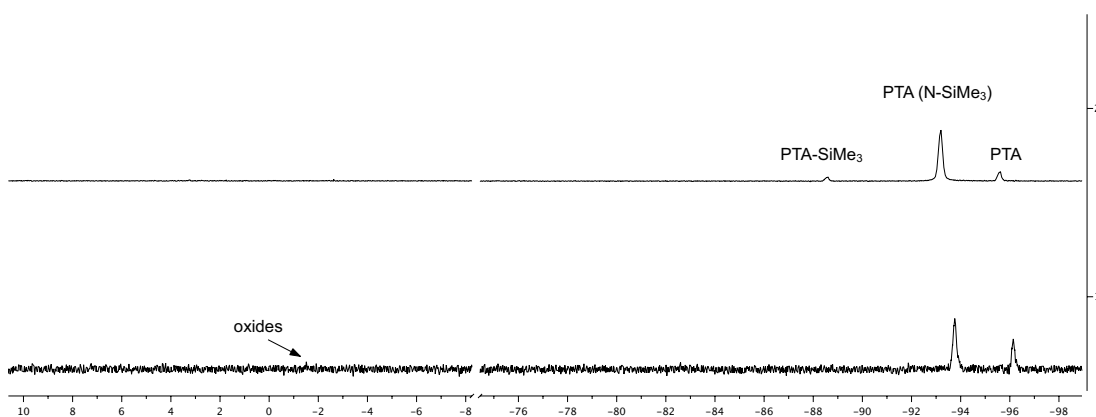


Figure 2.38. $^{31}\text{P}\{^1\text{H}\}$ NMR spectra of the reaction mixture of PTA-Li and SiMe_3Cl in THF (top) and the formation of oxides (bottom).

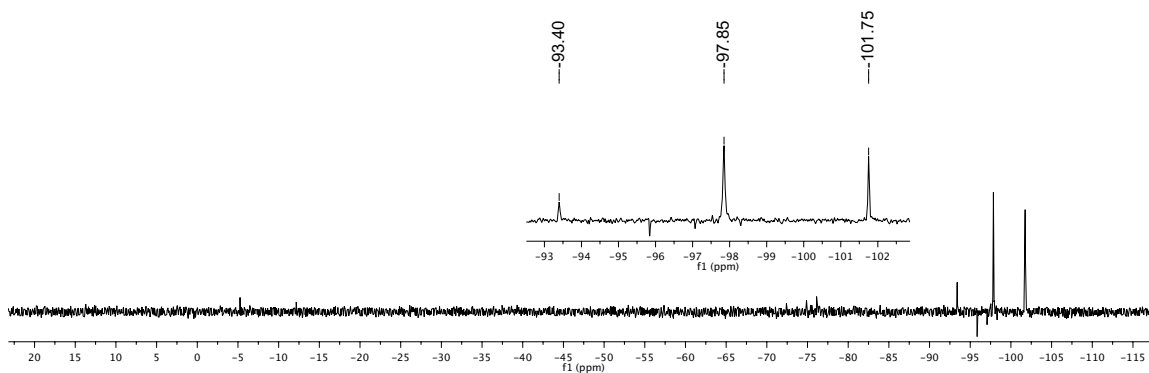
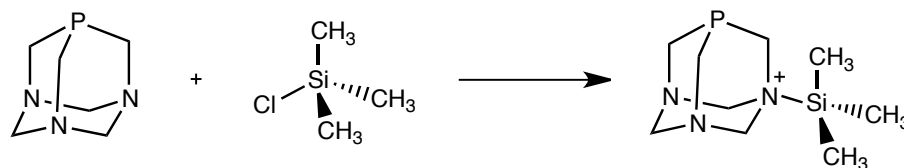


Figure 2.39. $^{31}\text{P}\{^1\text{H}\}$ NMR spectra of a PTA-Li and SiMe_3Cl in CDCl_3 .

2.2.2.1 Reaction of PTA with SiMe₃Cl



Scheme 2.10. Reaction of PTA with SiMe₃Cl depicting the expected product PTA(N-SiMe₃)

A NMR-scale experiment of the reaction of PTA (0.35 mmol) with SiMe₃Cl was monitored in CD₂Cl₂ in which both starting materials are soluble. The addition of 1 equiv. SiMe₃Cl caused the solution to turn from clear to a thick, white mixture that exhibits a ³¹P{¹H} NMR peak at -101.2 ppm (Figure 2.40). The addition of more PTA did not result in a new signal, signifying that the resonance at -101.2 ppm is unreacted PTA. Furthermore, ¹H NMR depicted peaks that are characteristic of PTA (Figure 2.41). The reaction was done at room temperature without prior drying of the NMR solvent. Future attempts should consider refluxing the reaction with degassed and dried solvent under nitrogen.

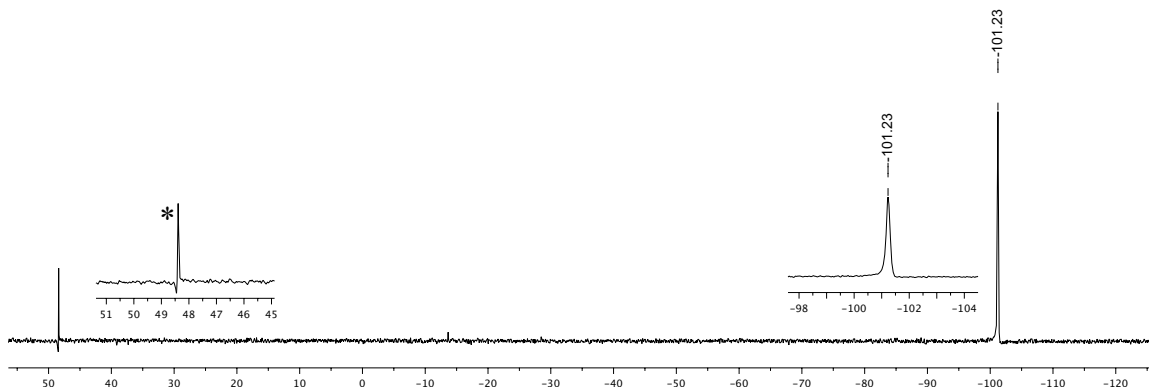


Figure 2.40. ³¹P{¹H} NMR spectrum of PTA with SiMe₃Cl in CD₂Cl₂. *Unidentified, possible digital noise

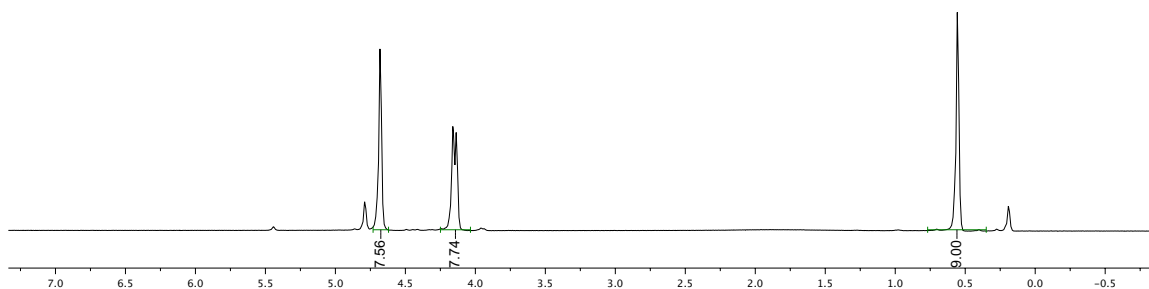
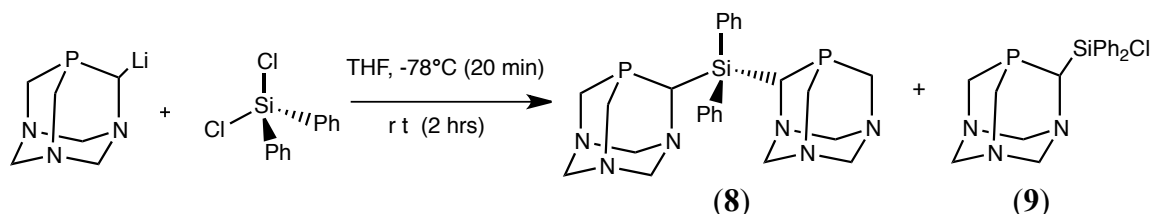


Figure 2. 41. ^1H NMR spectrum of PTA with SiMe_3Cl in CD_2Cl_2 .

Reaction with SiPh_2Cl_2



Scheme 2.11. Reaction of PTA-Li with SiPh_2Cl_2 depicting the expected product and side-product

The cloudy white solution resulting from the reaction of PTA-Li with liquid SiPh_2Cl_2 in THF exhibits a close group of singlets between -97 to -101 ppm (Figure 2. 42). One of the peaks is suggestive of unreacted PTA-Li. The rest of the singlets could include the mono- and disubstituted SiPh_2Cl_2 . The crude reaction mixture was pulled dry and dissolved C_6D_6 which exhibited overlapping peaks between -95 to -102 ppm with a minor peak at -0.69 ppm (Figure 2.43). This range in the $^3\text{P}\{^1\text{H}\}$ NMR spectrum is suggestive of oxidized material along with the visible observation of the discoloration of the solution to yellow over a short period of time. Chlorosilanes are generally air and moisture sensitive so appropriate measures must be taken to assure that these factors are avoided, if not possibly completely eliminated. For future attempts, washing with organic

solvent such as chloroform or dichloromethane could lead to isolation of the product and deuterated solvents and starting materials can be dried with activated molecular sieves.

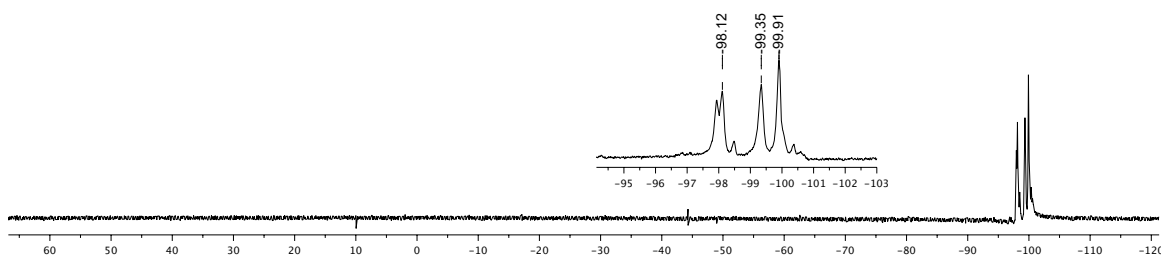


Figure 2.42. $^{31}\text{P}\{^1\text{H}\}$ NMR spectrum of the crude reaction mixture of PTA-Li and SiPh_2Cl_2 reaction in THF.

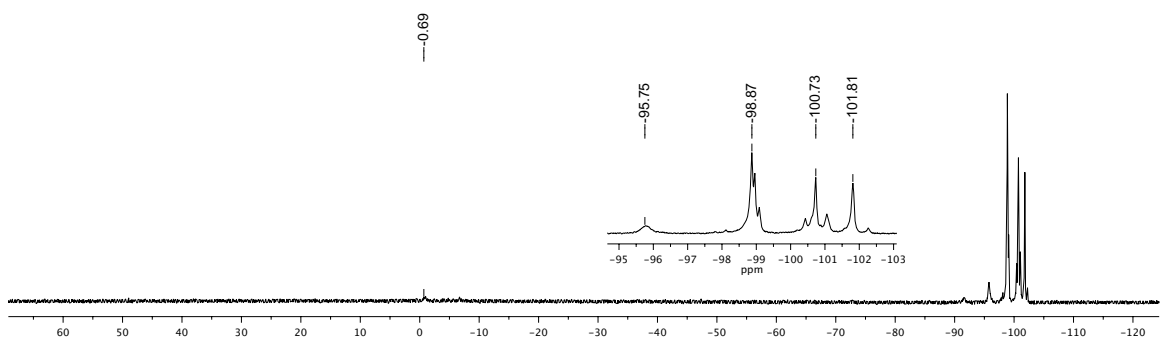


Figure 2.43. $^{31}\text{P}\{^1\text{H}\}$ NMR spectrum of the crude reaction mixture of PTA-Li and SiPh_2Cl_2 pulled dry and dissolved in C_6D_6 .

2.3 Concluding Remarks

Preparation of various stannylated and silylated PTA derivatives were attempted via PTA-Li. The seemingly straightforward reaction to obtain upper-rim PTA-derivatives appears more complicated than initially envisioned. PTA- SnMe_3 and O=PTA-SnMe_3 were successfully isolated. Full characterization of the compounds is highly recommended as well as their reactivity towards transition metals for catalysis such as tungsten and ruthenium.

2.4 Experimental

2.4.1 General

All manipulations, unless otherwise noted, were carried out on a double-manifold Schlenk vacuum line under nitrogen or in a nitrogen-filled glovebox. Tetrahydrofuran (THF) and hexanes were freshly distilled under nitrogen from sodium/benzophenone. *n*-BuLi, tin(IV) alkyl halides, and silicon alkyl- and aryl halides were all purchased from commercial sources and used as received. Water was deionized and deoxygenated before use. NMR solvents were purchased from Cambridge Isotopes and used as received. Tetrakis(hydroxymethyl)phosphonium chloride was obtained from Cytec and used without further purification. PTA and PTA-Li were synthesized according to literature.^{23,26} NMR spectra were recorded with Varian 500 or MR400 spectrometers at 25°C unless otherwise stated. ¹H and ¹³C NMR spectra were referenced to residual solvent relative to tetramethylsilane (TMS). Experiments involving SnMe₃Cl utilized CDCl₃ without TMS to avoid complications in overlapping resonance. ³¹P shifts are relative to an external standard of 85% H₃PO₄ in D₂O with positive values downfield of the reference. ¹¹⁹Sn shifts are relative to an external standard, either SnMe₃Cl in CDCl₃ (164 ppm) or SnMe₄ in C₆D₆ (0 ppm). Electrospray ionization mass spectra (ESI-MS) were recorded on a Waters Micromass 20 ESI mass spectrometer (positive ion mode).

2.4.2 Water Solubility. The water solubility was acquired by the slow addition of the compound into 0.5 mL of water, manually stirring, until saturation. The mixture was carefully filtered through a syringe filter into a pre-weighed vial. The solvent was evaporated and the mass of dry solid was weighed.

2.4.3 Synthesis

Synthesis of 1,3,5-Triaza-7-phosphaadamantane-6-yllithium (PTA-Li).

The synthesis of PTA-Li was previously reported by our group.⁴ To a suspension of dried PTA (3.10 g, 19.7 mmol) in 40 mL of THF was slowly added at room temperature *n*-butyllithium (2.5 M, 11 mL, 27.5 mmol) over the course of 5 min. The reaction was stirred at room temperature until the evolution of butane was no longer observed (approximately 2.5-3 h). The suspension was filtered under nitrogen and the precipitate washed with hexanes (2 × 15 mL), resulting in 3.20 g of a fine white highly pyrophoric powder. A yield of >90% for the synthesis of PTA-Li was determined by quenching PTA-Li with D₂O and measuring the ratio of PTA/PTA-D by ³¹P spectroscopy. PTA-D was characterized by ¹H, ¹³C{¹H} and ³¹P{¹H} NMR spectroscopies in D₂O and in CDCl₃. ¹H NMR (400 MHz, D₂O): 4.48 and 4.43 ppm (AB quartet, J = 12.4 Hz, 6H, NCH₂N), 3.91 ppm (d, ²J_{PH} = 8.8 Hz, 5H, PCH₂N, PCHDN). ¹³C{¹H} NMR (100 MHz, D₂O): 70.8 ppm (t, J_{PC} = 2.0 Hz, 3C, NCH₂N), 47.7 ppm (d, ¹J_{PC} = 19.6 Hz, 1C, PCH₂N), 47.6 ppm (d, ¹J_{PC} = 19.6 Hz, 1C, PCH₂N), 47.3 (~1:2:2:1 quartet, ¹J_{PC} = 21.1 Hz, ¹J_{DC} = 21.1 Hz, 1C, PCHDN). ³¹P{¹H} NMR (162 MHz, D₂O): -98.8 ppm (s, PTA- D), -98.4 ppm (s, PTA). PTA-D was also characterized in CDCl₃. The solvent of the D₂O solution was removed under reduced pressure. The resulting solid was dissolved in CDCl₃ followed by filtration to remove the lithium salts (LiOD). ¹H NMR (400 MHz, CDCl₃): 4.60 ppm (s, 6H, NCH₂N), 4.05 ppm (d, ²J_{PH} = 10.0 Hz, 5H, PCH₂N, PCHDN). ¹³C{¹H} NMR (100 MHz, CDCl₃): 73.66 ppm (vt, J_{PC} = 2 Hz, 3C, NCH₂N), 50.6 ppm (d, ¹J_{PC} = 20.6 Hz, 1C, PCH₂N), 50.5 ppm (d, ¹J_{PC} = 20.6 Hz, 1C, PCH₂N), 50.2 (~1:2:2:1 quartet, ¹J_{PC} = 21.1 Hz, ¹J_{DC} = 21.1 Hz, 1C, PCHDN).

$^{31}\text{P}\{^1\text{H}\}$ NMR (162 MHz, CDCl_3): -102.5 ppm (s, PTA-D), -102.1 ppm (s, PTA).

Synthesis of PTA-SnMe₃ (1)

To a suspension of PTA-Li (0.97 g, 6.0 mmol) in 30 mL of freshly distilled THF at -78°C was added solid SnMe_3Cl (0.95 g, 4.8 mmol) under positive nitrogen flow. The solution was left to stir at -78°C for about 20 minutes before warming up to room temperature. After 3 hours, the solvent was removed under reduced pressure. 10 mL of pentane was added to the crude product. After sonication, traces of unreacted PTA-Li and LiCl were filtered off and the solvent was removed under vacuum resulting in a white solid (0.7034 g, 46% yield). X-ray quality crystals were obtained by slow evaporation of pentane solution, resulting in colorless blocks over the course of 2 days. ^1H NMR (400 MHz, CDCl_3): δ 0.241 ppm (s, $^2J_{^1\text{H}^{119}\text{Sn}} = 56$ Hz, $^2J_{^1\text{H}^{117}\text{Sn}} = 52$ Hz 9H, SnCH₃), 3.95 - 4.20 ppm (m, 5H, PCH₂N, PCHSn), 4.50 - 4.77 ppm (m, 6H, NCH₂N). $^{13}\text{C}\{^1\text{H}\}$ NMR (125.7 MHz, CDCl_3): δ 76.8 ppm (d, $^3J_{\text{PC}} = 3.8$ Hz, 1C, NCH₂N), 74.5 ppm (d, $^3J_{\text{PC}} = 2.5$ Hz, 1C, NCH₂N), 73.0 ppm (d, $^3J_{\text{PC}} = 2.5$ Hz, 1C, NCH₂N), 53.3 ppm (d, $^1J_{\text{PC}} = 23.9$ Hz, 1C, PCH₂N), 52.7 ppm (d, $^1J_{\text{PC}} = 36.3$ Hz, 1C, PCHSn), 50.0 ppm (d, $^1J_{\text{PC}} = 20.1$ Hz, 1C, PCH₂N), -9.10 ppm (s, $^1J_{\text{SnC}} = 319.3$ Hz, 3C, SnCH₃). $^{31}\text{P}\{^1\text{H}\}$ NMR (162 MHz, CDCl_3): δ -86.79 ppm (s, $^2J_{^{31}\text{P}^{119}\text{Sn}} = 107$ Hz, $^2J_{^{31}\text{P}^{117}\text{Sn}} = 104.7$ Hz). $^{119}\text{Sn}\{^1\text{H}\}$ NMR (149.2 MHz, CDCl_3): δ -22.3 ppm (d, $^2J_{\text{SnP}} = 108$ Hz).

Synthesis of O=PTA-SnMe₃ (2)

The phosphine oxide was obtained by the addition of 30% H_2O_2 (0.2 mmol) to 1 mL solution of the stannylated phosphine (0.1 mmol). ^1H NMR (400 MHz, CDCl_3): δ 0.35 ppm (s, $^2J_{^1\text{H}^{119}\text{Sn}} = 56$ Hz, $^2J_{^1\text{H}^{117}\text{Sn}} = 53$ Hz, 9H, SnCH₃), 3.60 - 4.30 ppm (m,

11H, PCH₂N, PCHN, NCH₂N). ¹³C{¹H} NMR (125.7 MHz, CDCl₃): δ 75.2 ppm (d, ³J_{PC} = 9 Hz, 1C, NCH₂N), 73.1 ppm (d, ³J_{PC} = 9 Hz, 1C, NCH₂N), 71.6 ppm (d, ³J_{PC} = 10 Hz, 1C, NCH₂N), 58.4 ppm (d, ¹J_{PC} = 48 Hz, 1C, PCH₂N), 57.1 ppm (d, ¹J_{PC} = 40 Hz, 1C, PCH₂N), 55.3 ppm (d, ¹J_{PC} = 54 Hz, 1C, PCH₂N), -8.11 ppm (s, ¹J_{SnC} = 330 Hz, 3C, SnCH₃). ³¹P{¹H} NMR (162 MHz, CDCl₃): δ -4.54 ppm (s). ¹¹⁹Sn{¹H} NMR (149.2 MHz, CDCl₃): δ 5.68 ppm (d, ²J_{SnP} = 16 Hz).

Attempted Synthesis of PTA-(N-SnMe₃) (3)

A small-scale NMR reaction was carried out by adding 0.11 mmol of SnMe₃Cl to 0.10 mmol of PTA in CDCl₃. The NMR tube was left to sonicate for about 15 minutes before acquiring NMR data. ³¹P{¹H} NMR (162 MHz, CDCl₃): δ -97 ppm. A similar reaction was carried out in D₂O. ³¹P{¹H} NMR (162 MHz, CDCl₃): δ -90 ppm. The addition of excess PTA did not form a new peak on the spectrum, indicating that the resonance may be unreacted PTA or protonated PTA. ¹H NMR shows characteristic singlet and doublet of NCH₂N and CH₂N protons in PTA.

Attempted Synthesis of (PTA)₂-SnMe₂ (4)

To a suspension of PTA-Li (0.1638 g, 1 mmol) in 30 mL of freshly distilled THF at -78°C was added solid SnMe₂Cl₂ (0.108 g, 0.49 mmol). The solution was left to stir at -78°C for about 20 minutes before warming up to room temperature. After 3 hours, the solvent was removed under reduced pressure. The crude pale yellow solid was characterized by ³¹P NMR spectroscopy. ³¹P{¹H} NMR (162 MHz, CDCl₃): δ -63.4 ppm (s, ²J_{SnP} = 50.22 Hz, PTA-SnMe₂Cl), -86.5 ppm and -86.7 ppm (s, ²J_{SnP} = 106.9 Hz, PTA₂-SnMe₂ meso and RR/SS), -102 ppm (s, PTA).

Attempted Synthesis of PTA₂-SnPh₂ (6)

To a suspension of PTA-Li (0.1686 g, 1.0 mmol) in mL of freshly distilled THF at -78°C was added solid SnMe₂Cl₂ (0.108 g, 0.48 mmol) under positive nitrogen flow. The solution was left to stir at -78°C for about 20 minutes before warming up to room temperature. After 3 hours, the solvent was removed under reduced pressure. The crude pale yellow solid was characterized by ³¹P NMR spectroscopy. ³¹P{¹H} NMR (162 MHz, crude THF): δ -83.0 ppm (s, ²J_{SnP} = 162 Hz), -85.6 ppm (s, ²J_{SnP} = 97.2 Hz), -101.5 ppm (s, PTA). ³¹P{¹H} NMR (162 MHz, crude CDCl₃): δ -86.8.0 ppm (s, ²J_{SnP} = 108.5 Hz), -86.6 ppm (s, ²J_{SnP} = 108.5 Hz), -63.5 ppm (s, ²J_{SnP} = 50.2 Hz), -102 ppm (s, PTA). ¹¹⁹Sn{¹H} NMR (149 MHz, crude CDCl₃): δ -41.2 ppm (t, ²J_{SnP} = 116.4 Hz), -42.1 ppm (t, ²J_{SnP} = 116.4 Hz), -25.6 ppm (t, ²J_{SnP} = 50.7 Hz).

Attempted Synthesis of PTA-SiMe₃ (8)

To a suspension of PTA-Li (81.5 mg, 0.5 mmol) in 15 mL of freshly distilled THF at -78°C was added liquid SiMe₃Cl via syringe (0.064 mL, 0.5 mmol). The solution was left to stir at -78°C for about 20 minutes before warming up to room temperature. After 3 hours, the solvent was removed under reduced pressure. The crude pale yellow solid was characterized by NMR spectroscopy. ³¹P{¹H} NMR (162 MHz, crude THF): δ -93.76 ppm, -98.73 ppm, -101.31 ppm (PTA).

Attempted Synthesis of PTA₂-SiPh₂ (10)

To a suspension of PTA-Li (0.1661 g, 1 mmol) in 25 mL of freshly distilled THF at -78°C was slowly added liquid SiPh₂Cl₂ (0.10 mL, 0.5 mmol) via syringe. The solution was left to stir at -78°C for about 20 minutes before warming up to room temperature. After 3 hours, the solvent was removed under reduced pressure. 10 mL of hexanes was

added and LiCl filtered off. The solvent was pulled under vacuum and the resulting crude white solid was characterized by NMR spectroscopy. $^{31}\text{P}\{^1\text{H}\}$ NMR (162 MHz, CDCl_3): δ -98 to 101 ppm (set of singlets)

2.5 References

- (1) Bravo, J.; Bolano, S.; Gonsalvi, L.; Peruzzini, M. *Coord. Chem. Rev.* **2010**, *254*, 555–607.
- (2) Lee, W.-C.; Sears, J. M.; Enow, R. A.; Eads, K.; Krogstad, D. A.; Frost, B. J. *Inorg. Chem.* **2013**, *52*, 1737–1746.
- (3) Wong, G. W.; Lee, W.-C.; Frost, B. J. *Inorg. Chem.* **2008**, *47*, 612–620.
- (4) Wong, G. W.; Harkreader, J. L.; Mebi, C. A.; Frost, B. J. *Inorg. Chem.* **2006**, *45*, 6748–6755.
- (5) Erlandsson, M.; Gonsalvi, L.; Ienco, A.; Peruzzini, M. *Inorg. Chem.* **2008**, *47*, 8–10.
- (6) Guerriero, A.; Erlandsson, M.; Ienco, A.; Krogstad, D. A.; Peruzzini, M.; Reginato, G.; Gonsalvi, L. *Organometallics* **2011**, *30*, 1874–1884.
- (7) Krogstad, D. A.; Guerriero, A.; Ienco, A.; Manca, G.; Peruzzini, M.; Reginato, G.; Gonsalvi, L. *Organometallics* **2011**, *30*, 6292–6302.
- (8) Sears, J. M. *Synthesis and Coordination Chemistry of Novel Water Soluble Diphosphines: Application to Ruthenium Catalyzed Aqueous Nitrile Hydration*. M.S., University of Nevada, Reno, 2012.
- (9) Krogstad, D. A.; Gohmann, K. E.; Sunderland, T. L.; Geis, A. L.; Bergamini, P.; Marvelli, L.; Young, V. G. *Inorganica Chim. Acta* **2009**, *362*, 3049–3055.
- (10) Krogstad, D. A.; Gohmann, K. E.; Sunderland, T. L.; Geis, A. L.; Bergamini, P.; Marvelli, L.; Young Jr., V. G. *Inorganica Chim. Acta* **2009**, *362*, 3049–3055.
- (11) Weichmann, H.; Tzschach, A. *J. Organomet. Chem.* **1975**, *99*, 61–69.
- (12) Weichmann, H.; Tzschach, A. *J. Fuer Prakt. Chem. Leipz.* **1976**, *318*, 87–95.
- (13) Weichmann, H.; Quell, G.; Tzschach, A. *Z. Fuer Anorg. Allg. Chem.* **1980**, *462*, 7–17.
- (14) Weichmann, H.; Muegge, C.; Grand, A.; Robert, J. B. *J. Organomet. Chem.* **1982**, *238*, 343–356.
- (15) Weichmann, H.; Rensch, B. *Z. Fuer Anorg. Allg. Chem.* **1983**, *503*, 106–114.
- (16) Weichmann, H. *J. Organomet. Chem.* **1984**, *262*, 279–292.
- (17) Weichmann, H.; Richter, F. *Z. Fuer Chem.* **1989**, *29*, 409–410.
- (18) Karsch, H. H.; Appelt, A. *Z. Fuer Naturforschung Teil B Anorg. Chem. Org. Chem.* **1983**, *38B*, 1399–1405.
- (19) Weichmann, H.; Ochsler, B.; Duchek, I.; Tzschach, A. *J. Organomet. Chem.* **1979**, *182*, 465–476.
- (20) Wolfsberger, W. *Chem.-Ztg.* **1989**, *113*, 349–351.
- (21) Davies, A. G. *Organotin Chemistry*; Second.; John Wiley & Sons, 2006.
- (22) Kowall, B.; Heinicke, J. *Main Group Met. Chem.* **1997**, *20*, 379–386.

- (23) Daigle, D. J. *Inorg. Synth.* **1998**, 32, 40–45.
- (24) Frost, B. J.; Mebi, C. A.; Gingrich, P. W. *Eur. J. Inorg. Chem.* **2006**, 1182–1189.
- (25) Dörr, A.; Gudat, D.; Hänssgen, D.; Hens, H.; Stahlhut, E. **1994**, 131, 674–682.
- (26) Daigle, D. J.; Pepperman, A. B., Jr.; Vail, S. L. *J. Heterocycl. Chem.* **1974**, 11, 407–408.

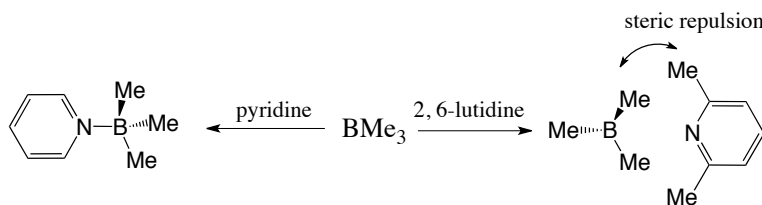
Chapter 3

PTA Phosphinoboranes

3.1 Introduction

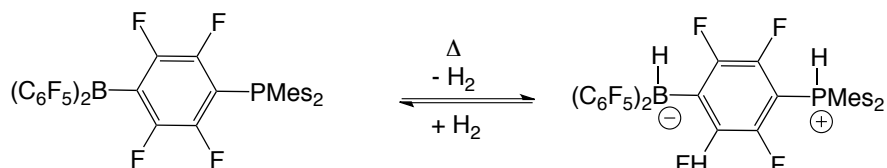
3.1.1 FLPs

Frustrated Lewis pairs (FLPs) are combinations of Lewis acids and bases that render characteristic reactivity because of steric congestion.¹ The acid/base functionalities are in close proximity with each other but are geometrically constrained so instead of the classical notion of neutralization, FLPs form “co-existing non-quenched pairs of acids and bases”.² The concept of frustrated Lewis pairs was introduced in 2006 by Stephan and coworkers^{1,3} but the idea of steric congestion as a primary reason for adduct formation was observed by Brown in 1942 in his study of coordination compounds of boron.⁵ In this particular experiment, trimethylborane (Lewis acid) was reacted with either pyridine or 2,6-lutidine (Lewis base) (Scheme 3.1). Steric repulsion between the methyl groups present in 2,6-lutidine and the trimethylborane prevent adduct formation while pyridine is readily ‘quenched’ to form an adduct.

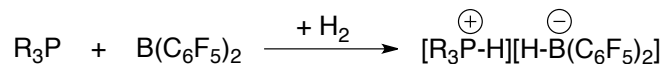


Scheme 3.1. Reaction of trimethylborane with different Lewis bases.⁵

Due to the conserved properties of the bulky Lewis acid and base, interesting reactions can be facilitated. One of the first to be reported is the reversible metal-free activation of H₂ by Stephan and coworkers.⁶ The reported FLP was intramolecular (Scheme 3.2) but was readily applied to intermolecular FLPs (Scheme 3.3).⁷



Scheme 3.2. Example of an intramolecular FLP system.



Scheme 3.3. Example of an intermolecular FLP system.

Common examples of these unusual acid/base systems are composites of bulky phosphines or amines with a strong electrophile like $RB(C_6F_5)_2$.⁸ More recent studies have employed Lewis acid entities based on C, Al, Zr, Si, and P.⁹ (Scheme 3.4) Since the discovery of the unique reactivity of FLPs in 2006,⁶ new attempts at the synthesis of more efficient acid/base pairs have been made. A variety of FLPs can react with a wide range of substrates including alkenes, alkynes, aldehydes, and most interestingly on the activation of small molecules like CO_2 , O_2 , and H_2 .¹⁰

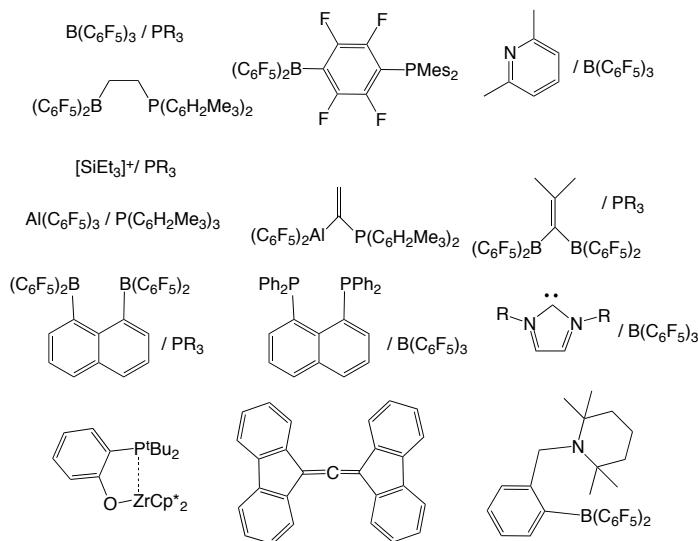


Figure 3.1. Examples of FLPs^{8,10-16}

With the tremendous growth in FLP research over the past few years, due to the fascination on the original discovery of reversible H₂ activation, and with our research group's main concern on water-soluble phosphines, it is within our interest to develop P/B FLP systems with the PTA framework via PTA-Li. Previous reports by Thomas and Peters¹⁷ on the synthesis of bis(phosphine)borates, a new generation of monoanionic chelating phosphine ligands has led to the investigation of similar synthetic methods. More of this shall be discussed in the following sub-chapter.

3.1.2 P/B FLP compounds

The breakthrough in P/B FLP systems has found a wide range of application including activations of olefins,^{18,19} acetylene,¹⁹⁻²⁴ disulfides,²⁶ carbon dioxide,^{18,19} N₂O,²⁹ NO³⁰ and the C-H bonds of propene.³¹ Examples of these unique acid/base combinations are shown in Scheme 3.5.

There have been studies that reveal FLP characteristics even for phosphines of low sterics such as P(Et)₃ when paired up with a very sterically hindered Lewis acid tris(perchloroaryl)borane or BAr^{Cl}.³² O'Hare and coworkers were able to show how R₃P/BAr^{Cl} FLPs (R=ethyl, cyclohexyl, ⁿbutyl, ^tbutyl, or *p*-tolyl) can split H₂ in thf-d₈.

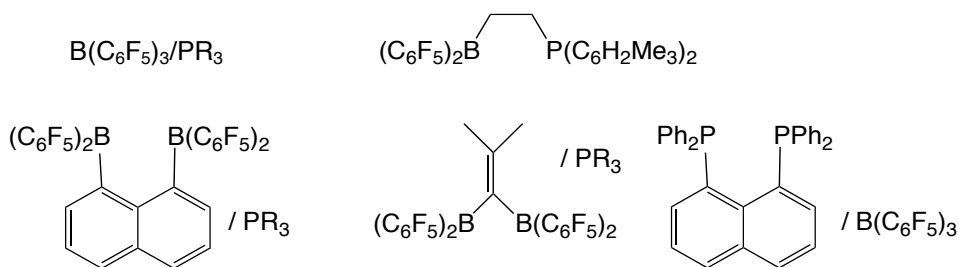
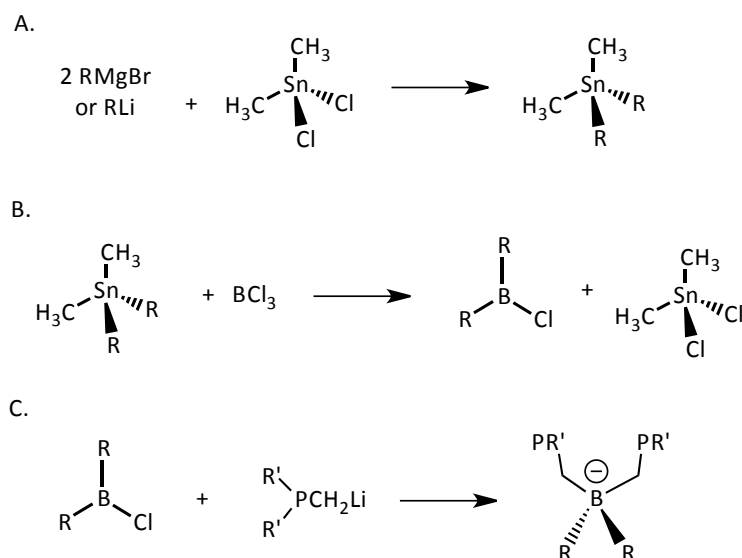


Figure 3.2. Examples of P/B FLP combinations.

3.1.3 Synthesis of Phosphinoborates and related compounds

In a recent report by Thomas and Peters,¹⁷ a series of bis(phosphino)borates were derived from the general reaction of a phosphinoalkyl carbanion to a borane electrophile. This method is advantageous, first of all, with the accessibility of numerous carbanions and borane electrophiles and second, borate-based ligands synthesized via nucleophilic addition to borane precursors are highly regarded in the literature.³³⁻³⁷ A general scheme for the synthesis of bis(phosphino)borates is shown in Scheme 3.4.



Scheme 3.4. Synthesis of bis(phosphine) borates. (R = *p*-MePh, *m,m*-(CH₃)₂Ph, *p*-^tBuPh, *p*-MeOPh, *p*-CF₃Ph, *o*-MeOPh, *o,o*-(MeO)₂Ph, *o*-CF₃Ph and R' = ^tBu, ⁱPr, Ph, *p*-^tBuPh, *p*-CF₃Ph)¹⁷

In this method presented by Thomas and Peters, the generation of Me₂SnR₂ (Scheme 3.6-A) from either a Grignard reagent or organolithium compound is based on previous literature - Me₂SnPh₂,³⁸⁻⁴² Me₂Sn(*p*-MePh)₂,^{38-40,43} Me₂Sn(*p*-MeOPh)₂,^{39,40,44} Me₂Sn(*p*-CF₃Ph)₂,³⁹ Me₂Sn(*o*-MeOPh)₂,⁴⁰ Me₂Sn(*o,o*-(MeO)₂Ph)₂.⁴⁵ Subsequent reaction with BCl₃ affords the diarylchloroboranes based on Chivers/Piers methodology.^{46,47} The reaction products of the lithiated phosphines with BR₂Cl (Scheme 3.6-C) were observed

via ^{31}P NMR and was proved successful. The bis(phosphine)borates have some solubility in toluene, THF, CH_3CN , acetone, ethanol, ether and benzene. Rapid decomposition of the compounds was evident upon dissolution in chlorinated solvents like CHCl_3 and CH_2Cl_2 . A similar reaction step was done for the commercially available bis(cyclohexyl)chloroborane, which was included in this thesis. Most of the compounds appeared downfield at about 10 to -10 ppm in the ^{31}P NMR with $^2J_{\text{B-P}}$ ranging from 10 to 70 Hz.

The Frost group reported the first N-bound PTA derivative with BH_3 , having an uncoordinated phosphorus atom.⁵¹ This synthesis was done in cold CH_2Cl_2 with 1.1 equiv. $\text{BH}_3\cdot\text{THF}$. In a study by Peruzzini and coworkers, a stepwise addition of up to 4 equiv. BH_3 to PTA, in dry THF, afforded the tetrakis-borane PTA adduct. They reported a preference for N-bound BH_3 which correlates to computational investigation of the energies involved in complex formation of hetero-substituted caged phosphines like PTA. The formation of the adducts was monitored via ^{31}P NMR but due to its extreme air and water sensitivity, attempts to isolate in the solid state were unsuccessful. Observed products of hydrolysis of the monoboranyl adduct were noted as PTA and boric acid, H_3BO_3 .⁵²

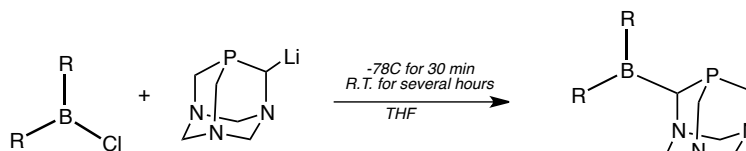
A former research group member, Wei-chih Lee, conducted further experiments by reacting PTA in cold CH_2Cl_2 with 4 equiv $\text{H}_3\text{B}\cdot\text{SMe}_2$. Precipitation with dry hexane and filtration allowed isolation of a solid that has $\delta^{31}\text{P} \{^1\text{H}\}$ of -34.0 ppm in C_6D_6 . This is comparable to the tetrakis-borane adduct by Peruzzini and coworkers (-28.8 ppm). An attempt to isolate this solid was unsuccessful. Instead, a single-crystal X-ray analysis showed a solid-state structure of $[\text{H}_3\text{B}(\text{O}=\text{PTA})]$, previously reported by our group.⁵¹

This further suggests how these types of compounds are unstable towards oxidation. These previous studies along with the recent reports on P/B frustrated lewis pairs sparked interest in the synthesis of PTA phosphinoborane derivatives.

3.2 Results and Discussion

3.2.1 Reaction of PTA-Li with BCy₂Cl

In an attempt to extend the library of PTA coordination compounds with potential FLP reactivity, we have considered exploring the reaction of lithiated PTA with boron-containing electrophiles, R₂BCl, similar to the method reported by Thomas and Peters.¹⁷ The synthetic method was expected to be a straightforward approach to generating upper-rim PTA derivatives. (Scheme 3.5)



Scheme 3.5. Reaction of PTA-Li with R₂BCl (R=Cy, Ph).

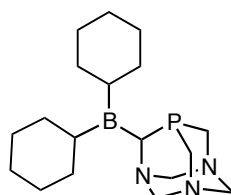


Figure 3.3. Depiction of PTA-BCy₂ (**12**)

An attempt to synthesize PTA-BCy₂ in an NMR-scale experiment was conducted by the addition of BCy₂Cl (0.400 mmol) to a THF solution of PTA-Li (0.407 mmol). The addition of the colorless liquid BCy₂Cl resulted in a yellow-orange solution within a few minutes. The reaction was monitored via ³¹P{¹H} NMR at 35°C (Figure 3.4). The disappearance of the PTALi signal (-101 ppm) and the immediate formation of a major

peak at -80.7 ppm (88.5%) and a minor peak at -77.3 ppm (11.5%) was observed. This is deshielded in comparison to PTA(N-BH₃) reported by Peruzzini and coworkers (-94.85 ppm, Table 3.1).⁵² It is unclear why the NMR signals on the arrayed spectra appear to split and shift. The sharp ³¹P{¹H} NMR resonance at -80.7 ppm is suggestive of the the α-boranyl species depicted in Figure 3.3, and not the P-boranyl product which would be expected to give a broad signal further downfield. Furthermore, the minor peak at -77.3 ppm present in spectrum number 1 of the arrayed spectra, was no longer observed at the end of the NMR acquisition. This could be the N-bound BCy₂Cl side product, possibly formed from the PTA contained in the starting PTA-Li, usually less than 10%. A notable decrease in intensity of the peak at -80.7 ppm was accompanied by the formation of a new peak at -22.0 ppm. This is comparable to the reported tetrakis-boranyl PTA derivative, in which all three nitrogens and the phosphorus are bound to BH₃ (-28.82 ppm, Table 3.1).⁴⁸ The identity of this resonance is unclear but it could be the P-bonded derivative or the oxidized PTA-BCy₂.

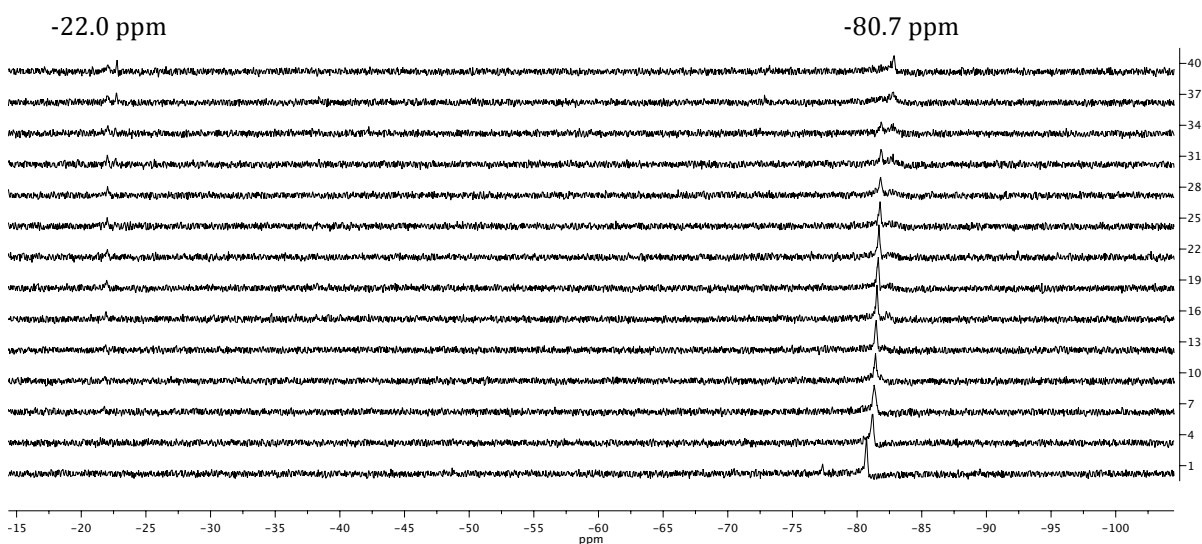
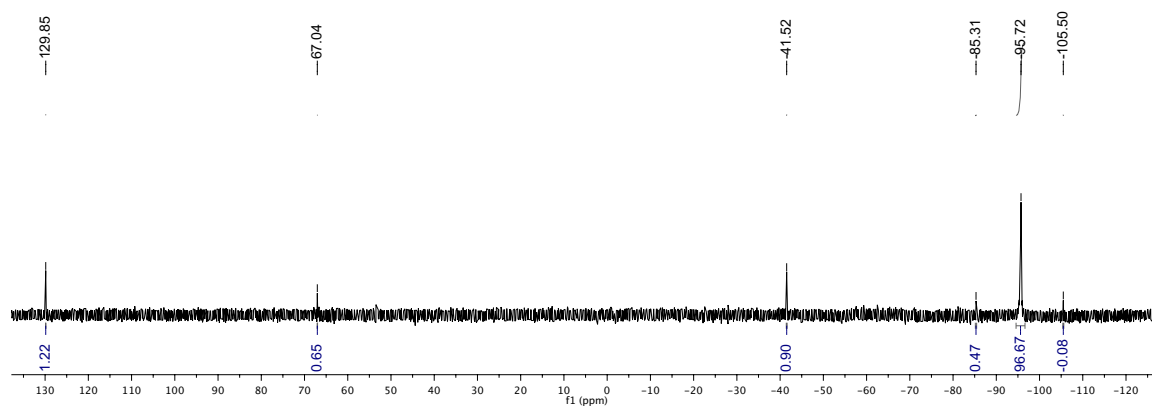


Figure 3.4. Kinetic ³¹P{¹H} NMR spectra of the reaction of PTA-Li and BCy₂Cl in THF at 35°C. Time elapsed can be calculated from the multiplication of the spectrum number by 5 minutes. Full study is shown in the appendix.

Table 3.1. $^{31}\text{P}\{^1\text{H}\}$ NMR shifts of PTA-BH₃ adducts in THF⁴⁸

BH ₃ bond mode	1 N-BH ₃	2 N-BH ₃	1 N-BH ₃ , 1 P-BH ₃	3 N-BH ₃	2 N-BH ₃ , 1 P-BH ₃	3 N-BH ₃ , 1 P-BH ₃	PTA
$\delta^{31}\text{P}$, ppm	-94.85	-92.37	-43.41	-93.45	-34.01	-28.83	-101.3

The same reaction carried out in a larger scale (1.297 mmol BCy₂Cl, 1.490 mmol PTA-Li) generated a cloudy orange mixture in THF. Low intensity, narrow peaks in the $^{31}\text{P}\{^1\text{H}\}$ NMR spectrum in Figure 3.5 gave low relative integration of 0.08 to 1.22% (-129.9 ppm, -67.0 ppm, -41.52 ppm, -85.31 ppm, -105.5 ppm). Although the intense peak at -95.7 ppm is within the range of other α -substituted PTA derivatives, it is shifted upfield in comparison to the previous NMR scale experiment by about about 15ppm. Instead, it is comparable to the $\delta^{31}\text{P}$ shift of the PTA(N-BH₃) reported by Peruzzini and coworkers. The product from this reaction is suggestive of PTA(N-BCy₂Cl) which is a probable consequence of a larger scale experiment that is easily introduced to moisture and air contamination as it was ran at a longer period of time.

**Figure 3.5.** $^{31}\text{P}\{^1\text{H}\}$ NMR spectrum of the reaction of PTA-Li and BCy₂Cl in THF at 25°C after 23 hours.

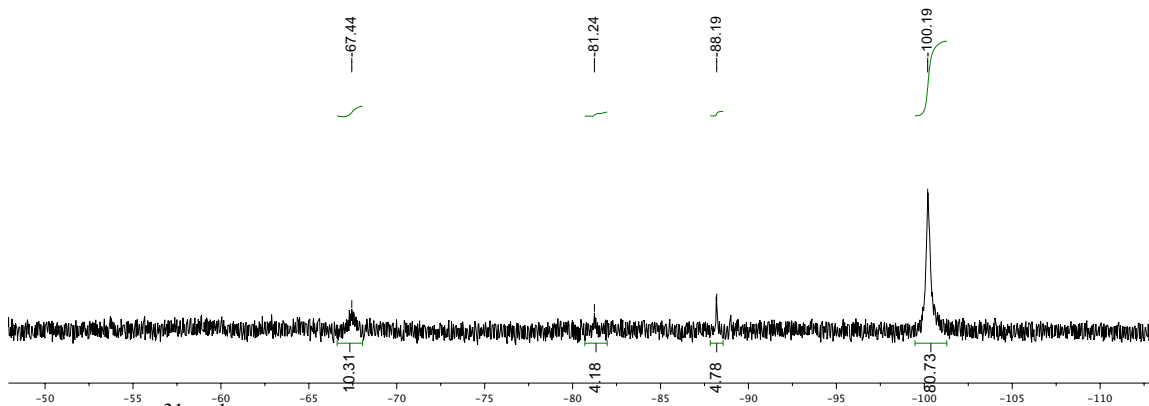


Figure 3.6. $^{31}\text{P}\{^1\text{H}\}$ NMR spectrum of the crude reaction mixture of PTA-Li and BCy_2Cl after filtering over celite.

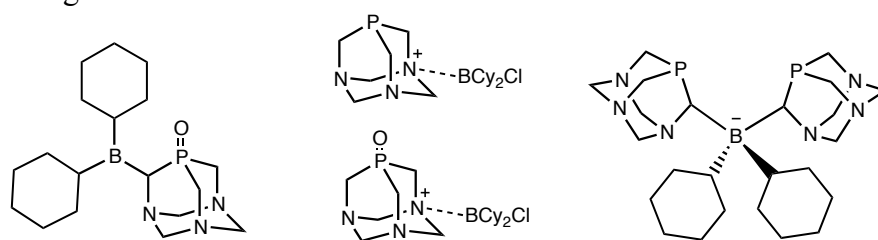


Figure 3.7. Depiction of possible side products of the reaction of PTA-Li with BCy_2Cl .

The crude reaction mixture was filtered over celite in an attempt to isolate the product. The $^{31}\text{P}\{^1\text{H}\}$ NMR spectrum of the filtrate was evaluated and integrated as shown in Figure 3.6. The low intensity peak at -81.2 ppm can be correlated to the peak at -77.3 ppm of the NMR experiment while the -67.4 ppm peak may be an open-cage PTA derivative. Meanwhile, the THF-soluble compounds showed up as singlets in the $^{31}\text{P}\{^1\text{H}\}$ NMR spectrum in C_6D_6 (-49.4 ppm, -100.8 ppm, Figure 3.8). Even though the α -methylene bonded BCy_2 is expected to appear downfield, the resonance at -49.4 ppm is too narrow in comparison to the resonance peak at -100.8 ppm. Also, a distinguished feature for boronated phosphines, B-P, is peak broadening.⁵² Therefore, the possibility that this is a P bonded BCy_2 can also be eliminated. The narrow base peak dimension is suggestive of digital noise which was also observed in other $^{31}\text{P}\{^1\text{H}\}$ NMR spectra.

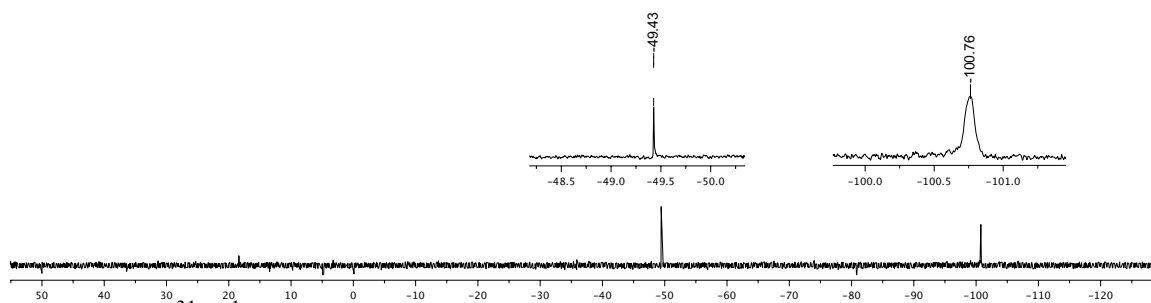


Figure 3.8. $^{31}\text{P}\{^1\text{H}\}$ NMR spectrum of the THF-soluble product from the reaction of PTA-Li and BCy_2Cl in C_6D_6 .

In CD_3OD , singlets at -6.9 ppm (36.9%), -67.1 ppm (6.5%), -83.77 ppm (2.5%), -96.4 ppm (54.1%) appeared (Figure 3.9). The peak at -6.9 ppm is a typical chemical shift for $\text{O}=\text{PTA}$ and -96.4 ppm for PTA in CD_3OD . ^1H NMR of the sample further suggests the presence of characteristic PTA and $\text{O}=\text{PTA}$ peaks (Figure 3.10). This may imply that the product is not stable in polar solvent and oxidizes to $\text{O}=\text{PTA}$. A similar observation was noted in D_2O (Refer to Appendix).

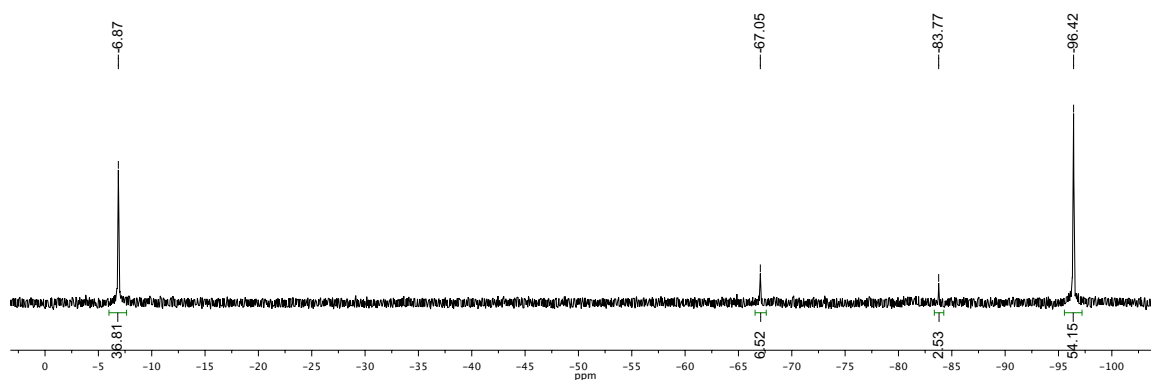


Figure 3.9. $^{31}\text{P}\{^1\text{H}\}$ NMR spectrum of the THF-soluble product from the crude reaction mixture of PTA-Li and BCy_2Cl in CD_3OD .

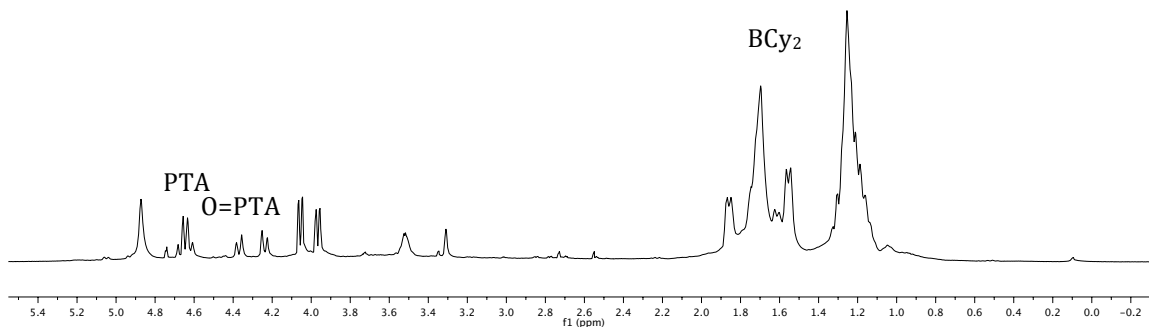


Figure 3.10. ^1H NMR spectrum of the THF-soluble product from the crude reaction mixture of PTA-Li and BCy_2Cl in CD_3OD .

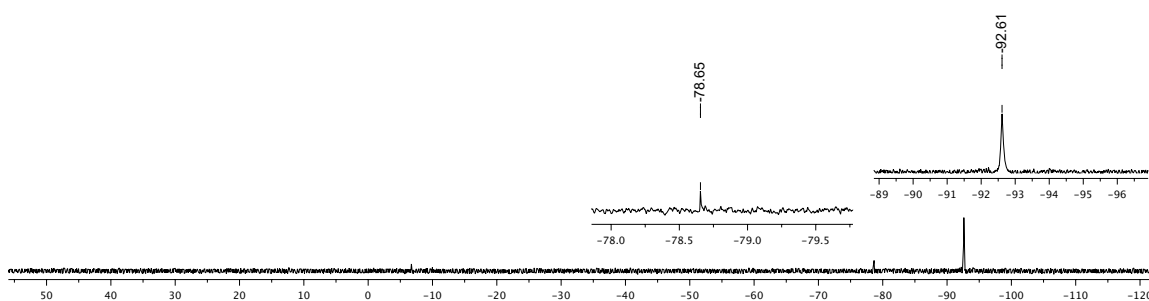


Figure 3.11. $^{31}\text{P}\{^1\text{H}\}$ NMR spectrum of the crude yellow precipitate from the reaction of PTA-Li and BCy_2Cl in CD_3OD .

The yellow precipitate dissolved in CD_3OD exhibited peaks at -6.72 ppm (4.03%), -78.65 ppm (0.91%), and -92.6 ppm (95.1%) (Figure 3.11). The peak at -6.72 ppm may be O=PTA and the peaks upfield may correspond to the N-bonded and α -methylene bonded BCy_2 . In D_2O , peaks at -2.60 ppm, -85.6 ppm and -98.0 ppm may correspond to O=PTA, PTA- BCy_2 , and PTA. Attempts to isolate the products were unsuccessful due to minute yield and inability to separate from PTA in addition to air and water sensitivity. However, the ESI m/z data correlates to the theoretical value of PTA- BCy_2 and O=PTA- BCy_2 (Figure 3.12).

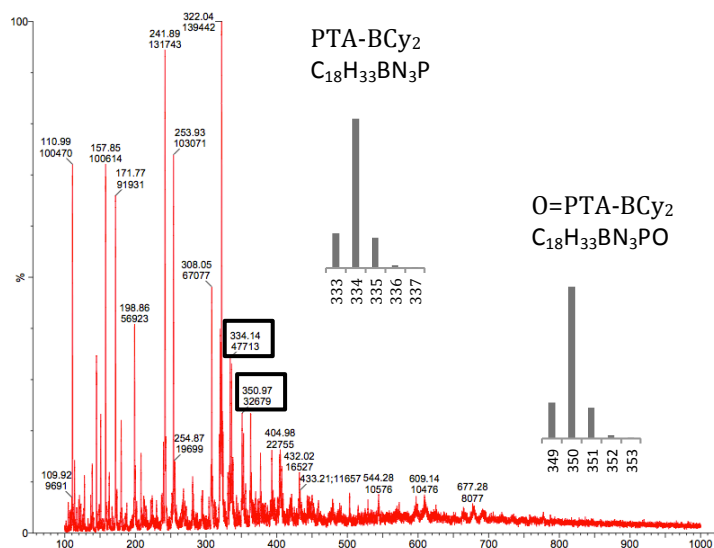


Figure 3.12. ESI+ mass spectrum of a crude reaction mixture of PTA-Li and BCy₂Cl in methanol. Inset shows the simulated isotopic distribution pattern for M⁺.

Several other attempts were made using a different solvent like toluene at 1:1 and 2:1 mole ratio of PTA-Li with BCy₂Cl. The reaction in THF in a 1:1 ratio (0.487 mmol) shows a clean reaction with the formation of a single, slightly broad peak at -79.6 ppm (Figure 3.13), somewhere near the average between the N-bound and P-bound PTA-boranyl adducts.

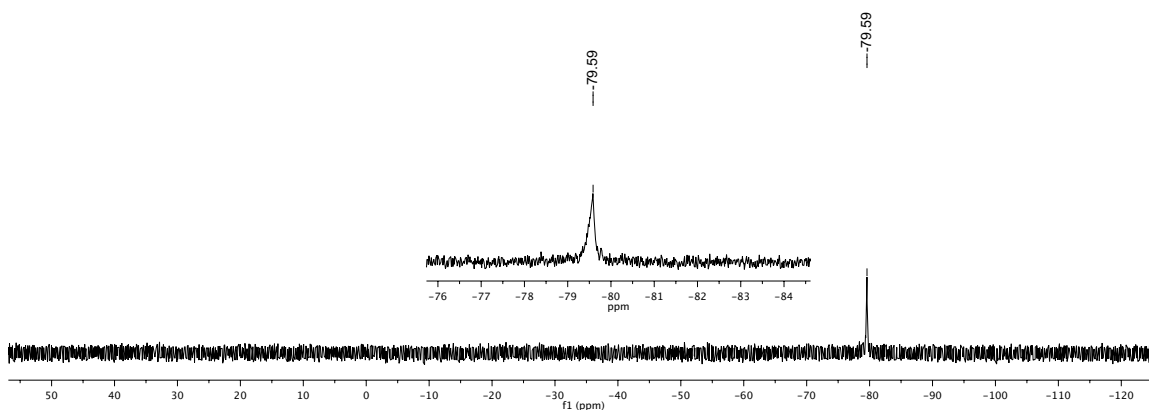


Figure 3.13. ³¹P{¹H} NMR spectrum of PTA-Li and BCy₂Cl in THF.

3.2.2 Reaction of PTA with BCy₂Cl

To aid in characterizing the products from the reaction of PTA-Li with BCy₂Cl, a similar NMR scale experiment was monitored for the reaction of PTA with BCy₂Cl in toluene (1 equiv., 0.20 mmol). The ³¹P{¹H} NMR spectra stacked together shows the formation of the PTA(N-BCy₂Cl) product as the PTA peak (top) disappears and the peak at -81.1 ppm appears after 30 minutes (Figure 3.15). This suggests that the peak at -81.4 ppm from the reaction of PTA-Li and BCy₂Cl is probably N-bound. In addition to the appearance of additional peaks due to the amine adducts, a test for air sensitivity shows that within just 3 hours (or less) of exposure to air, the boronated phosphine oxidizes and decompose into unidentified species (Figure 3.15).

To be able to gain detailed information on the reactivity of PTA, a systematic approach of adding increasing equiv. of BCy₂Cl can be monitored by ³¹P NMR which can then be compared to the results of the PTA-BH₃ study by Peruzzini and coworkers. Effective oxygen and moisture removal from organic solvents should be tested. To avoid sources of moisture contact with the product, optimizing NMR characterization procedure such as degassing (by freeze-pump-thaw cycles) and drying (over molecular sieves) deuterated solvent should be considered.¹⁶

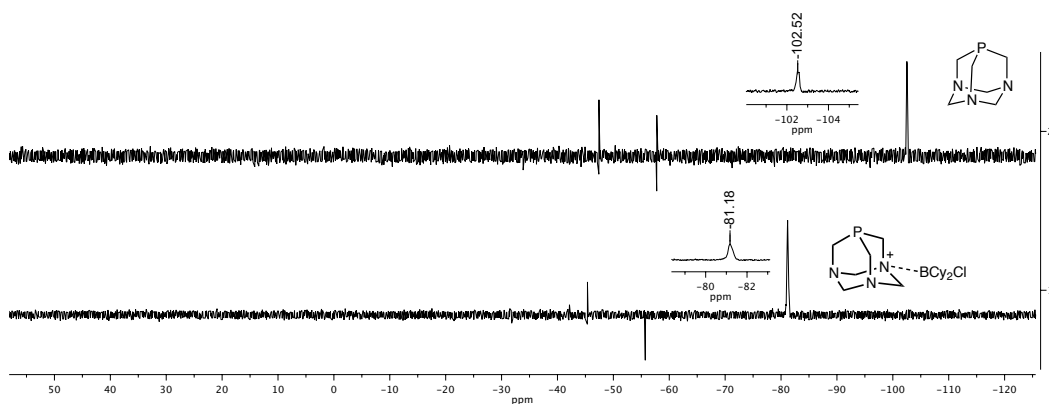


Figure 3.14. $^{31}\text{P}\{^1\text{H}\}$ NMR spectrum of PTA and BCy_2Cl in toluene. The PTA peak (top) disappears and a new peak downfield appears (bottom).

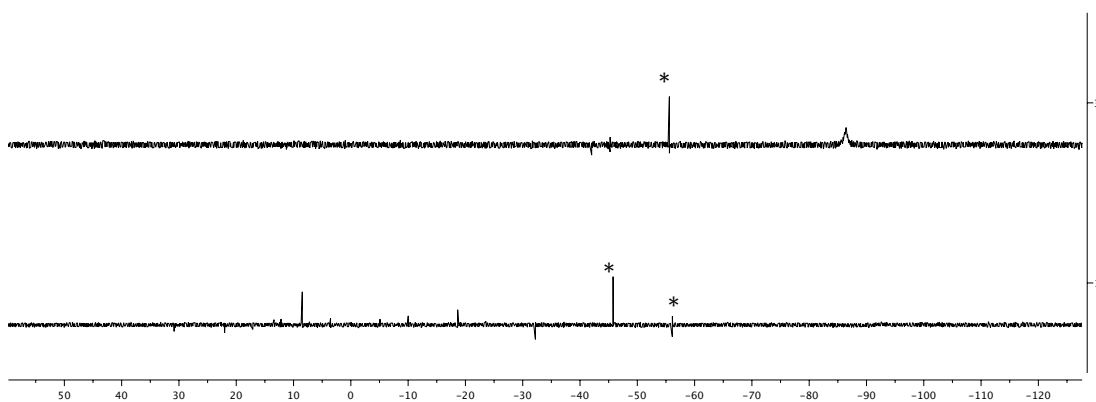
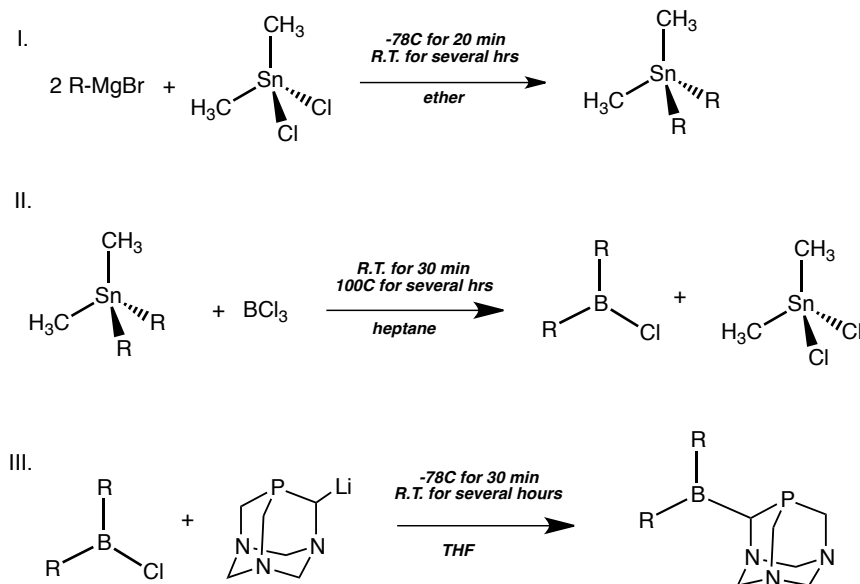


Figure 3.15. $^{31}\text{P}\{^1\text{H}\}$ NMR spectrum for air-sensitivity of PTA and BCy_2Cl in toluene. The solution in toluene (top) oxidizes and decomposes within 3 hours (bottom). *Unidentified

3.2.3 Attempted Synthesis of PTA-BPh₂

The synthetic method devised by Thomas and Peters¹⁷ to synthesize a variety of bis(phosphine)borates involve the reaction of SnR_2Me_2 and BCl_3 to form BR_2Cl . The first stage of their method is the generation of SnR_2Me_2 from a suitable Grignard reagent and SnMe_2Cl_2 . In this method, the relatively toxic and expensive alkyltin chloride can be recovered by simply decanting the solution. Heptane was the choice of solvent since ether

and THF can undergo cleavage by BCl_3 .⁵³ BPh_2Cl was obtained at 43% yield whereas literature reported 73% yield.



Scheme 3.6. Synthesis of BR_2PTA via BR_2Cl .

The difference in yield may be due to a large difference in the scale of the reaction which was originally reported at 5 g while this experiment was done at mg scale. Future experiments should be extended to about 48 hours to ensure a complete reaction. Nevertheless, for the purpose of conducting preliminary attempts, upon reaction with PTA-Li , the $^{31}\text{P}\{^1\text{H}\}$ NMR of the crude THF solution revealed 4 distinct peaks (-92.6 ppm, -90.1 ppm, -42.2 ppm, -12.0 ppm), as shown in Figure 3.17. The set of peaks upfield is unclear but it is similar to the resonance observed by Peruzzini and coworkers (-94.85 ppm, -92.37 ppm, and -93.45 ppm for mono-, bis-, and tris-boronated PTA, respectively).⁵² The peak at -42 ppm may correspond to the P-B adduct which is also similar to the observed $\delta^{31}\text{P}$ shift (-43.41 ppm) of the bis-boranyl species in which one BH_3 is N-bonded and the other, P-bonded. The tetrakis-boranyl adduct was previously

reported at -28.83 ppm by Perruzzini and coworkers. Meanwhile, the peak at -12 ppm could be the oxidized product from PTA(α -BPh₂) since O=PTA-BH₃ appears at -9.8 ppm.

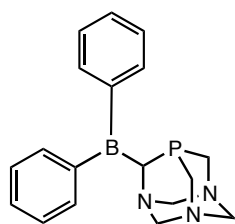


Figure 3.16. Depiction of PTA-BPh₂.

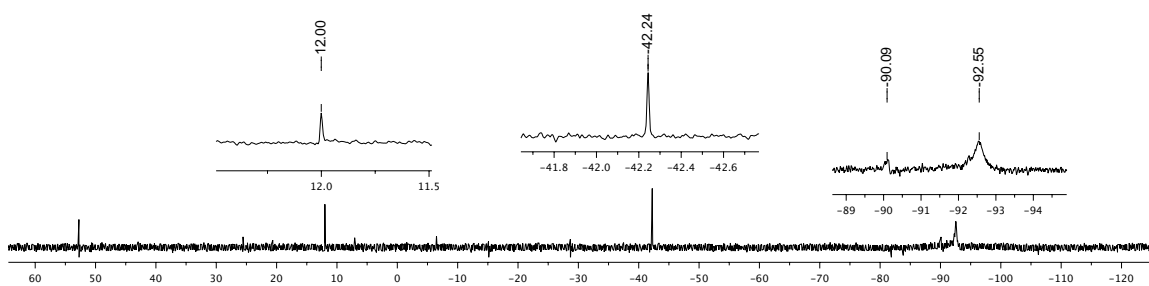


Figure 3.17. ³¹P{¹H} NMR spectrum of PTA-Li with BPh₂Cl in THF.

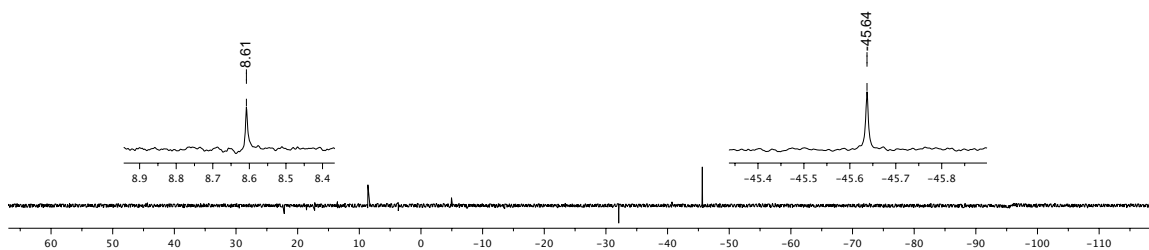


Figure 3.18. ³¹P{¹H} NMR spectrum of PTA-Li with BPh₂Cl in CDCl₃.

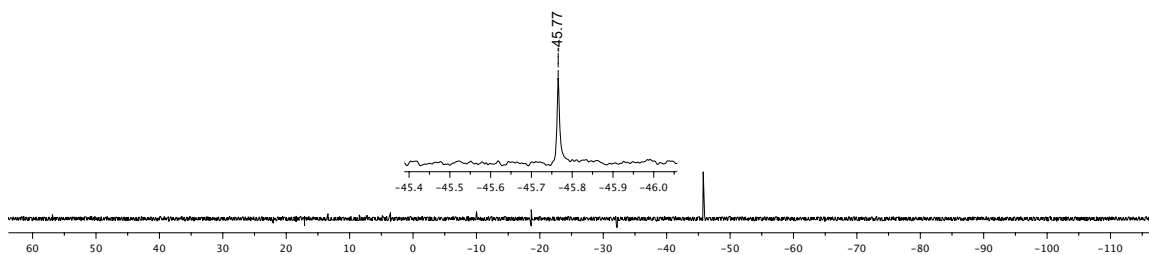


Figure 3.19. $^{31}\text{P}\{^1\text{H}\}$ NMR spectrum of PTA-Li with BPh_2Cl in CDCl_3 after washing with hexanes.

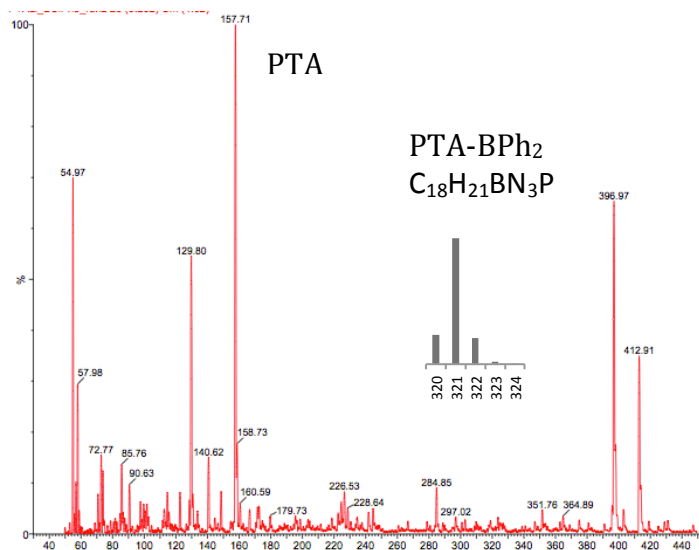


Figure 3.20. ESI+ mass spectrum of PTA-Li with BPh_2Cl in methanol. Inset shows the simulated isotopic distribution curve for PTA- BPh_2 (M^+).

The previous NMR sample was pulled dry and re-dissolved in CDCl_3 . Only 2 peaks at -8.5 ppm and -45.64 ppm was observed and upon washing with hexanes, the peak at -8.5 ppm was no longer observed (Figure 3.17, 3.18). The acquired ^1H NMR spectrum for this product (refer to Appendix) showed overlapping peaks at 7 to 8 ppm

which is the range for BPh_2Cl proton shifts. Weak resonance at 3-4 ppm, presumably from PTA, is difficult to identify. The computer-generated isotopic distribution pattern for BPh_2PTA is 321 m/z but the mass spectrum of the sample dissolved in methanol exhibited a PTA peak and unidentified peaks at 397 m/z and 412 m/z (Figure 3.20). Attempts to run the experiment in a systematic addition of excess BPh_2Cl is highly recommended in order to gain details on the reactivity of PTA-Li as well as the reaction of PTA with BPh_2Cl .

3.3 Concluding Remarks

Attempts at synthesizing the PTA-B compounds proved promise for the reactivity of PTA-Li but the presence of various side-products including N-coordination can be a challenge to isolate, in addition to the known air- and water-sensitivity of these compounds. Due to the hard-type acidic nature of borane, quenching by common O_2 and/or N_2 containing molecules can take place easily so the need to increase the steric demand around the Lewis base arises. The Frost group has a library of PTA derivatives that can be investigated for potential FLP systems. The boron/phosphorus FLPs can be assessed through solid state NMR as well as additional NMR parameters like ^{11}B chemical shifts that can provide information on the strength of the acid-base interaction.

3.4 Experimental

3.4.1 General

All manipulations, unless otherwise noted, were carried out on a double-manifold Schlenk vacuum line under nitrogen or in a nitrogen-filled glovebox. Glassware were oven dried overnight prior to use. Tetrahydrofuran (THF) was freshly distilled under nitrogen from sodium/benzophenone. Hexanes was freshly distilled under nitrogen. Heptane, ether, and toluene were dried with activated molecular sieves and degassed before use. n-BuLi, tin(IV) alkyl and aryl halides, BCl₃, and BCy₂Cl were all purchased from commercial sources and used as received. NMR solvents were purchased from Cambridge Isotopes and used as received. Tetrakis(hydroxymethyl)phosphonium chloride was obtained from Cytec and used without further purification. PTA was synthesized according to literature.^{54,55} NMR spectra were recorded with Varian 500 or MR400 spectrometers at 25°C unless otherwise stated. ¹H and ¹³C NMR spectra were referenced to residual solvent relative to tetramethylsilane (TMS). ³¹P shifts are relative to an external standard of 85% H₃PO₄ in D₂O with positive values downfield of the reference. Electrospray ionization mass spectra (ESI-MS) were recorded on a Waters Micromass 20 ESI mass spectrometer (positive ion mode).

3.4.2 Synthesis

Reaction of PTA-Li with BCy₂Cl

An NMR scale experiment was done by adding BCy₂Cl (0.400 mL, 0.400 mmol from 1.0 M hexane solution) to a 0.5 mL solution of PTA-Li (66.4 mg, 0.407 mmol) in THF. The milky white solution turned yellowish upon addition of the clear liquid BCy₂Cl. A series of ³¹P{¹H} NMR spectra was acquired every 15 minute interval at

35°C. The kinetic $^{31}\text{P}\{^1\text{H}\}$ NMR spectra for this reaction is shown in the appendix.
 $^{31}\text{P}\{^1\text{H}\}$ NMR (162 MHz, THF): δ -81 ppm, -22 ppm.

In a separate experiment, a schlenk flask was charged with PTA-Li (0.2149 g, 1.146 mmol) and suspended in 15 mL THF. This flask was cooled to -78°C and BCy_2Cl (1.10 mL, 1.1 mmol) was added dropwise for 30 seconds via syringe. The resulting mixture was left to stir at -78°C for 30 minutes, after which the solution was slowly warmed to room temperature. The initial milky white suspension turned into a pale yellow solution over a few minutes. The solution was kept stirring at room temperature. Subsequent addition of THF was done to keep the solution from drying out. A crude ^{31}P NMR of the resulting cloudy, orange mixture was acquired. $^{31}\text{P}\{^1\text{H}\}$ NMR (162 MHz, THF): δ 129.85 ppm, 67.04 ppm, -41.52 ppm, -85.31 ppm, -95.72 ppm, -105.50 ppm. The mixture was simply filtered over celite. A ^{31}P NMR of the clear orange mixture (THF-soluble product) was acquired. $^{31}\text{P}\{^1\text{H}\}$ NMR (162 MHz, THF): δ -67.44 ppm, -81.24 ppm, -88.19 ppm, -100.19 ppm. The clear orange THF solution was then pulled dry under vacuum. $^{31}\text{P}\{^1\text{H}\}$ NMR in C_6D_6 and CD_3OD were acquired separately. $^{31}\text{P}\{^1\text{H}\}$ NMR (162 MHz, C_6D_6): δ -100.76 ppm, -49.43 ppm. $^{31}\text{P}\{^1\text{H}\}$ NMR (162 MHz, CD_3OD): δ -6.87 ppm, -67.05 ppm, -83.77 ppm, -96.42 ppm. The yellow solid (THF insoluble product) was dissolved in CD_3OD . $^{31}\text{P}\{^1\text{H}\}$ NMR (162 MHz, CD_3OD): δ -78.6 ppm, -92.61 ppm. NMR scale reaction in THF was done by mixing PTA-Li (0.0317 g, 0.200 mmol) with BCy_2Cl (0.20 ml, 0.200 mmol). $^{31}\text{P}\{^1\text{H}\}$ NMR (162 MHz, THF): δ -79.6 ppm.

Reaction of PTA with BCy₂Cl

An NMR scale experiment was conducted by adding BCy₂Cl (0.20 mL, 0.20 mmol) to a 0.5 mL solution of PTA (0.0317 g, 0.202 mmol) in toluene. The milky white suspension turned into pale yellow. After 30 minutes, a ³¹P{¹H} NMR spectra was acquired at 25°C. ³¹P{¹H} NMR (162 MHz, toluene): δ -81.2 ppm. This sample was diluted to test for air sensitivity. ³¹P{¹H} NMR (162 MHz, toluene, diluted): δ -86.63 ppm, -55.62 ppm. ³¹P{¹H} NMR (162 MHz, toluene, air-exposed 3 hours): δ 8.57 ppm, 3.55 ppm, -10.27 ppm, -18.83 ppm, -45.94 ppm.

Attempted synthesis of PTA-BPh₂

Synthesis of Dimethyldiphenyltin, SnMe₂Ph₂

The Grignard reagent, PhMgBr, was prepared with the corresponding aryl bromide. A schlenk flask charged with magnesium turnings was purged with nitrogen for at least 3 minutes before adding anhydrous ether. The flask was placed in an oil bath at 35-40°C before the addition of PhMgBr. The solution was allowed to reflux for a few hours before filtering through celite. The filtrate is collected in a pre-weighed schlenk flask and solvent is pulled dry under vacuum for 2 days. The Grignard reagent was assumed at 75% recovery and the corresponding equiv. of dimethyltin dichloride was added. After 24 hours, the mixture was pulled dry. The resulting solid was washed with hexanes and MgBr₂/MgCl₂ filtered over celite. The dimethyldiphenyltin was collected as a pale yellow oil and characterized based on previous literature data for Me₂SnPh₂.¹⁷

¹H NMR (400 MHz, CDCl₃): δ 7.54 (m), 7.36 (m), 0.53 (s, ²J_{Sn-H} = 54 Hz).

Synthesis of Diphenylchloroborane, Ph₂BCl

This method was adapted from the reported synthesis of different R₂BCl compounds by Thomas and Peters.¹⁶ Dimethyldiphenyltin (0.6181g, 2.04 mmol) was weighed in a thick-walled vial. Degassed heptane was added followed by BCl₃ (2.04 mL, 1 M heptane solution). The vial was sealed and allowed stir for 30 minutes at room temperature after which it was transferred to an oil bath (100°C). The pale yellow solution was left to stir for about 48 hours. Upon cooling down to room temperature, dimethyltin dichloride crashed out. The solution was decanted and evaporated to dryness under reduced pressure to obtain a pale yellow oil. Any traces of dimethyltin dichloride that wasn't effectively removed by decanting was removed by vacuum distillation. The sample was used without further purification. Characterization was based on previous literature data.¹⁷ ¹H NMR (400 MHz, CDCl₃): δ 8.05 ppm (d), 7.65 ppm (t), 7.54 ppm (t). ¹³C {¹H} NMR (75.4 MHz, CDCl₃): δ 137.2 ppm, 133.1 ppm, 128.0 ppm.

Synthesis of 1,3,5-Triaza-7-phosphaadamantane-6-yllithium (PTA-Li)

The synthesis of PTA-Li was previously reported by our group.⁵⁶ To a suspension of dried PTA (3.10 g, 19.7 mmol) in 40 mL of THF was slowly added at room temperature *n*-butyllithium (2.5 M, 11 mL, 27.5 mmol) over the course of 5 min. The reaction was stirred at room temperature until the evolution of butane was no longer observed (approximately 2.5-3 h). The suspension was filtered under nitrogen and the precipitate washed with hexanes (2 × 15 mL), resulting in 3.20 g of a fine white highly pyrophoric powder. A yield of >90% for the synthesis of PTA-Li was determined by quenching PTA-Li with D₂O and measuring the ratio of PTA/PTA-D by ³¹P spectroscopy. PTA-D was characterized by ¹H, ¹³C {¹H} and ³¹P {¹H} NMR

spectroscopies in D₂O and in CDCl₃. ¹H NMR (400 MHz, D₂O): 4.48 and 4.43 ppm (AB quartet, J = 12.4 Hz, 6H, NCH₂N), 3.91 ppm (d, ²J_{PH} = 8.8 Hz, 5H, PCH₂N, PCHDN). ¹³C{¹H} NMR (100 MHz, D₂O): 70.8 ppm (t, J_{PC} = 2.0 Hz, 3C, NCH₂N), 47.7 ppm (d, ¹J_{PC} = 19.6 Hz, 1C, PCH₂N), 47.6 ppm (d, ¹J_{PC} = 19.6 Hz, 1C, PCH₂N), 47.3 (~1:2:2:1 quartet, ¹J_{PC} = 21.1 Hz, ¹J_{DC} = 21.1 Hz, 1C, PCHDN). ³¹P{¹H} NMR (162 MHz, D₂O): -98.8 ppm (s, PTA-D), -98.4 ppm (s, PTA). PTA-D was also characterized in CDCl₃. The solvent of the D₂O solution was removed under reduced pressure. The resulting solid was dissolved in CDCl₃ followed by filtration to remove the lithium salts (LiOD). ¹H NMR (400 MHz, CDCl₃): δ 4.60 ppm (s, 6H, NCH₂N), 4.05 ppm (d, ²J_{PH} = 10.0 Hz, 5H, PCH₂N, PCHDN). ¹³C{¹H} NMR (100 MHz, CDCl₃): δ 73.66 ppm (vt, J_{PC} = 2 Hz, 3C, NCH₂N), 50.6 ppm (d, ¹J_{PC} = 20.6 Hz, 1C, PCH₂N), 50.5 ppm (d, ¹J_{PC} = 20.6 Hz, 1C, PCH₂N), 50.2 (~1:2:2:1 quartet, ¹J_{PC} = 21.1 Hz, ¹J_{DC} = 21.1 Hz, 1C, PCHDN). ³¹P{¹H} NMR (162 MHz, CDCl₃): δ -102.5 ppm (s, PTA-D), -102.1 ppm (s, PTA).

Attempted reaction of PTA-Li with BPh₂Cl

A schlenk flask was charged with 0.1413 g PTA-Li (0.861 mmol) and 10 mL freshly distilled THF added. The solution was placed in a dry ice/acetone bath (-78°C) before transferring a THF solution of BPh₂Cl (0.1746 g, 0.871 mmol) via cannula. The solution turned from milky white to yellow-orange within a few minutes. After 30 minutes of stirring, the flask was taken out of the dry ice/acetone bath and allowed to stir at room temperature for 3 days. Within this time frame, the solution ran dry and THF was added accordingly. The solution was concentrated to about 3 mL to obtain a ³¹P{¹H} NMR sample of the crude solution. ³¹P{¹H} NMR (162 MHz, THF): δ -92.6 ppm, -90

ppm, -42ppm, -12 ppm. The crude solution was pulled dry under reduced pressure and redissolved in CDCl₃. ³¹P{¹H} NMR (162 MHz, CDCl₃): δ -8.5 ppm, -45.64 ppm. The previous sample was washed with hexanes, pulled dry under vacuum, and redissolved in CDCl₃. ³¹P{¹H} NMR (162 MHz, CDCl₃): δ -45.77 ppm.

3.5 References

- (1) Stephan, D. W. *Org. Biomol. Chem.* **2008**, *6*, 1535–1539.
- (2) Wiegand, T.; Eckert, H.; Ekkert, O.; Froehlich, R.; Kehr, G.; Erker, G.; Grimme, S. *J. Am. Chem. Soc.* **2012**, *134*, 4236–4249.
- (3) Stephan, D. W. *Dalton Trans.* **2009**, 3129–3136.
- (4) Brown, H. C.; Schlesinger, H. I.; Cardon, S. Z. *J. Am. Chem. Soc.* **1942**, *64*, 325–329.
- (5) Welch, G. C.; San Juan, R. R.; Masuda, J. D.; Stephan, D. W. *Sci. Wash. DC U. S.* **2006**, *314*, 1124–1126.
- (6) Paradies, J. *Angew. Chem. Int. Ed.* **2014**, *53*, 3552–3557.
- (7) Stephan, D. W.; Erker, G. *Angew. Chem. Int. Ed.* **2010**, *49*, 46–76.
- (8) Jiang, C.; Stephan, D. W. *Dalton Trans.* **2013**, *42*, 630–637.
- (9) Stephan, D. W.; Erker, G. *Chem. Sci.* **2014**, *5*, 2625–2641.
- (10) Takenaga, N. *Yuki Gosei Kagaku Kyokaishi* **2010**, *68*, 409–410.
- (11) Stephan, D. W.; Greenberg, S.; Graham, T. W.; Chase, P.; Hastie, J. J.; Geier, S. J.; Farrell, J. M.; Brown, C. C.; Heiden, Z. M.; Welch, G. C.; Ullrich, M. *Inorg. Chem.* **2011**, *50*, 12338–12348.
- (12) Wang, P.; Sun, X.; Gao, P. *Youji Huaxue* **2011**, *31*, 1369–1376.
- (13) Erker, G. *Pure Appl. Chem.* **2012**, *84*, 2203–2217.
- (14) Stephan, D. W. *Org. Biomol. Chem.* **2012**, *10*, 5740–5746.
- (15) Kehr, G.; Schwendemann, S.; Erker, G. *Top. Curr. Chem.* **2013**, *332*, 45–84.
- (16) Thomas, J. C.; Peters, J. C. *Inorg. Chem.* **2003**, *42*, 5055–5073.
- (17) Zhao, X.; Stephan, D. W. *J. Am. Chem. Soc.* **2011**, *133*, 12448–12450.
- (18) Voss, T.; Sortais, J.-B.; Frohlich, R.; Kehr, G.; Erker, G. *Organometallics* **2011**, *30*, 584–594.
- (19) Voss, T.; Chen, C.; Kehr, G.; Nauha, E.; Erker, G.; Stephan, D. W. *Chem. - Eur. J.* **2010**, *16*, 3005–3008, S3005/1–S3005/7.
- (20) Tanur, C. A.; Stephan, D. W. *Organometallics* **2011**, *30*, 3652–3657.
- (21) Liedtke, R.; Froehlich, R.; Kehr, G.; Erker, G. *Organometallics* **2011**, *30*, 5222–5232.
- (22) Dureen, M. A.; Brown, C. C.; Stephan, D. W. *Organometallics* **2010**, *29*, 6594–6607.
- (23) Dureen, M. A.; Stephan, D. W. *J. Am. Chem. Soc.* **2009**, *131*, 8396–8397.

- (24) Chen, C.; Froehlich, R.; Kehr, G.; Erker, G. *Chem. Commun. Camb. U. K.* **2010**, *46*, 3580–3582.
- (25) Dureen, M. A.; Welch, G. C.; Gilbert, T. M.; Stephan, D. W. *Inorg. Chem.* **2009**, *48*, 9910–9917.
- (26) Peuser, I.; Neu, R. C.; Zhao, X.; Ulrich, M.; Schirmer, B.; Tannert, J. A.; Kehr, G.; Froehlich, R.; Grimme, S.; Erker, G.; Stephan, D. W. *Chem. - Eur. J.* **2011**, *17*, 9640–9650, S9640/1–S9640/38.
- (27) Zhao, X.; Stephan, D. W. *Chem. Commun. Camb. U. K.* **2011**, *47*, 1833–1835.
- (28) Otten, E.; Neu, R. C.; Stephan, D. W. *J. Am. Chem. Soc.* **2009**, *131*, 9918–9919.
- (29) Cardenas, A. J. P.; Culotta, B. J.; Warren, T. H.; Grimme, S.; Stute, A.; Froehlich, R.; Kehr, G.; Erker, G. *Angew. Chem. Int. Ed.* **2011**, *50*, 7567–7571, S7567/1–S7567/41.
- (30) Menard, G.; Stephan, D. W. *Angew. Chem. Int. Ed.* **2012**, *51*, 4409–4412, S4409/1–S4409/5.
- (31) Travis, A. L.; Binding, S. C.; Zaher, H.; Arnold, T. A. Q.; Buffet, J.-C.; O'Hare, D. *Dalton Trans.* **2013**, *42*, 2431–2437.
- (32) Ohrenberg, C.; Ge, P.; Schebler, P.; Riordan, C. G.; Yap, G. P. A.; Rheingold, A. L. *Inorg. Chem.* **1996**, *35*, 749–754.
- (33) Ge, P.; Riordan, C. G.; Yap, G. P. A.; Rheingold, A. L. *Inorg. Chem.* **1996**, *35*, 5408–5409.
- (34) Schebler, P. J.; Riordan, C. G.; Guzei, I. A.; Rheingold, A. L. *Inorg. Chem.* **1998**, *37*, 4754–4755.
- (35) Ohrenberg, C.; Liable-Sands, L. M.; Rheingold, A. L.; Riordan, C. G. *Inorg. Chem.* **2001**, *40*, 4276–4283.
- (36) Ge, P.; Rheingold, A. L.; Riordan, C. G. *Inorg. Chem.* **2002**, *41*, 1383–1390.
- (37) Kula, M. R.; Amberger, E.; Mayer, K. K. *Chem. Ber.* **1965**, *98*, 634–637.
- (38) Wilt, J. W.; Belmonte, F. G.; Zieske, P. A. *J. Am. Chem. Soc.* **1983**, *105*, 5665–5675.
- (39) Harada, G.; Yoshida, M.; Iyoda, M. *Chem. Lett.* **2000**, 160–161.
- (40) Wursthorn, K. R.; Kuivila, H. G.; Smith, G. F. *J. Am. Chem. Soc.* **1978**, *100*, 2779–2789.
- (41) Reich, H. J.; Holladay, J. E.; Mason, J. D.; Sikorski, W. H. *J. Am. Chem. Soc.* **1995**, *117*, 12137–12150.
- (42) Nagelberg, S. B.; Reinhold, C. E.; Willeford, B. R.; Bigwood, M. P.; Molloy, K. C.; Zuckerman, J. J. *Organometallics* **1982**, *1*, 851–858.
- (43) Rieke, R. D.; Tucker, I.; Milligan, S. N.; Wright, D. R.; Willeford, B. R.; Radonovich, L. J.; Eyring, M. W. *Organometallics* **1982**, *1*, 938–950.
- (44) Wada, M.; Wakamori, H.; Hiraiwa, A.; Erabi, T. *Bull. Chem. Soc. Jpn.* **1992**, *65*, 1389–1391.
- (45) Chambers, R. D.; Chivers, T. *J. Chem. Soc.* **1965**, 3933–3939.
- (46) Parks, D. J.; Piers, W. E.; Yap, G. P. A. *Organometallics* **1998**, *17*, 5492–5503.
- (47) Frost, B. J.; Mebi, C. A.; Gingrich, P. W. *Eur. J. Inorg. Chem.* **2006**, 1182–1189.
- (48) Bolano, S.; Albinati, A.; Bravo, J.; Gonsalvi, L.; Peruzzini, M. *Inorg. Chem. Commun.* **2006**, *9*, 360–363.
- (49) Bhatt, M. V.; Kulkarni, S. U. *Synthesis* **1983**, 249–282.

- (50) Daigle, D. J. *Inorg. Synth.* **1998**, 32, 40–45.
- (51) Daigle, D. J.; Pepperman, A. B., Jr.; Vail, S. L. *J. Heterocycl. Chem.* **1974**, 11, 407–408.
- (52) Wong, G. W.; Harkreader, J. L.; Mebi, C. A.; Frost, B. J. *Inorg. Chem.* **2006**, 45, 6748–6755.

Chapter 4

General Conclusions

Preparation of various stannylated, silylated, and borylated PTA derivatives were attempted via PTA-Li. Successful isolation of the water-soluble PTA-SnMe₃ and O=PTA-SnMe₃ can provide insight into future attempts at isolating other derivatives. Full characterization of the compounds including X-ray analysis is recommended. Synthesis of the silylated derivative, PTA-SiMe₃, was attempted and initial characterization suggests a possible mixture of the N- and α -methylene bound SiMe₃. PTAH⁺ was also found as a potential side-product since the starting materials, SnMe₃Cl and SiMe₃Cl, react readily with traces of water. In pursuit of bis-PTA derivatives via SnR₂Cl₂ and SiR₂Cl₂, mixtures of the mono- and -disubstituted products were encountered. Open-ring PTA derivatives were also likely to be present. To expand the source for data comparison, additional reactivity studies of PTA with organotin and organosilicon chlorides is recommended. This includes investigating the effects of adding different equivalents of the reactants in different solvents particularly on whether there is a preference for binding on either phosphorus or nitrogen. Due to the possibility of autoassociation between tin and silicon compounds, varying concentrations and temperatures should also be considered.

The synthesis of PTA-BR₂ (R = Cy, Ph) was pursued because of the potential frustrated lewis pair reactivity. The reaction of PTA-Li with BCy₂Cl and BPh₂Cl provided a number of side products in attempt to carry out the reaction in a large scale and to isolate the products. The seemingly straightforward reaction is limited by the sensitivity of the starting materials and the final products to air and moisture, leading to a

significant decrease in yield. Methods to assure effective oxygen and moisture removal from starting materials and solvents, including deuterated solvents should be considered. Previous studies with phosphinoborates indicated deoxygenation and drying organic solvents by thorough sparging with N₂ followed by passage through activated alumina column or drying by storing over molecular sieves. Furthermore, general addition of excess PTA-Li in these electrophilic addition reactions can improve overall yield since PTA-Li contains about 10% PTA. Attempts to crystallize products should be carried out in the dry box. Future related studies on the reactivity towards transition metals for catalysis such as tungsten and ruthenium and their application in hydration reactions in comparison to other upper-rim PTA derivatives is highly recommended.

APPENDIX

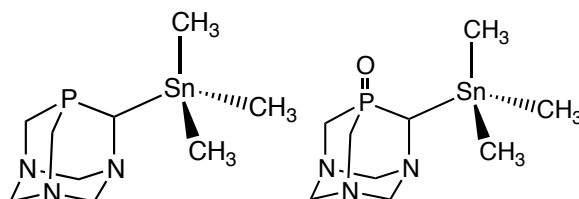


Figure A-1. Depiction of PTA-SnMe₃ (**1**) and O=PTA-SnMe₃ (**2**)

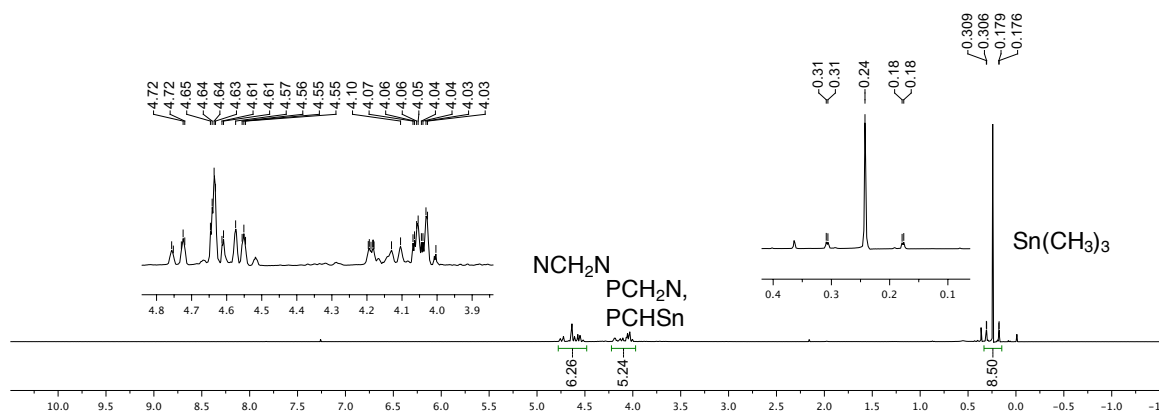


Figure A-2. ¹H NMR of PTA-SnMe₃ in CDCl₃.

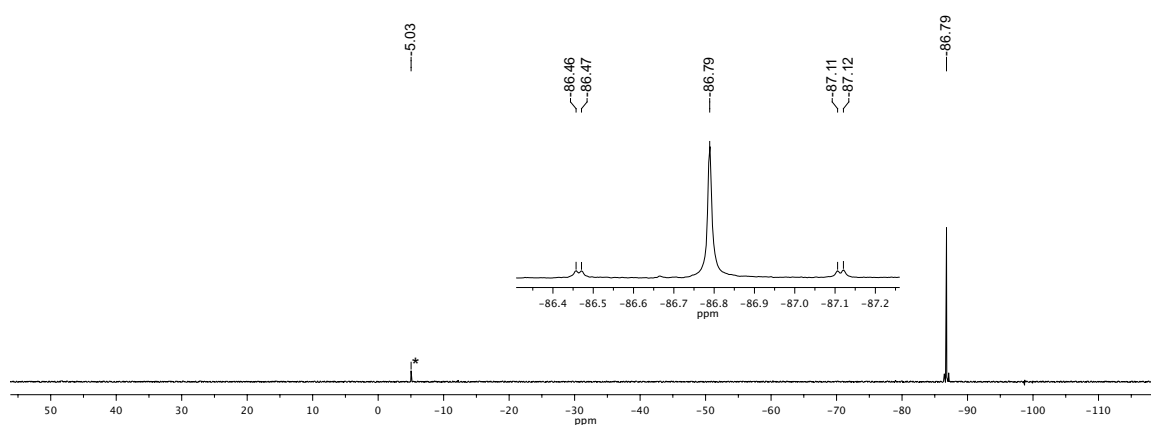
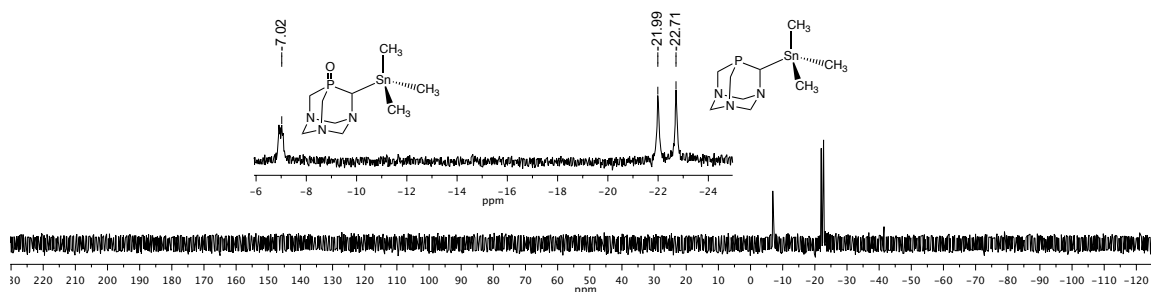
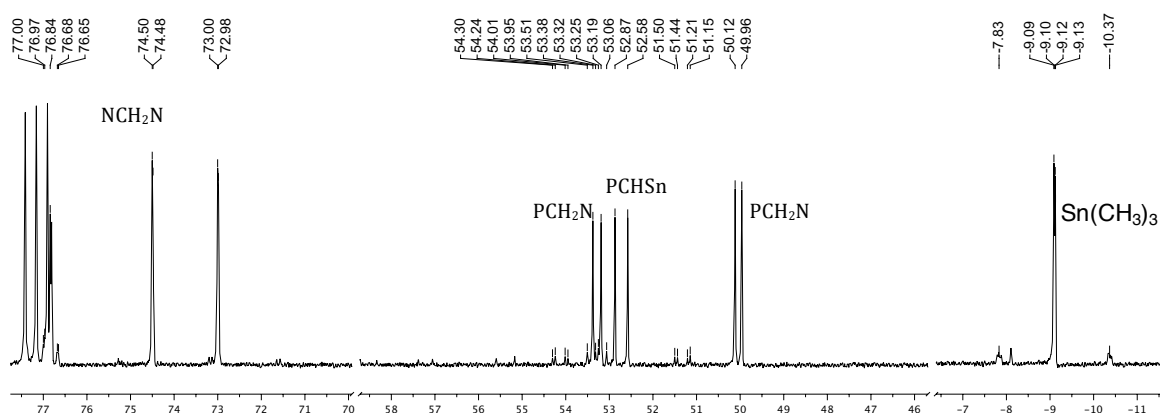
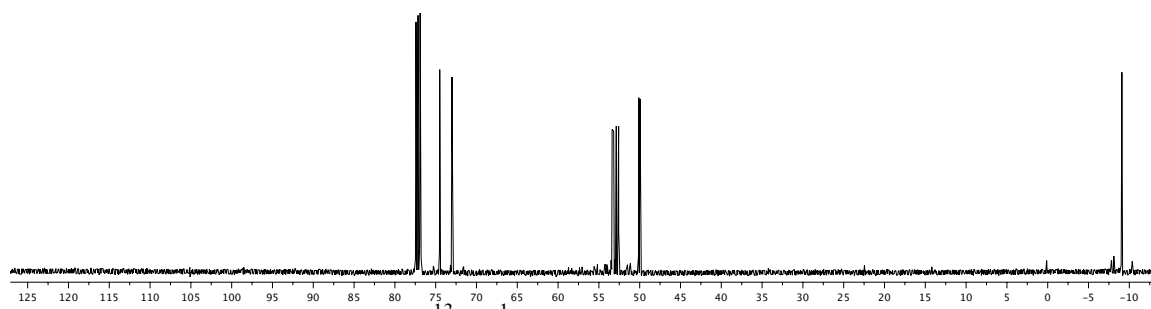


Figure A-3. Full ³¹P {¹H} NMR of PTA-SnMe₃ in CDCl₃. *Oxidized product



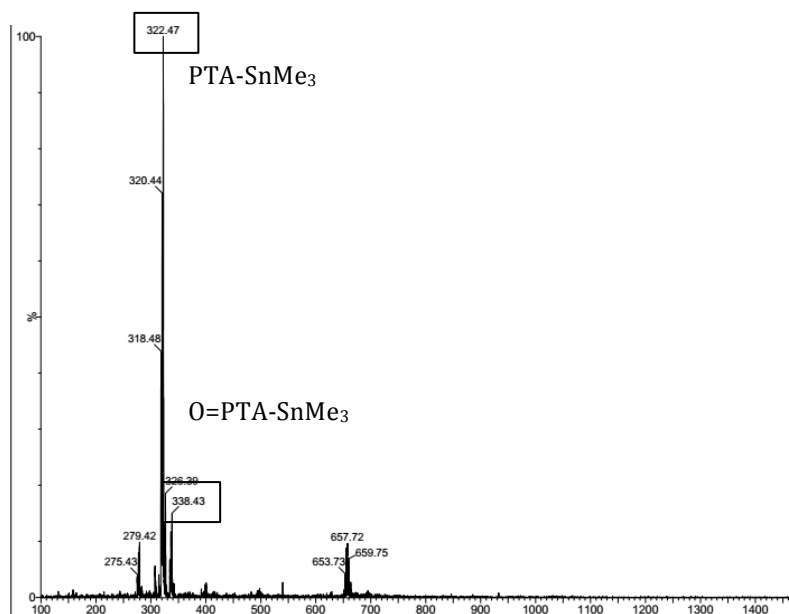


Figure A-7. Full electrospray mass spectrum (positive mode) of PTA-SnMe₃ and O=PTA-SnMe₃.

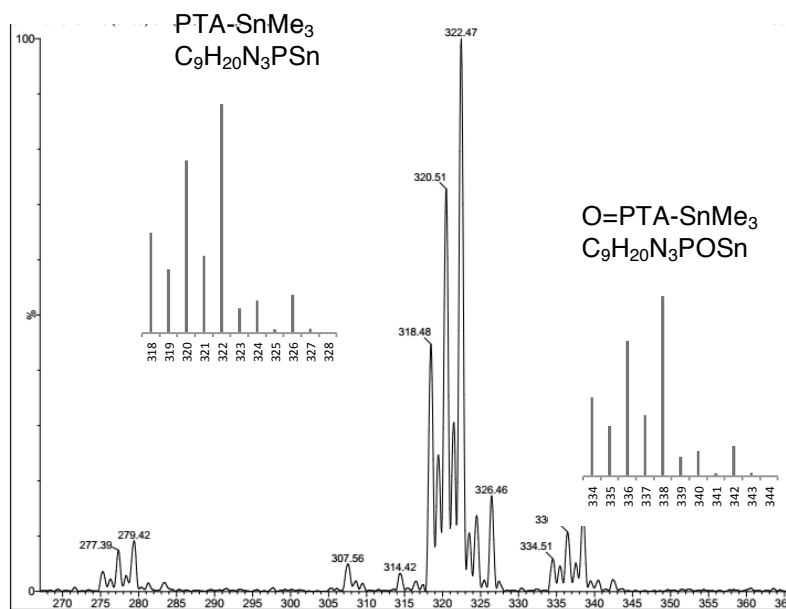
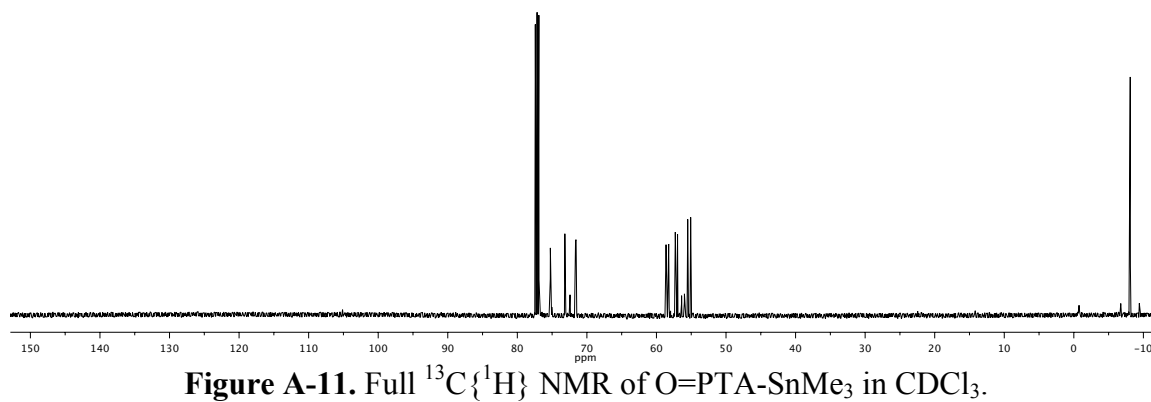
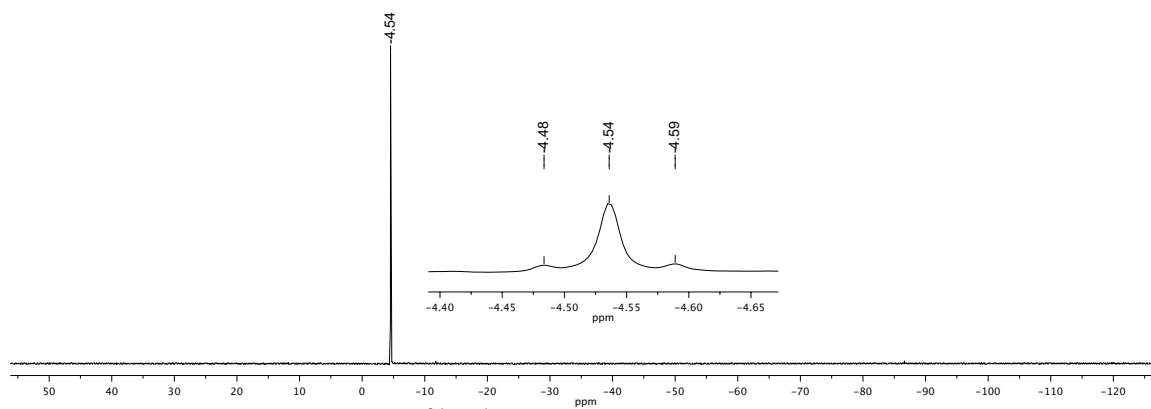
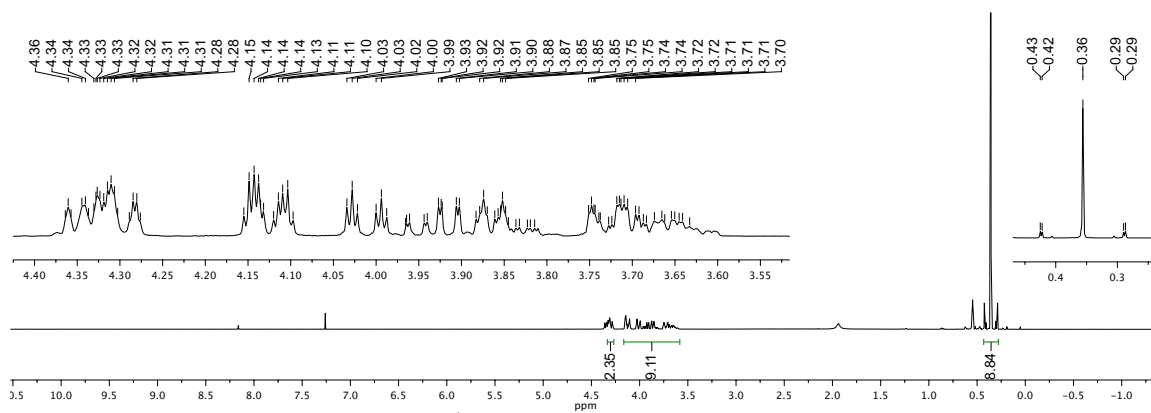


Figure A-8. Expanded electrospray mass spectrum (positive mode) of PTA-SnMe₃ and O=PTA-SnMe₃. Inset shows the simulated isotopic distribution pattern (MH⁺) for PTA-SnMe₃.



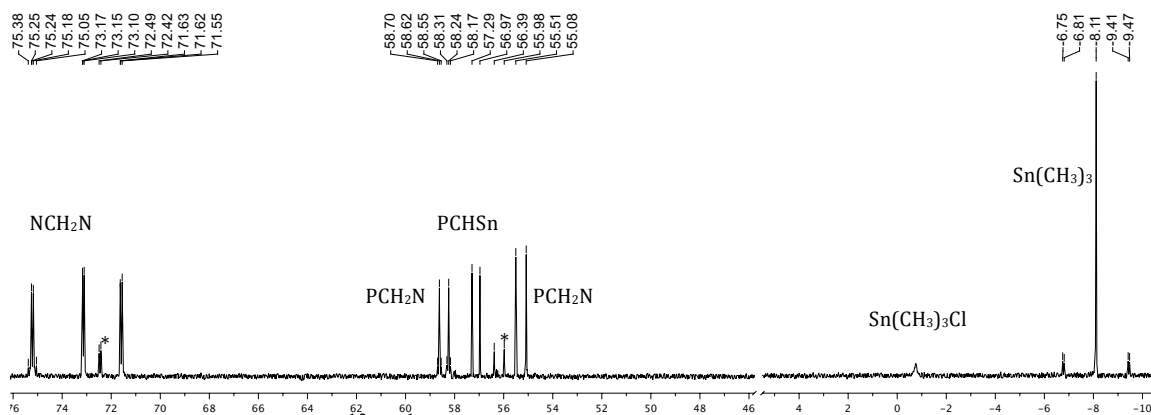


Figure A-12. Expanded $^{13}\text{C}\{^1\text{H}\}$ NMR of $\text{O}=\text{PTA}-\text{SnMe}_3$ in CDCl_3 . *Possibly trace $\text{O}=\text{PTA}$

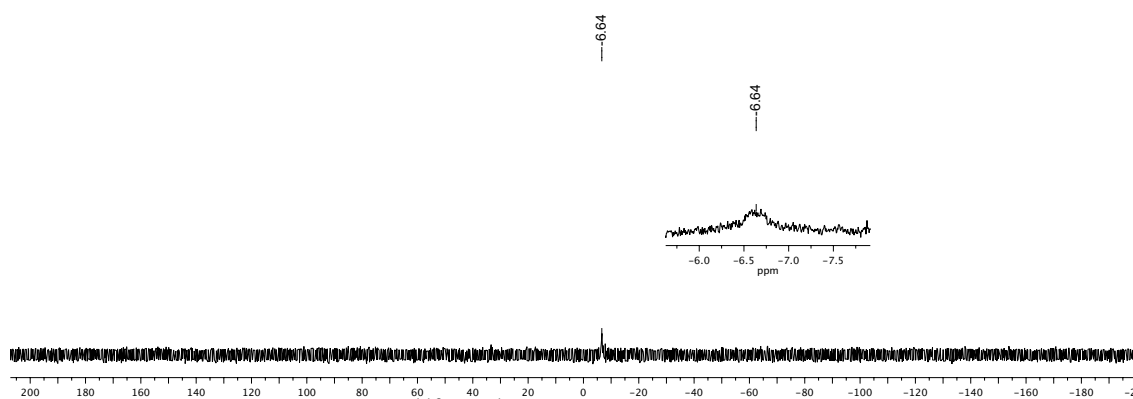


Figure A-13. Full $^{119}\text{Sn}\{^1\text{H}\}$ NMR of $\text{O}=\text{PTA}-\text{SnMe}_3$ in CDCl_3 .

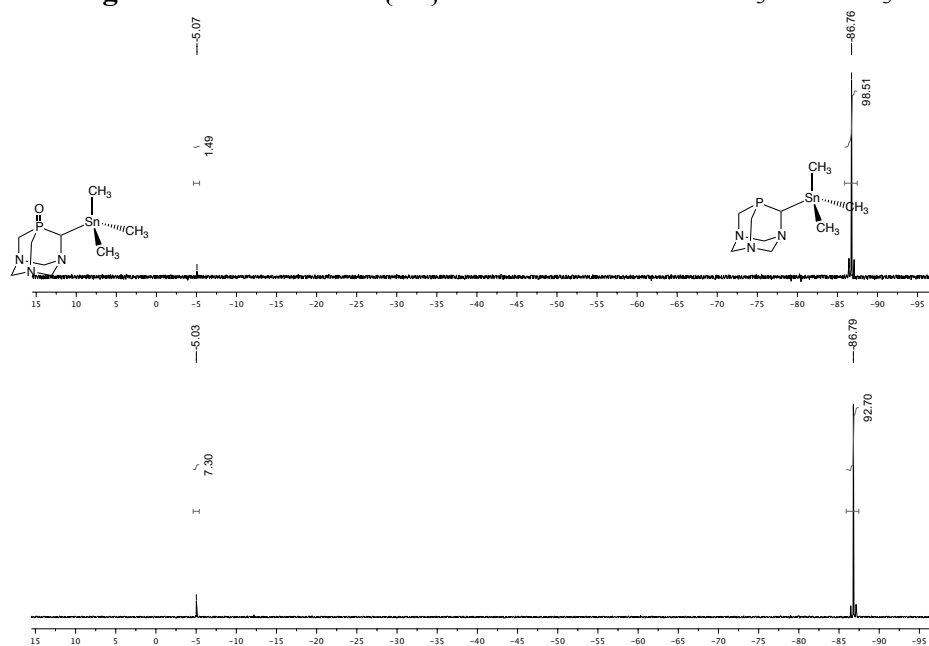


Figure A-14. Oxidation rate of $\text{PTA}-\text{SnMe}_3$ to $\text{O}=\text{PTASnMe}_3$ over 24 hrs in CDCl_3 . (top: original sample, bottom: sample after 24 hrs).

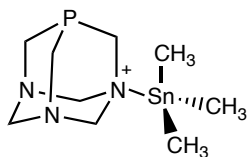


Figure B-1. Depiction of PTA(N-SnMe₃) (**3**).

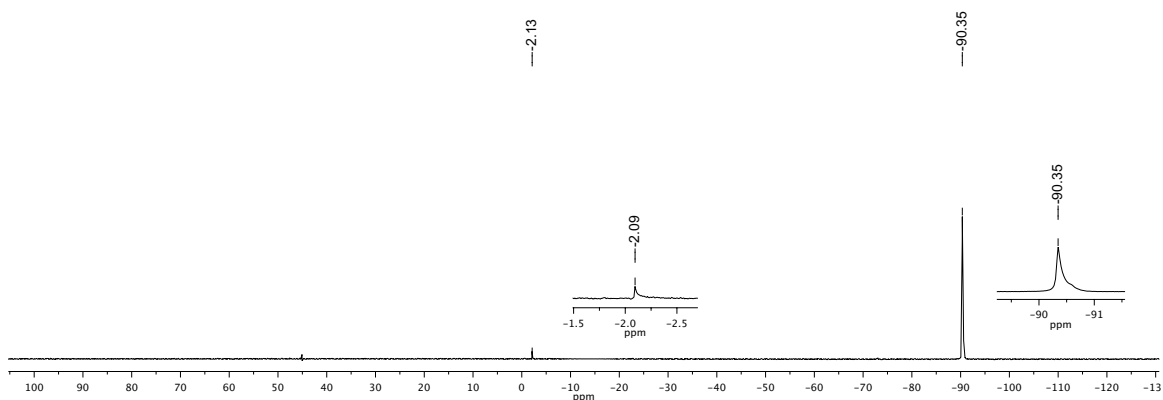


Figure B-2. Full $^{31}\text{P}\{^1\text{H}\}$ NMR of PTA with 1.1 equiv. SnMe₃Cl in D₂O.

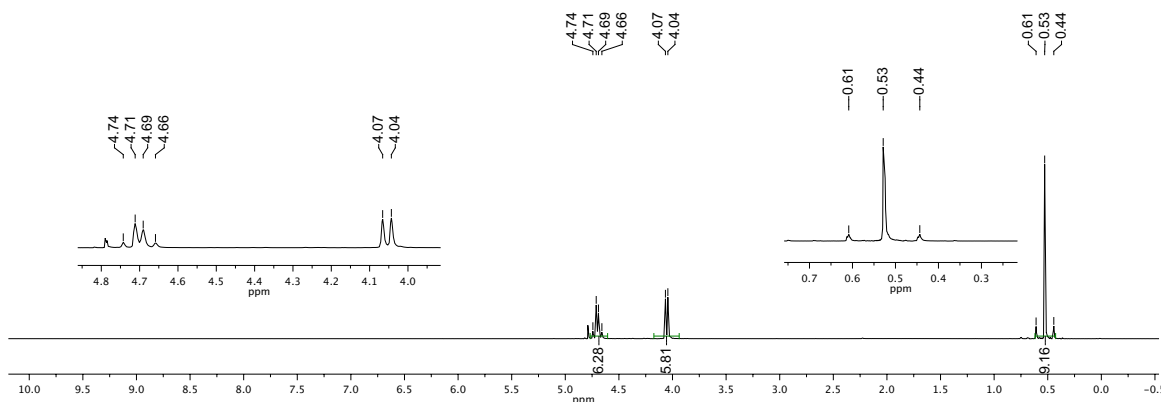


Figure B-3. Full ^1H NMR of PTA with 1.1 equiv. SnMe₃Cl in D₂O.

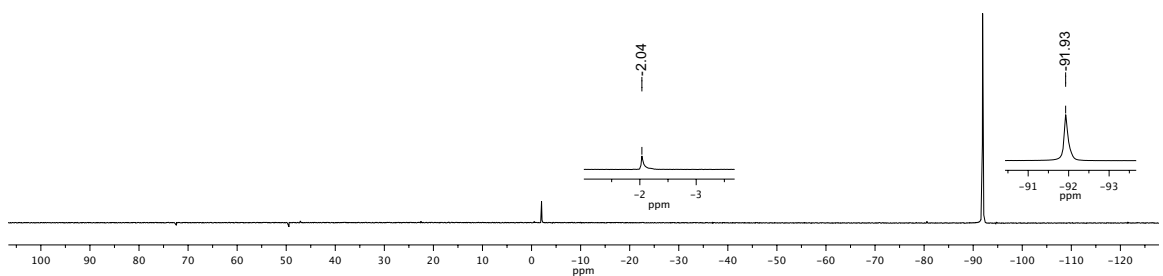


Figure B-4. Full $^{31}\text{P}\{^1\text{H}\}$ NMR of PTA (4 equiv. excess) with SnMe₃Cl in D₂O.

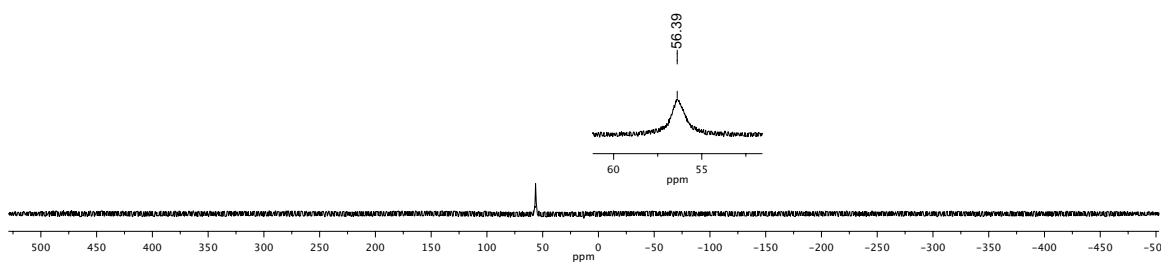


Figure B-5. Full ^{119}Sn $\{^1\text{H}\}$ NMR spectrum of PTA (4 equiv. excess) with SnMe_3Cl in D_2O .

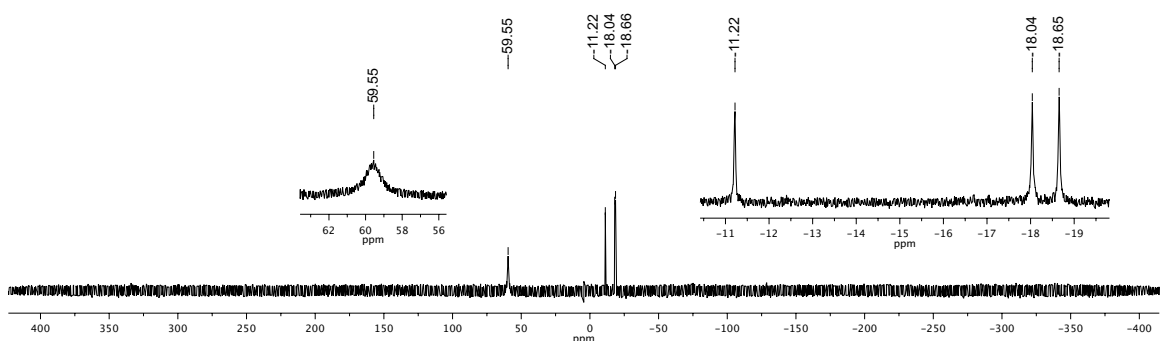


Figure B-6. Full ^{119}Sn $\{^1\text{H}\}$ NMR spectrum of a sample of PTA- SnMe_3 in D_2O .

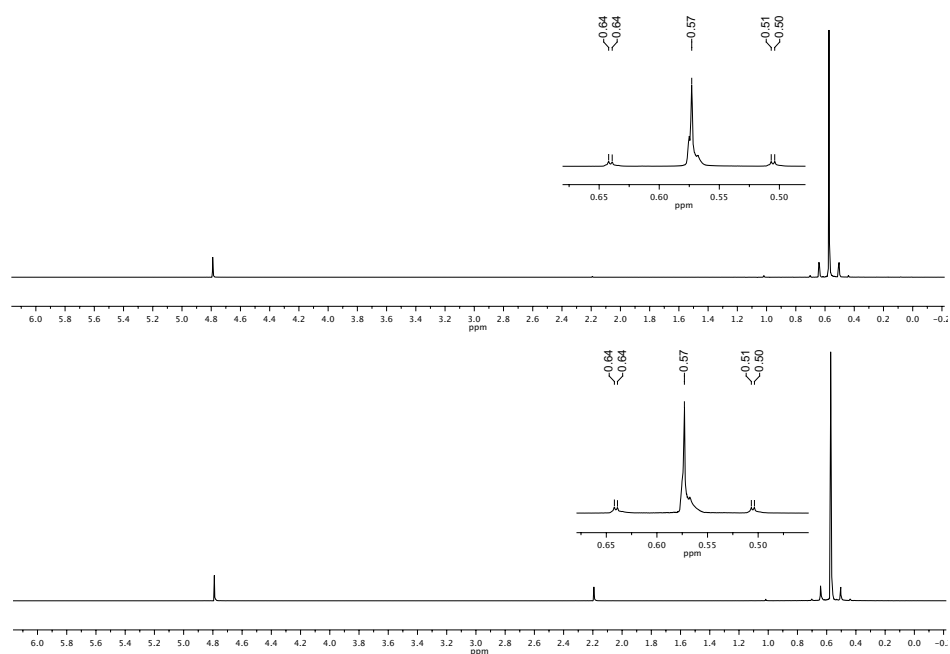


Figure B-7. ^1H NMR spectrum of SnMe_3Cl in D_2O from day 1 (top) to day 39 (bottom).

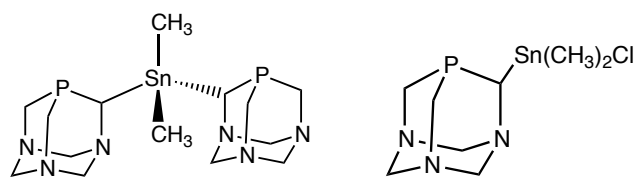


Figure C-1. Depiction of PTA₂-SnMe₂ (**4**) and the mono-substituted product PTA-SnMe₂Cl (**5**).

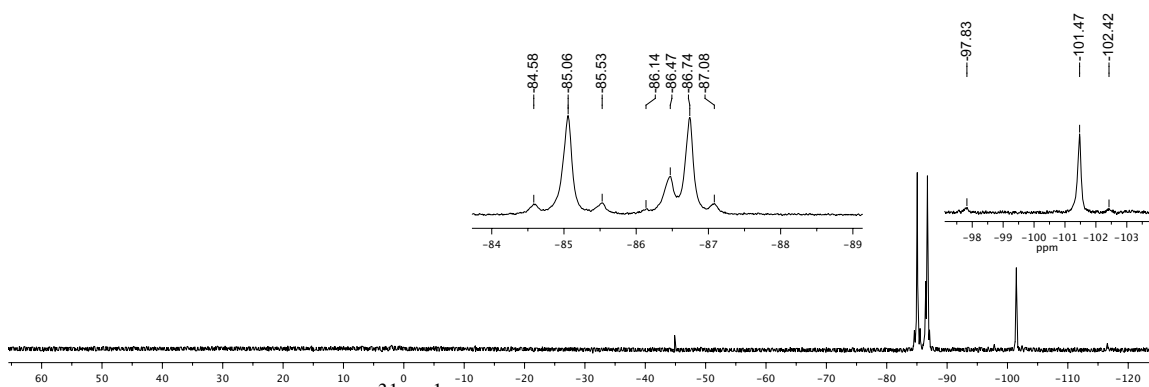


Figure C-2. Full ³¹P{¹H} NMR of PTA-Li with SnMe₂Cl₂ in THF.

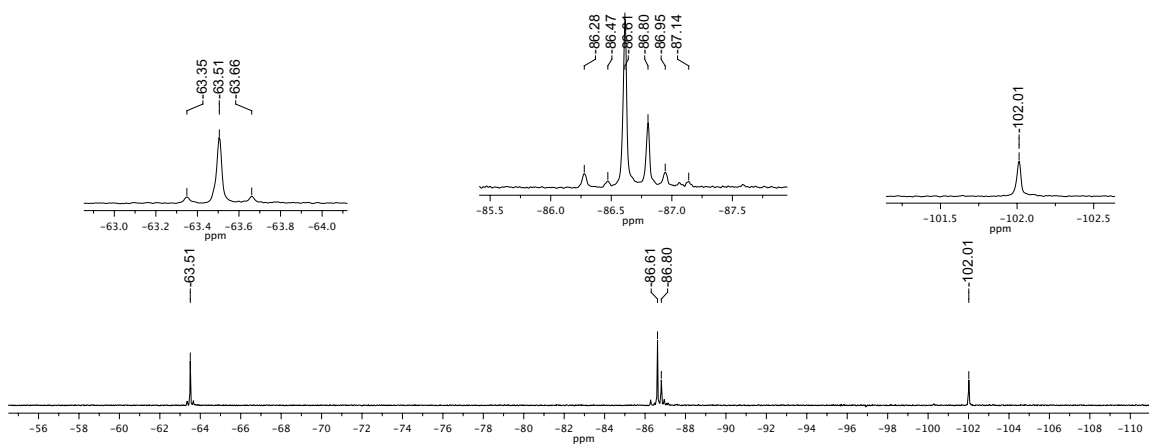


Figure C-3. Full ³¹P{¹H} NMR of PTA-Li with SnMe₂Cl₂ in CDCl₃.

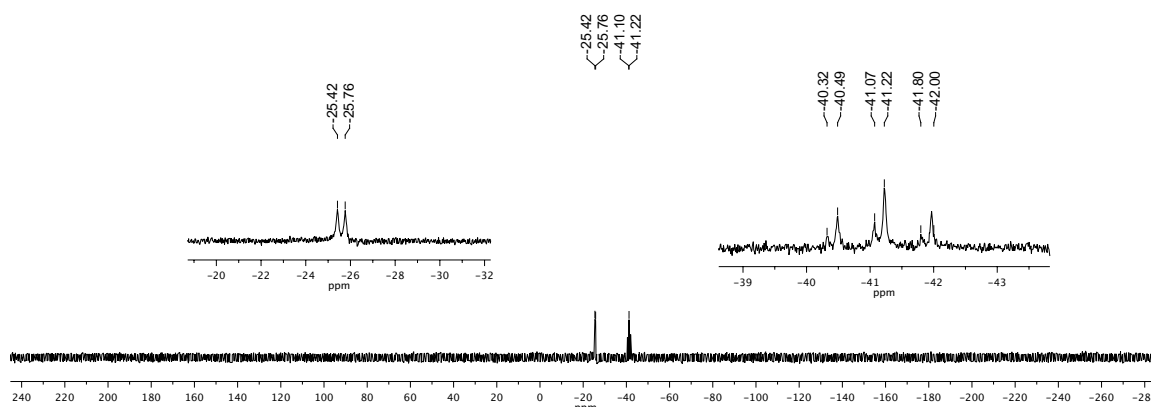


Figure C-4. Full $^{119}\text{Sn}\{^1\text{H}\}$ NMR of PTA-Li with SnMe_2Cl_2 in CDCl_3

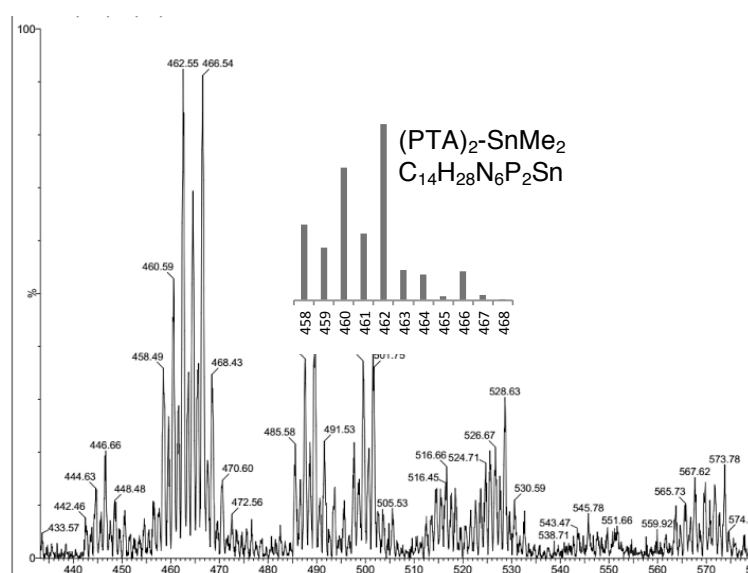


Figure C-5. Expanded ESI+ electrospray mass spectrum (positive mode) of $(\text{PTA})_2\text{-SnMe}_2$. Inset shows the simulated isotopic distribution pattern for $(\text{PTA})_2\text{-SnMe}_2$ (M^+).

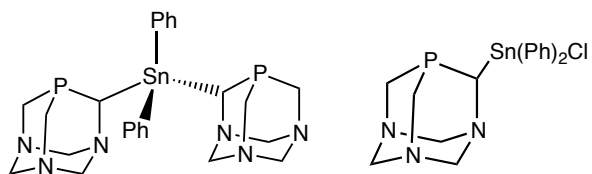


Figure D-1. Depiction of $\text{PTA}_2\text{-SnPh}_2$ (**6**) and PTASnPhCl (**7**).

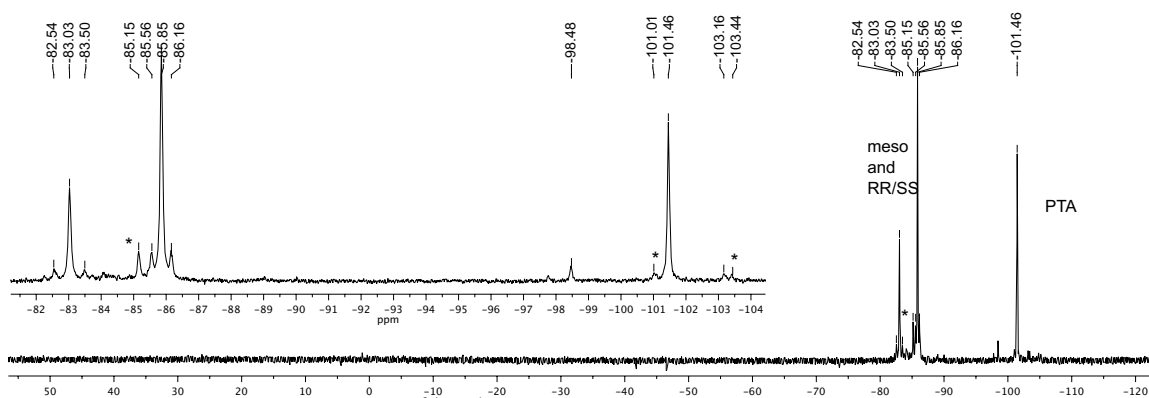


Figure D-2. Expanded $^{31}\text{P}\{^1\text{H}\}$ NMR of PTA-Li with SnPh_2Cl_2 in THF.

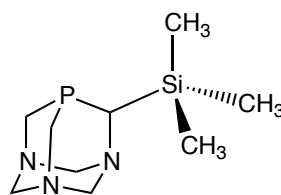


Figure E-1. Depiction of PTA-SiMe_3 (**8**)

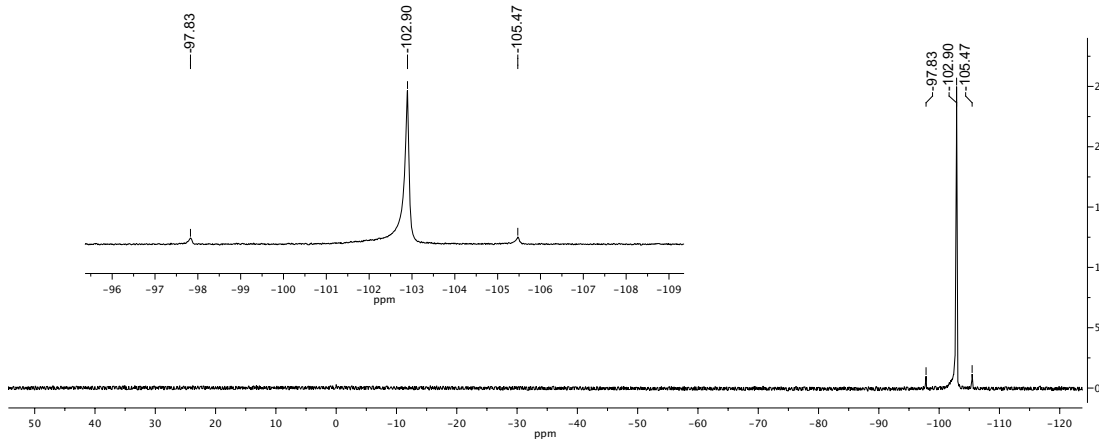


Figure E-2. Full $^{31}\text{P}\{^1\text{H}\}$ NMR of PTA-Li with SiMe_3Cl in THF.

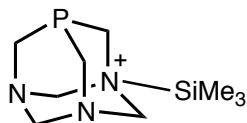


Figure F-1. Depiction of PTA-(N-SiMe₃) (9)

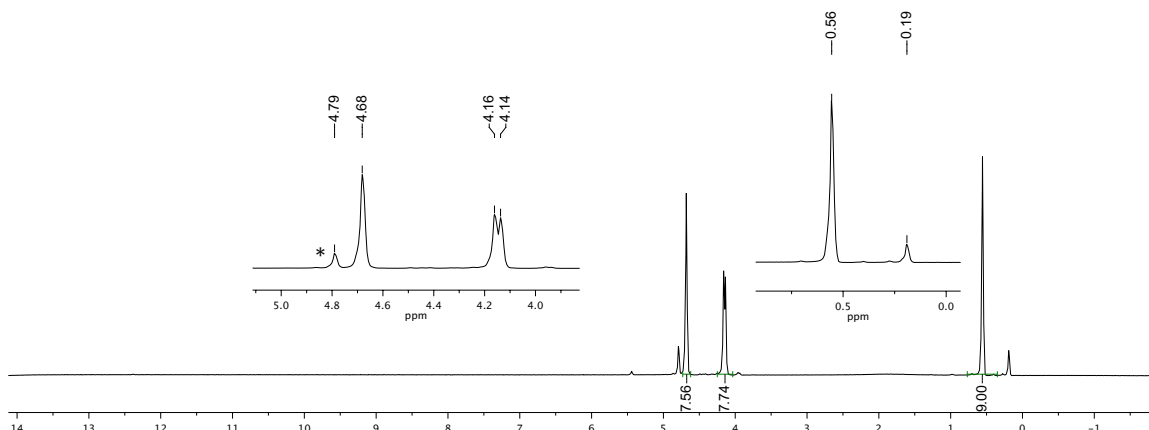


Figure F-2. Full ¹H NMR of the reaction PTA with SiMe₃Cl in CD₂Cl₂. *Trace HMTA from PTA synthesis

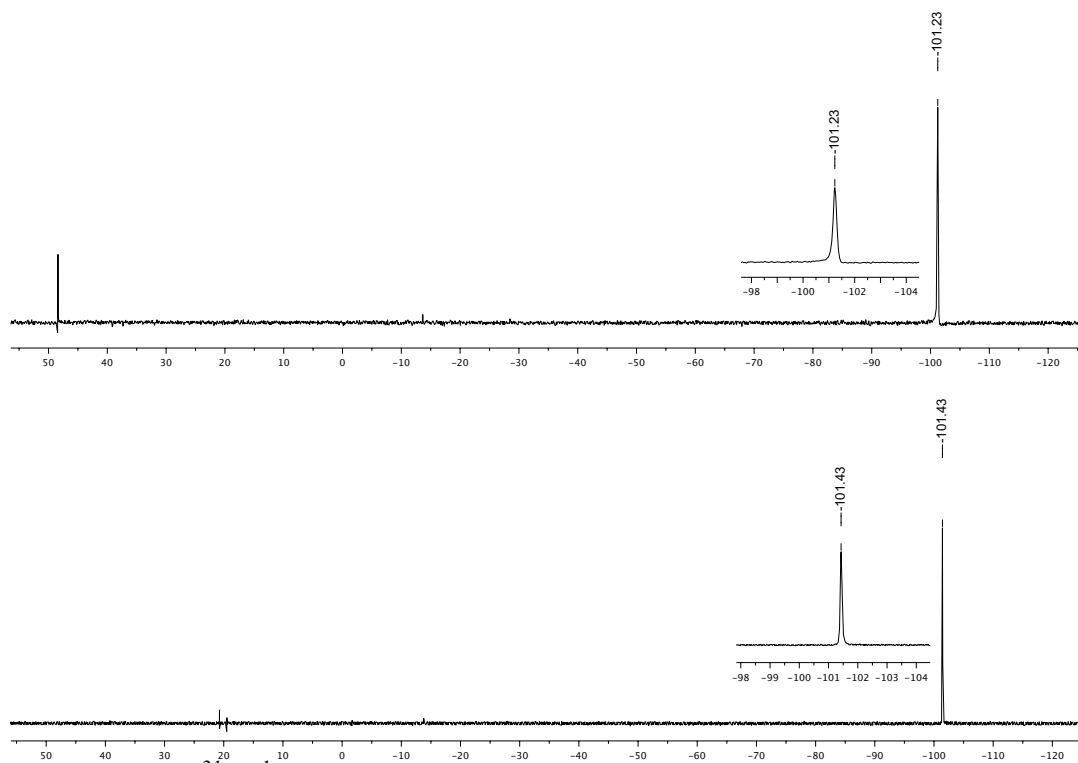


Figure F-3. Full ³¹P {¹H} NMR of the reaction PTA with SiMe₃Cl in CD₂Cl₂. Top (1.1 equiv. SiMe₃Cl), bottom (after addition of PTA)

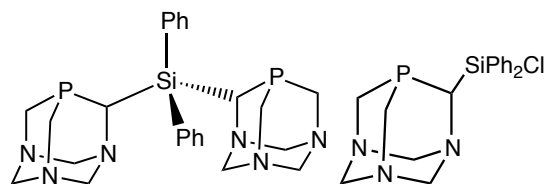


Figure G-1. Depiction of PTA₂-SiPh₂ (**10**) and PTASiPhCl (**11**).

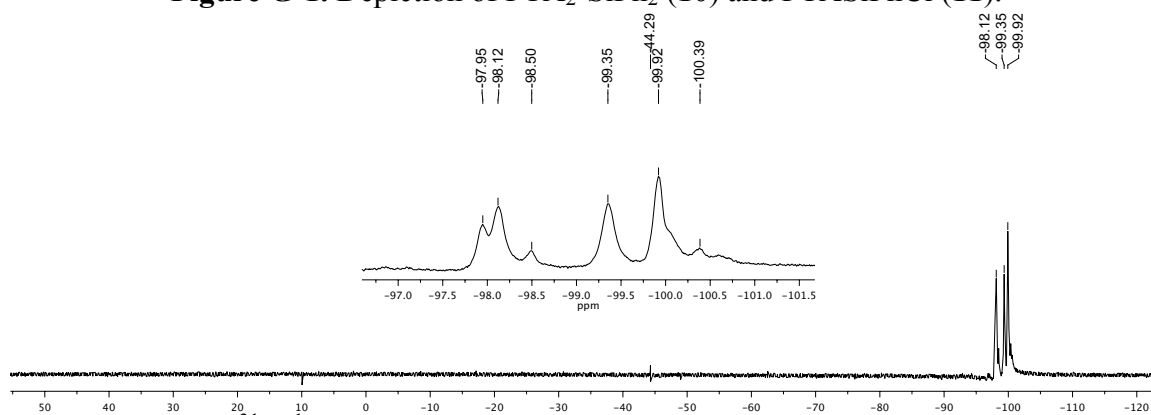


Figure G-2. Full ³¹P{¹H} NMR of the crude reaction mixture of PTA-Li with SiPh₂Cl in THF.

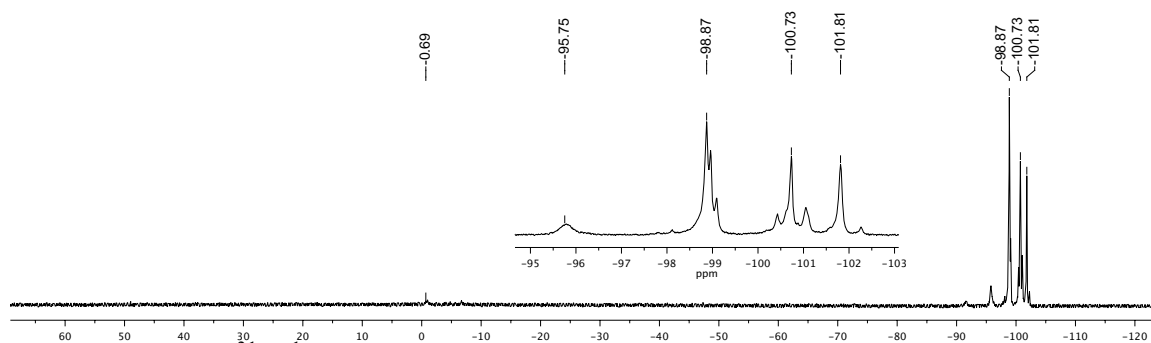


Figure G-3. Full ³¹P{¹H} NMR of the crude mixture of PTA-Li with SiPh₂Cl, pulled dry, and dissolved in C₆D₆.

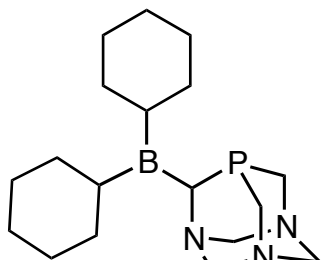


Figure H-1. Depiction of PTA-BCy₂ (**12**).

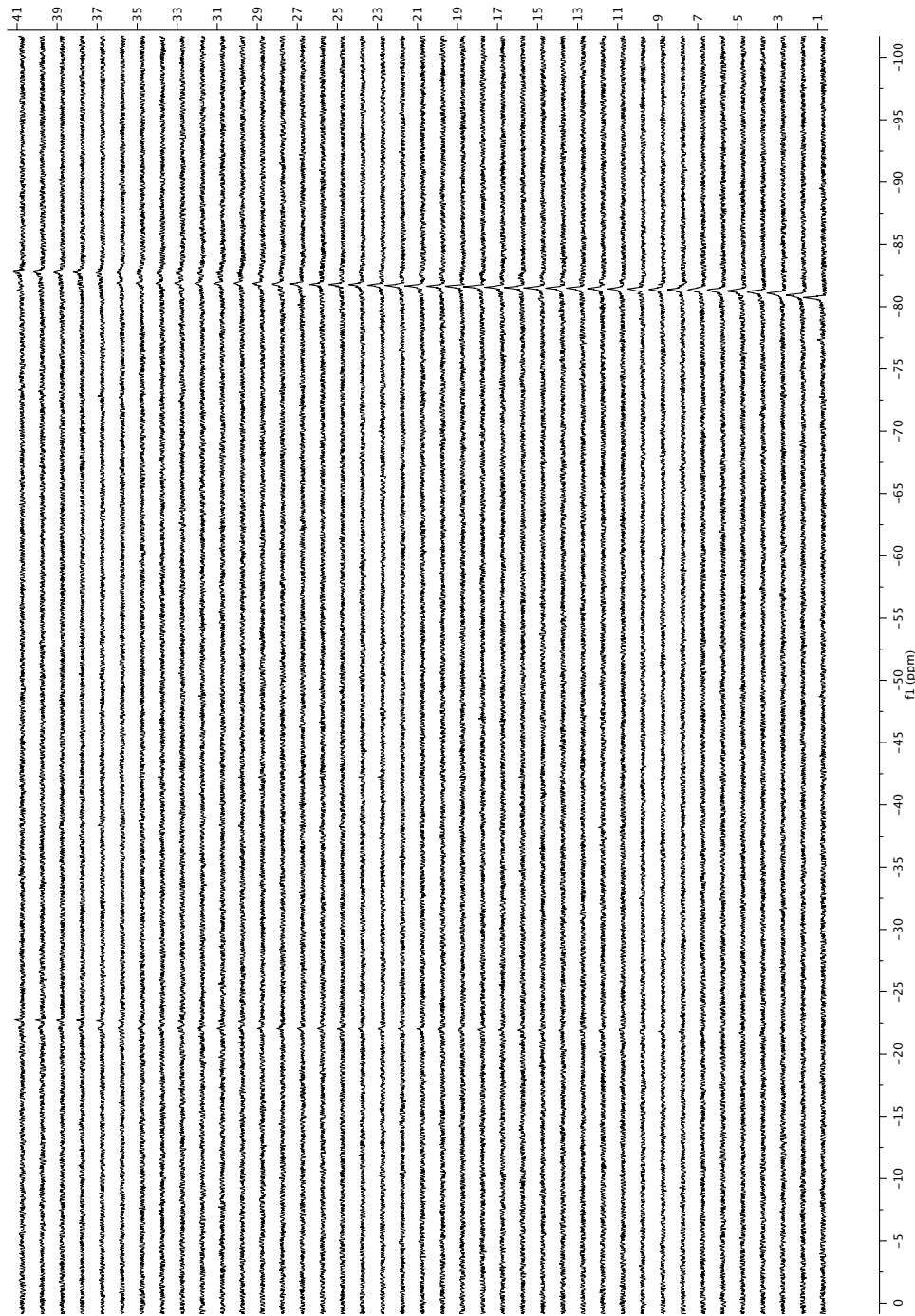


Figure H-2. Kinetic $^{31}\text{P}\{^1\text{H}\}$ NMR spectra of the reaction of PTA-Li and BCy_2Cl in THF at 35°C . Time elapsed can be calculated from the multiplication of the spectrum number by 5 minutes.

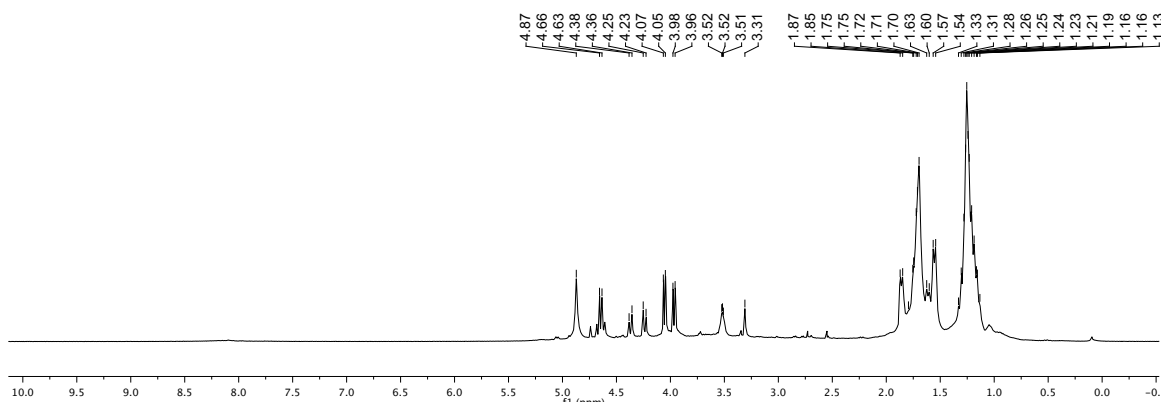


Figure H-3. Full ^1H NMR spectrum of the THF-soluble product from the crude reaction mixture of PTA-Li and BCy_2Cl , pulled dry and dissolved in CD_3OD .

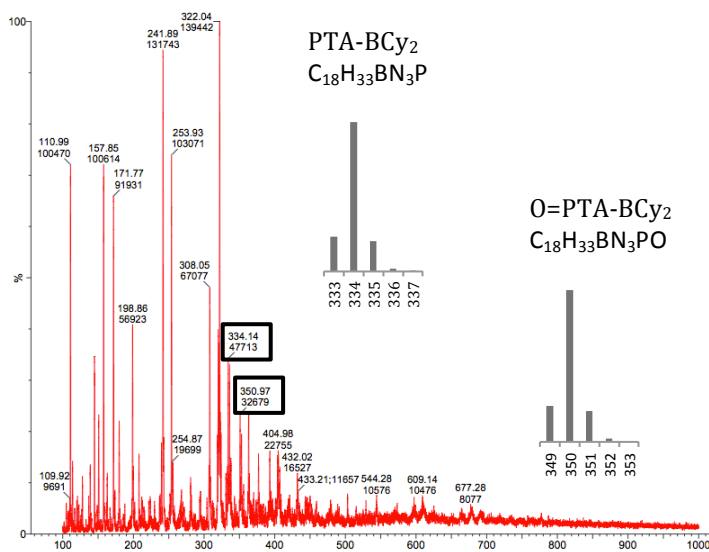


Figure H-4. ESI-MS (positive mode) of the reaction between PTA-Li and BCy_2Cl in methanol. Inset shows the simulated distribution pattern (M^+).

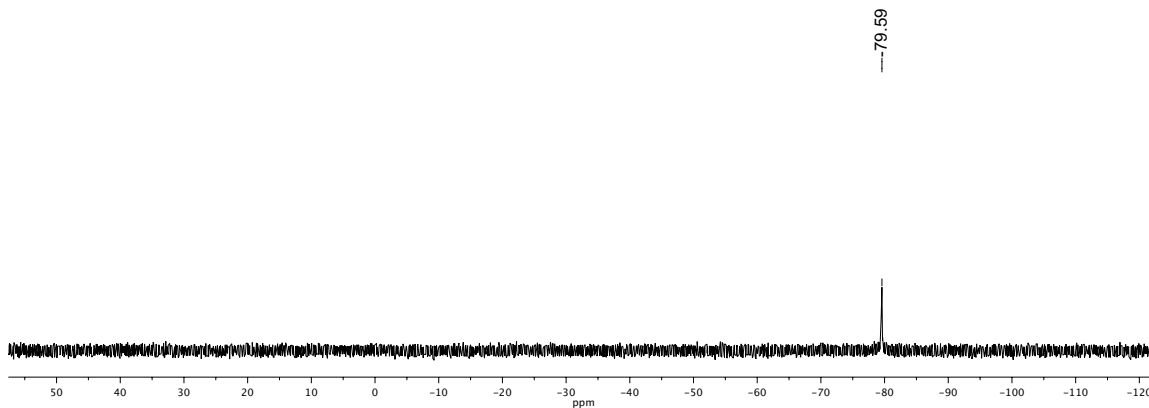


Figure H-5. Full $^{31}\text{P}\{^1\text{H}\}$ NMR spectrum of PTA-Li and BCy_2Cl (1 equiv.) in THF.

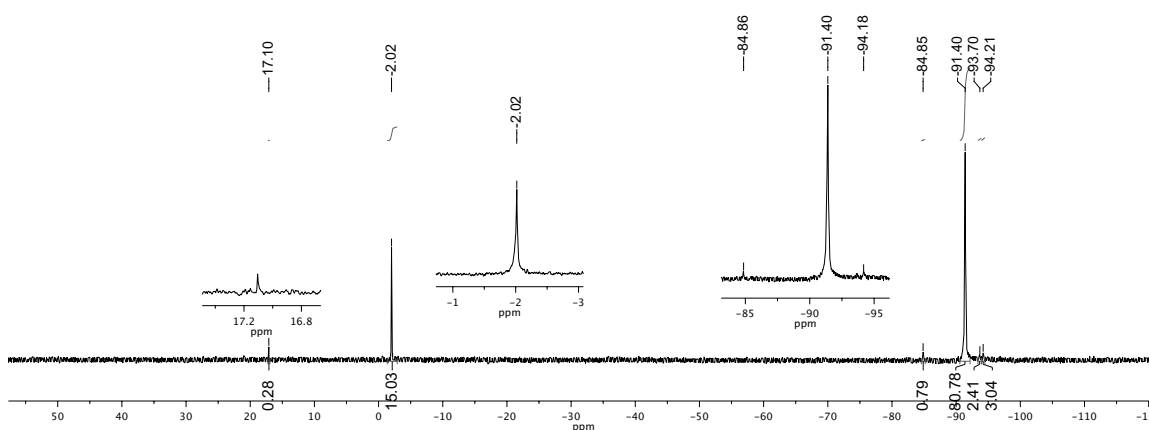


Figure H-6. $^{31}\text{P}\{^1\text{H}\}$ NMR spectrum of PTA-Li and BCy_2Cl in D_2O .

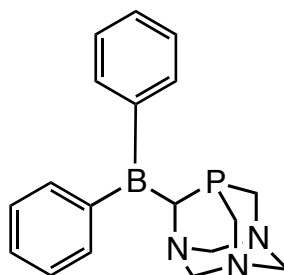


Figure I-1. Depiction of PTA-BPh₂ (13).

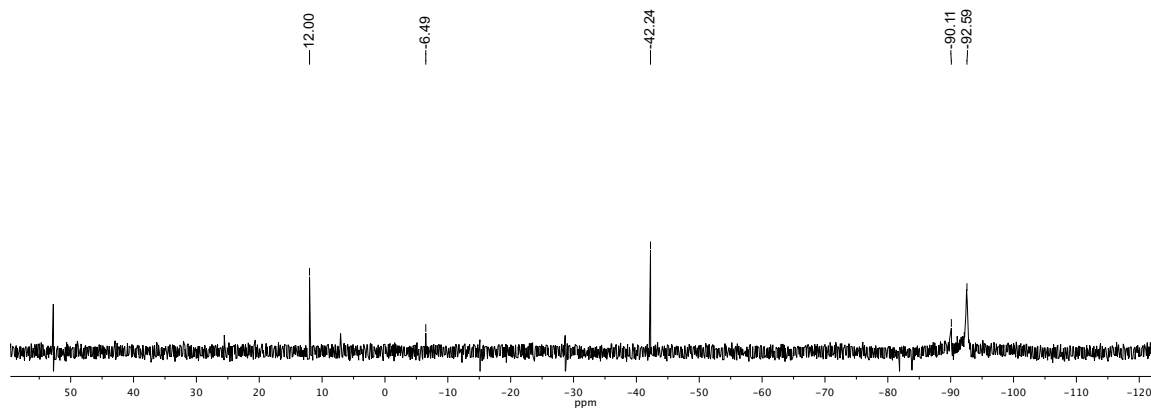


Figure I-2. Full $^{31}\text{P}\{^1\text{H}\}$ NMR spectrum of the reaction of PTA-Li with BPh_2Cl in THF.

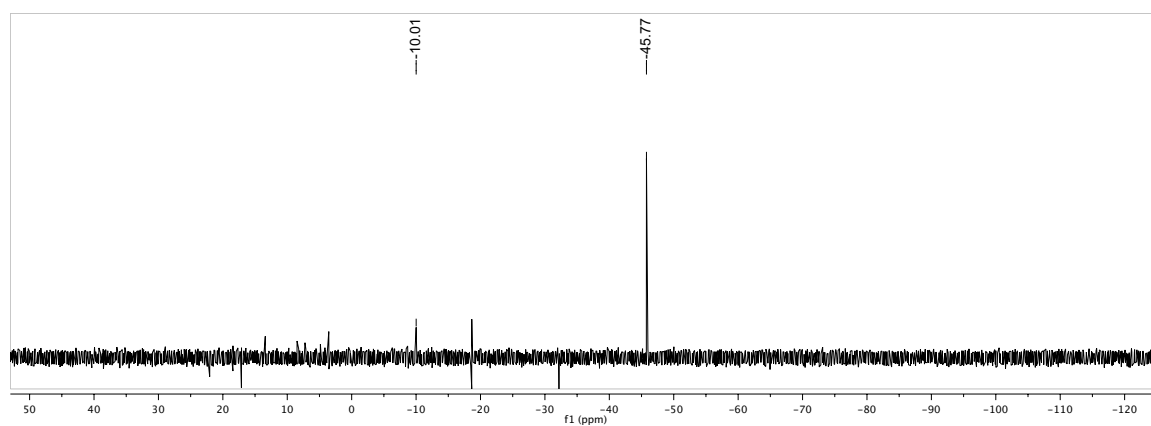


Figure I-3. Full $^{31}\text{P}\{^1\text{H}\}$ NMR spectrum of the reaction of PTA-Li with BPh_2Cl in CDCl_3 after washing with hexanes.

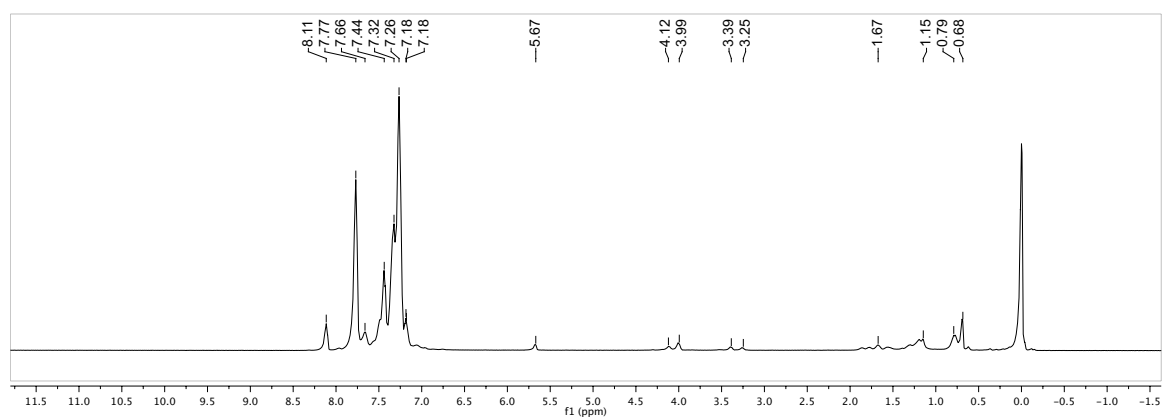


Figure I-5. Full ^1H NMR spectrum of the reaction of PTA-Li with BPh_2Cl in CDCl_3 after washing with hexanes.

VITA

June Pinky T. Acay was born in Isabela, Philippines in 1989. From 2005 to 2009, she pursued her Bachelor of Science degree in Chemistry at the University of the Philippines – Diliman Campus. In August 2011, she entered the master's program in chemistry at the University of Nevada, Reno. She conducted her research on PTA derivatives with tin, silicon, and boron moieties under the supervision of Brian J. Frost, PhD. Any questions or comments may be directed to june.acay@nevada.unr.edu.